

**SYSTEM MODELING AND CONTROL DESIGN OF A  
TWO-STAGE METERING POPPET-VALVE SYSTEM**

---

**A Dissertation  
presented to  
the Faculty of the Graduate School  
University of Missouri-Columbia**

---

**In Partial Fulfillment  
of the Requirements for the Degree  
Doctor of Philosophy**

---

**by  
YAMIN LUO**

**Dr. Noah Manring, Dissertation Supervisor**

**MAY 2006**


The undersigned, appointed by the Dean of the Graduate School, have examined the dissertation entitled,

SYSTEM MODELING AND CONTROL DESIGN OF A TWO-STAGE METERING  
POPPET-VALVE SYSTEM


Presented by YAMIN LUO

A candidate for the degree of Doctor of Philosophy

And hereby certify that in their opinion it is worthy of acceptance.

  
Dr. Noah Manning

  
Dr. Steven Borgelt (External Supervisor)

  
Dr. Roger Fales

  
Dr. Frank Feng

  
Dr. Craig Kluever

  
Dr. Yuyi Lin

*To my family*

献给我亲爱的家人

## ACKNOWLEDGEMENT

I would first thank to my advisor, Dr. Noah Manning, for his valuable guidance, patience and support throughout the past three years. His enthusiasm for work and dedication to his family present me America in a good light. It would be a quite hard task for me to find a better advisor.

I would also like to thank Dr. Mark Vonderwell and Dr. Hongliu Du. Without their help, patience and guidance, I would have never understood nor had the appreciation for this project. And I am grateful to Caterpillar Inc. to offer me the opportunity to work on poppets.

Thanks to my committee member, Dr. Steven C. Borgelt, Dr. Roger Fales, Dr. Zaichun Feng, Dr. Craig A. Kluever and Dr. Yuyi Lin for warm help and precious suggestions during my study.

My thanks also go to my workmates and friends for all happy and tough hours of research, classes as well as entertainment we shared. It is your accompany that makes my Mizzou experience brilliant and provides me many unforgettable memories.

Last, but certainly not least, I wish to thank my family that consists of my respectable parents, my intelligent brother, my beautiful elder sister and my lovely twin sister, for their ever-present support and encouragement. Foremost, though, I would like to thank my wonderful husband for his intimate consideration and everlasting support, especially his crucial “push” when I am working in a languid mood.

## TABLE OF CONTENTS

ACKNOWLEDGEMENT .....	iv
LIST OF TABLES .....	ix
LIST OF FIGURES .....	x
LIST OF NOMENCLATURE.....	xiii
ABSTRACT.....	xxii
CHAPTER 1. INTRODUCTION .....	1
1.1 Introduction.....	1
1.2 Description.....	2
1.2.1 Configuration of A Relief Control Poppet .....	2
1.2.2 Configuration of the Metering Poppet Valve System .....	3
1.3 Literature Review .....	7
1.3.1 Poppet Valve Research .....	7
1.3.2 Automatic Control History .....	12
1.4 Thesis Objective and Organization.....	16
CHAPTER 2. SYSTEM MODELING .....	19
2.1 Introduction.....	19
2.2 Poppet Analysis.....	20
2.2.1 Poppet Valve Flow Force .....	22
2.2.2 Nominal Conditions.....	29
2.2.3 Equation of Motion for the Poppet Valve .....	30
2.3 Back-side Pressure Analysis.....	31
2.3.1 Flow Rates in Back-side Chamber .....	33

2.3.2 Nominal Conditions.....	38
2.3.3 Back-side Pressure Equation .....	40
2.4 Control Pressure Analysis .....	41
2.4.1 Nominal Conditions.....	43
2.4.2 Control Pressure Equation.....	44
2.5 Nonlinear Governing Equations for the Open-loop System.....	45
2.6 Linear Governing Equations for the Full-model Open-loop System .....	46
2.7 Steady-State Solution .....	48
2.8 Linear Governing Equations for the Reduced-order Open-loop System .....	48
2.8.1 Non-Dimensional Governing Equations for the Full-model Linear Open-loop System.....	48
2.8.2 Linear Governing Equations for the Reduced-order Linear Open-loop System.....	50
2.9 Summary.....	54
CHAPTER 3. CONTROL DESIGN.....	55
3.1 Introduction.....	55
3.2 Modified PI Control .....	56
3.2.1 Control Law.....	56
3.2.2 Characteristic Equation of the Reduced-order Linear Closed-loop System	59
3.2.3 Control Gain Analysis.....	60
3.3 LQG Control.....	63
3.3.1 State-Space Equations for the Full-model Linear Open-loop System.....	64
3.3.2 Kalman Estimator.....	69
3.3.3 Full-State Feedback LQR.....	71

3.3.4 Summary of the Closed-loop System with the LQG Controller .....	73
3.4 $H_\infty$ Control.....	74
3.4.1 System Uncertainty .....	74
3.4.2 Mixed Sensitivity $H_\infty$ Control Design .....	76
3.4.2.1 Standard Control Configuration for a Common System with Uncertainty .....	76
3.4.2.2 Common $H_\infty$ Control Design.....	80
3.4.2.3 Mixed Sensitivity $H_\infty$ Control Design .....	84
3.5 Nonlinear Controller Design for the Nonlinear System.....	88
3.5.1 System Nonlinearities.....	88
3.5.2 Control Law.....	89
3.5.3 Lyapunov Function and Globally Asymptotical Stability.....	93
3.6 Summary.....	96
CHAPTER 4. SIMULATION RESULTS .....	97
4.1 Introduction.....	97
4.2 System Requirements.....	99
4.3 Influences of Key Parameters on the Open-loop System Stability .....	99
4.3.1 Characteristic Equation of the Full-model Linear Open-loop System .....	100
4.3.2 Non-Dimension Stability Criteria of the Full-model Linear Open-loop System.....	100
4.3.3 System Pressures $P_1, P_{2d}$ .....	101
4.3.4 Leakage Coefficients $K_2, K$ .....	104
4.3.5 System Geometries $V_L, rA_c$ .....	107

4.3.6 Fluid Properties $\beta, C_d$ .....	109
4.3.7 Spring Rate $k$ .....	112
4.4 Regulation Problem of Open-loop Systems .....	115
4.5 Regulation Problem of the First Group of Closed-loop Systems .....	117
4.6 Regulation Problem for the Second Group of Closed-loop Systems .....	122
4.7 Tracking Problem of the First Group of Closed-loop Systems .....	124
4.8 Tracking Problem of the Second Group of Closed-loop Systems.....	129
4.9 Summary.....	131
CHAPTER 5. CONCLUSIONS AND CONTRIBUTIONS .....	133
5.1 Introduction.....	133
5.2 System Modeling.....	133
5.3 Control Design.....	134
5.4 Contributions.....	137
CHAPTER 6. FUTURE WORK.....	138
6.1 System Modeling.....	138
6.2 Control Design.....	138
REFERENCE.....	140
VITA.....	147



## LIST OF TABLES

Table	Page
Table 4- 1. Parameters of system operation conditions .....	98
Table 4- 2. Poppet parameters .....	98

## LIST OF FIGURES

Figure	Page
Figure 1-1. Common relief poppet valve structure.....	3
Figure 1-2. A two-stage poppet valve system structure .....	5
Figure 1-3. Sectional view of a MOOG D633/D634 direct drive servo-proportional control valve .....	6
Figure 2-1. Forces acting on the poppet.....	20
Figure 2-2. Poppet nose-side control volume for calculating the poppet flow force .....	23
Figure 2-3. Poppet instantaneous discharging area .....	25
Figure 2-4. Flows entering or exiting the back-side chamber .....	33
Figure 2-5. Leakage between the poppet land and its containing bore .....	34
Figure 2-6. Spool valve rectangular port geometry .....	37
Figure 2-7. Control pressure analysis .....	42
Figure 2-8. Block diagram for the open-loop poppet-valve system .....	46
Figure 2-9. Block diagram for the full-model linear open-loop poppet-valve system .....	47
Figure 2-10. Pressures for calculating non-dimension governing equation coefficients... 51	51
Figure 2-11. Non-dimension equation coefficients for the poppet analysis.....	52
Figure 2-12. Non-dimension equation coefficients for the back-side pressure analysis ..	52
Figure 2-13. Non-dimension equation coefficients for the control pressure analysis .....	53
Figure 3-1. Block diagram for the closed-loop poppet-valve system .....	59
Figure 3-2. Structure of the linear closed-loop system with the LQG controller.....	64
Figure 3-3. State-space structure of the linear closed-loop system with the LQG controller .....	69

Figure 3-4. Plant with the lumped multiplicative uncertainty: $G_p$ .....	75
Figure 3-5. Standard system structure with uncertainty for control design and robust analysis .....	77
Figure 3-6. Standard control design configuration for a system with uncertainty .....	78
Figure 3-7. NA-structure for analyzing robustness of a system with uncertainty .....	80
Figure 3-8. System structure for mixed sensitivity $H_\infty$ control design.....	86
Figure 4-1. F-M O-L system stability criteria for the 1 <sup>st</sup> set of working pressures.....	102
Figure 4-2. F-M O-L system stability criteria for the 2 <sup>nd</sup> set of working pressures .....	103
Figure 4-3. F-M O-L system stability criteria for Case 1 of leakage coefficients .....	105
Figure 4-4. F-M O-L system stability criteria for Case 2 of leakage coefficients .....	106
Figure 4-5. F-M O-L system stability criteria for Case 1 of system geometries.....	107
Figure 4-6. F-M O-L system stability criteria for Case 2 of system geometries.....	109
Figure 4-7. F-M O-L system stability criteria for Case 1 of fluid properties.....	110
Figure 4-8. F-M O-L system stability criteria for Case 2 of fluid properties.....	111
Figure 4-9. F-M O-L system stability criteria for Case 1 of spring rate .....	113
Figure 4-10. F-M O-L system stability criteria for Case 2 of spring rate .....	114
Figure 4-11. Regulation of open-loop systems .....	116
Figure 4-12. Input uncertainty and weight function $W_I$ (red line) for regulation problem .. .....	119
Figure 4-13. Regulation of nonlinear/linear closed-loop systems- $y$ and $x_v$ .....	120
Figure 4-14. Regulation of nonlinear/linear closed-loop systems- $P_2$ and $\dot{y}$ .....	121
Figure 4-15. Regulation of nonlinear closed-loop systems- $y$ and $x_v$ .....	123
Figure 4-16. Regulation of nonlinear closed-loop systems- $P_2$ and $\dot{y}$ .....	123

Figure 4-17. Input uncertainty and weight function $W_l$ (red line) for tracking problem.	125
Figure 4-18. Tracking of nonlinear/linear closed-loop systems- $y$ and $x_v$ .....	126
Figure 4-19. Tracking of nonlinear/linear closed-loop systems- $P_2$ and $\dot{y}$ .....	128
Figure 4-20. Gains of the modified PI controller for tracking problem .....	129
Figure 4-21. Tracking of nonlinear/linear closed-loop systems- $y$ and $x_v$ .....	130
Figure 4-22. Tracking of nonlinear closed-loop systems- $P_2$ and $\dot{y}$ .....	130

## LIST OF NOMENCLATURE

- $A$  cross-section area of the incompressible poppet nose-side control chamber
- $A_c$  cross-section area of the poppet land
- $\mathbf{A}_h, \mathbf{B}_{h1}, \mathbf{B}_{h2}, \mathbf{C}_{h1}, \mathbf{C}_{h2}, \mathbf{D}_{h11}, \mathbf{D}_{h12}, \mathbf{D}_{h21}, \mathbf{D}_{h22}$  system matrices of  $H_\infty$  control
- $A_i$  steady-state error percentage
- $A_k$  constant cross-section area of the orifice in the back-side pipeline
- $\mathbf{A}_{KF}, \mathbf{B}_{KF}, \mathbf{C}_{KF}, \mathbf{D}_{KF}$  system matrices of the Kalman filter
- $A_m$  cross-section area of a control volume boundary surface
- $\mathbf{A}_{op}, \mathbf{B}_{op}, \mathbf{C}_{op}, \mathbf{D}_{op}$  open-loop system matrices
- $A_p$  instantaneous discharge area of the poppet opening
- $A_1$  instantaneous discharge area of the spool valve with rectangular port
- $a_0, a_1, a_2, a_3, d_0, d_1, d_2, d_3$  coefficients of characteristics equations of linear systems
- $C_d$  discharge coefficient
- $c$  viscous drag coefficient of the poppet valve
- $e$  eccentricity dimension between the center of the inside insert and the center of the outside tube
- $D$  diameter of the poppet valve nose-side port

$D_c$	diameter of the poppet land
$D_{bore}$	diameter of the hole that contains the poppet land
$D_k$	diameter of the orifice in the back-side pipeline
$d_c$	diameter clearance between the poppet land and the hole that contains it
$E$	expectation operator
$F_f$	flow force acting on the poppet head yielded by the fluid linear momentum change
$F_{ft}$	transient flow force
$F_{fs}$	steady flow force
$F_p$	resultant flow force produced by the fluid passage across the poppet nose-side chamber
$F_{sp}$	instantaneous spring force of the poppet valve
$\vec{f}$	body force vector for the fluid in a control chamber
<b>G</b>	general plant
<b>G<sub>norm</sub></b>	nominal plant
<b>G<sub>p</sub></b>	plant with the lumped multiplicative input uncertainty
<b>I</b>	identity matrix
$h$	rectangular height of spool port

$h_o$	clearance of the circular walls between the inside insert and the outside tube
$K$	leakage coefficient of the leakage in the back-side pipeline
$K_c$	flow pressure coefficient of the poppet valve
$K_{cl}$	flow pressure coefficient of the back-side pipeline fluid
$K_{c1}$	flow pressure coefficient of the spool valve
$K_{fct}$	flow force pressure coefficient of the poppet valve
$K_{fq}$	flow force gain of the poppet valve
$\mathbf{K}_h$	$H_\infty$ controller
$K_I$	constant integral gain of the PI controller
$K_{I2}$	various integral gain of the PI controller
$K_p$	constant proportional gain of the PI controller
$K_{pp}$	various pressure gain of the PI controller
$K_{p2}$	various proportional gain of the PI controller
$K_Q, K_{QK}, K_y$	positive constants
$K_{qt}$	flow gain of the poppet valve
$K_{q1t}$	flow gain of the spool valve
$\mathbf{K}_r$	gain matrix of LQR

$K_s, K_v$	coefficients of linear governing equations
$K_2$	leakage coefficient of the leakage across the poppet land gap
$k$	poppet-valve spring rate
$\mathbf{J}_r$	quadratic cost function of LQR
$L$	length of the incompressible poppet nose-side control chamber
$l_c$	metering length of the poppet land
$M_{i_v}$	constant greater than the maximum peak value of $ S_{i_v} $
$m$	mass of the poppet valve
$n$	number of the system eigenvalues
$n_b$	maximum number of sample times in the whole chosen simulation time
$n_v$	number of the output disturbances
$\mathbf{M}_r$	Kalman filter innovation gain matrix
$\mathbf{N}_h$	generalized closed-loop plant
$P_1$	poppet nose-side pressure
$P_2$	poppet back-side pressure
$P_c$	control pressure in the control chamber
$P_k$	constant pressure provided by a fluid reservoir



- $\mathbf{P}_h$  generalized open-loop plant
- $\mathbf{P}_{h11}, \mathbf{P}_{h12}, \mathbf{P}_{h21}, \mathbf{P}_{h22}$  system transfer function matrices
- $\Delta P$  pressure drop across the poppet head
- $\nabla p$  gradient of the fluid pressure in a control chamber
- $Q$  flow rate going through the poppet
- $Q_c$  flow rate entering or exiting the control chamber
- $Q_L$  flow rate from the back-side chamber to the reservoir with a constant pressure
- $\mathbf{Q}_h$  stable proper transfer function
- $\mathbf{Q}_n, \mathbf{R}_n$  flat constant power spectral density matrices
- $Q_2$  leakage from the control chamber to the back-side chamber
- $rA_c$  ratio of the cross-section poppet land area and the cross-section poppet port area
- $StN_1, StN_2, StN_3, StN_4,$  non-dimension system stability criteria
- $\mathbf{S}, \mathbf{T}_1$  sensitivity function
- $s$  Laplace variable
- $t$  time variable
- $\mathbf{u}$  system control-signal vector
- $\mathbf{u}_\Delta$  input vector due to system uncertainties
- $u$  system control signal

$\vec{u}$	fluid velocity vector of a control volume
$V(\mathbf{x})$	Lyapunov function
$V_{co}$	volume of the poppet control chamber
$V_L$	volume of the poppet back-side chamber
$V_m$	changeable nose-side control volume
$\mathbf{V}_n$	measurement noise matrix
$\mathbf{W}$	input disturbance matrix
$\mathbf{W}_I$	uncertainty weight function
$\mathbf{W}_p, \mathbf{W}_u$	weight functions
$w$	rectangular width of the spool port
$w_1$	process disturbance
$\mathbf{x}$	system state vector
$\tilde{\mathbf{x}}$	internal Kalman state vector
$x_v$	spool valve displacement measured from the poppet asymmetric center line
$x_1$	horizontal direction of a control chamber
$\mathbf{x}_h$	internal state of the $H_\infty$ closed system
$\mathbf{Y}_f, \mathbf{Y}_r, \mathbf{X}_\infty, \mathbf{Y}_\infty$	solutions of algebraic Riccati equations
$\mathbf{y}_m$	measured system output vector

$\mathbf{y}_r$	output vector for the open-loop system
$\mathbf{y}_\Delta$	output vector due to system uncertainties
$y$	instantaneous poppet valve displacement measured from the poppet seat
$y_1$	vertical direction of a control chamber
$\tilde{\mathbf{y}}$	estimated full-state output vector
$\Delta y$	axial displacement derivation of the poppet from the nominal position
$\mathbf{z}$	output vector of a system with uncertainty

**Greek symbols**

$\beta$	fluid bulk modulus of elasticity
$\mu$	viscosity of 10WT hydraulic oil at 50C
$\tau$	characteristic time in which the main dynamic behavior of the system may occur
$\varepsilon$	eccentricity ratio
$\rho$	fluid density
$\theta$	poppet valve conical angle
$\varphi$	jet angle of the fluid flowing out of the poppet valve
$\sigma$	singular value
$\bar{\sigma}$	largest singular value of a matrix
$\gamma$	value of the infinite norm of a matrix

$\lambda$  eigenvalue

$\omega$  frequency variable

$\omega_B$  bandwidth frequency

$\Psi_1, \Psi_2, \Psi_3, \Psi_4, \Psi_5, \Xi_1, \Xi_2, \Xi_3, Z_1, Z_2, Z_3$  non-dimension coefficients of linear governing equations

$\nabla$  gradient operator

$\nabla^2$  Laplacian operator

$\Delta_R, \Delta_u, \Delta_T$  fictitious uncertainties that constitute  $\Delta_p$

$\Delta_p$  fictitious uncertainty come from  $H_\infty$  performance specification

$\Delta_l$  lumped complex perturbation

### Subscripts

$\hat{\phantom{x}}$  non-dimension

$\sim$  variable of Kalman filter

$d$  desired

$eff$  coefficient for linear governing equations

$g, clg$  for the closed-loop system with the LQG controller

$i_v$  about the  $i_v$  weight function for shaping the sensitivity function  $S$

$nd, ND$  non-dimension

$y_1$  sub-vector in  $y_1$  direction

$y_{1L}$  sub-vector along  $y_1$  direction at the exiting port of a control chamber

$y_{1o}$  sub-vector along  $y_1$  direction at the entering port of a control chamber

$\Delta$  about uncertainty

### **Superscripts**

$H$  complex conjugate transpose of a matrix

$T$  transpose of a matrix

$-1$  inverse of a matrix

## ABSTRACT

The goal of this work is to develop mathematical models, stability criteria, and control designs for a two-stage poppet valve system with a simple back-side pipeline condition that may be used in a valve stack to create an independent metering function for a hydraulic circuit.

First, this system is modeled as a nonlinear open-loop model as well as a linear one. The completely linear form of the flow force acting on the poppet head is derived from simplified Navier-Stokes Equations. Second, four control methods that comprise modified PI control, LQG control,  $H_\infty$  control, and nonlinear feedback control are used to make a closed-loop poppet system. The first three linear controllers are verified by being combined with the linear system as well as the nonlinear system in the simulation. The nonlinear controller is only applied to the nonlinear system and certified by Lyapunov theorem to be globally asymptotically stable. The basic guidelines for selecting control gains are derived by Routh-Hurwitz method. Finally, important system parameters are discussed to reveal their effects on the open-loop system stability. The transient flow force and two leakages have very close relationships with the system stability. Simulations results illustrate that the closed-loop poppet system with either the modified PI controller or the nonlinear controller can track the desired poppet displacement represented by a sine wave with 10 HZ frequency. The LQG controller and the  $H_\infty$  controller having fixed weighting functions or matrices are not flexible enough to satisfy the global nonlinear systems, though they exhibit the acceptable regulation behavior.

## CHAPTER 1. INTRODUCTION

### 1.1 Introduction

Poppet valves are extensively used in hydraulic systems as relief valves, check valves, cartridge valves, and pressure regulators due to their obvious advantages. First, they are easy to manufacture. They have positive metal-to-metal seals. Therefore tight machining tolerances are not necessary. Second, they are insensitive to jamming the seat by dirt particles due to a self-cleaning function. Third, they only have very small leakages. Poppet valves can essentially make zero leakage; thereby do not need check valves. Fourth, as a metering device, poppet valves do not need a pilot system, because they can directly use the system pressure as their pilot pressure. Therefore, a metering poppet valve system with low cost and small passage is possible. The final highlighted advantage of poppets is that they have high pressure-sensitivity to the valve displacement. A relatively small uplifting movement of the poppet can bring a large orifice area. However, there are two primary disadvantages of poppet valves. First, instability of the system is easy to occur accompanying with self-excited oscillations. Instability can be caused by many influences, for example, the unsteady flow forces through the poppet, uncertainty of discharge coefficient, upstream configurations, fluid delivery lines and the interference of the valve motion with other system components. Second, compared with the spool valves, the poppet valves cannot balance the pressure forces acting on the entire poppet by itself due to its geometry. Usually a compressed spring with preload is installed on the land side of the poppet to push the poppet tightly contact with the seat. Therefore, a poppet valve is very sensitive to fluid characteristics of the upstream and downstream of

the system. In this research, the working conditions linking with the back-side chamber will be considered.

The purpose of this research is to investigate the dynamic behavior and to carry out the control design for a two-stage metering poppet-valve system that may be used in a valve stack to create independent metering functions for a hydraulic circuit. The physical model of this study is quite similar to that in Du's work [1] except adding a simple back-side pipeline condition that contains a fixed-area orifice and a constant pressure reservoir to his system. The differences between Du's work and this work will be discussed in detail later in the literature review. The results of this work will be used for the upfront design of pressure compensators and for troubleshooting valve instabilities that are experienced in various applications.

## 1.2 Description

### 1.2.1 Configuration of A Relief Control Poppet

Figure 1-1 shows the general configuration of a seating type poppet valve that can relieve the over-high pressure flow to protect other components in hydraulic circuits. A typical poppet valve mainly comprises a moving element (or poppet) with spherical or conical or other head shapes, a fixed seat with different seat angles, and a force balance device e.g. attaching a spring or attaching a piston to the high-pressure side of the poppet. In Figure 1-1, the spring preload can be adjusted by altering the vertical height of the cartridge.

In this dissertation, the poppet lateral deviation from the center position due to the transverse flow force is ignored [2]. Therefore, the poppet is considered to only execute



vertical movements. As the pressure force from the nose side becomes big enough to overcome the sum of the inertia force, the damping force, the balance force and the pressure forces (including the flow force) acting on the poppet, the poppet is lifted away from the seat and the annular fluid passage allows to flow through the poppet valve from the high-pressure side to the low-pressure side. The relief function of the fluid accomplishes the basic pressure-drop of the poppet valve. The inverse process can happen when the back-side pressure is big enough to prevail over the sum of other forces acting on the poppet.

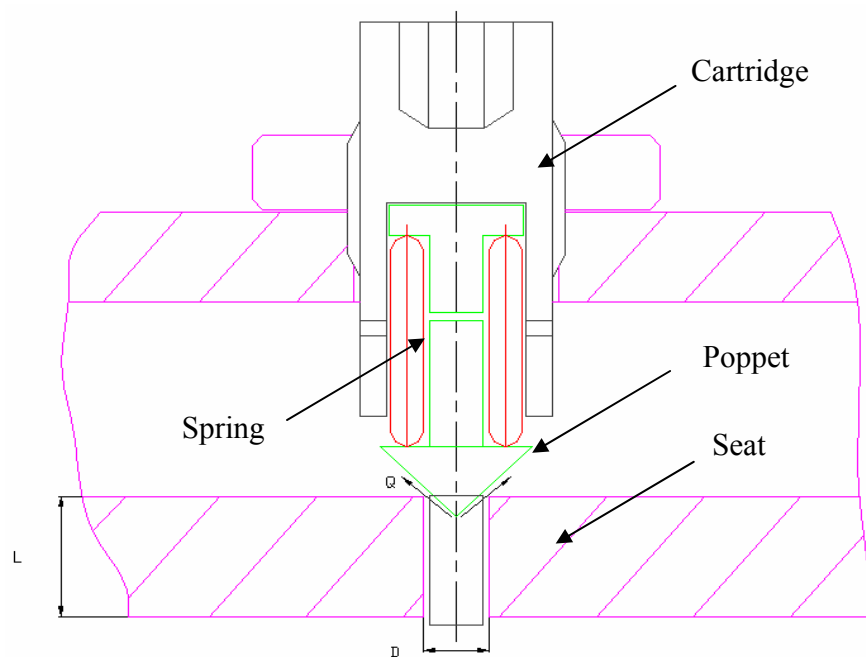


Figure 1-1. Common relief poppet valve structure

### 1.2.2 Configuration of the Metering Poppet Valve System

This system is a bi-direction two-stage metering poppet valve system, shown in Figure 1-2. The first stage is a 3-way piloting spool valve that is critically-centered with

the land width the same as that of the control-chamber port. The control orifice that is built up by the spool land and this port can open in both sides depending on which side has the higher pressure. However, no matter which side has the higher pressure, at the steady-state condition, this control opening always connects the control chamber with the poppet nose-side chamber, i.e. the port always opens at its right side. And this control orifice can be small enough to make up the leakage loss  $Q_2$  in the control chamber. The size and the response speed of this opening decide the reaction of the main poppet to the load changes. The displacement of the spool valve  $x_v$  is the input to the system, which might be fulfilled by operators or through other electric equipment according to load requirements.

The dynamics of the spool can be neglected by choosing the spool with fast response. The MOOG D633/D634 direct drive servo-proportional control valve in Figure 1-3 is a very fast valve that exhibits a frequency response of 90 HZ. The valve may be used to provide the first stage spool-valve function by connecting the T-port to the back-side chamber, the A-port to the poppet control chamber, the P-port to the nose-side chamber, while the B-port is blocked. Note: the Y-port remains open to the tank. Two simple working components connecting with the poppet back-side chamber are included in the system: an orifice with a fixed cross-section area  $A_k$  and a fluid reservoir with a constant pressure  $P_k$ .

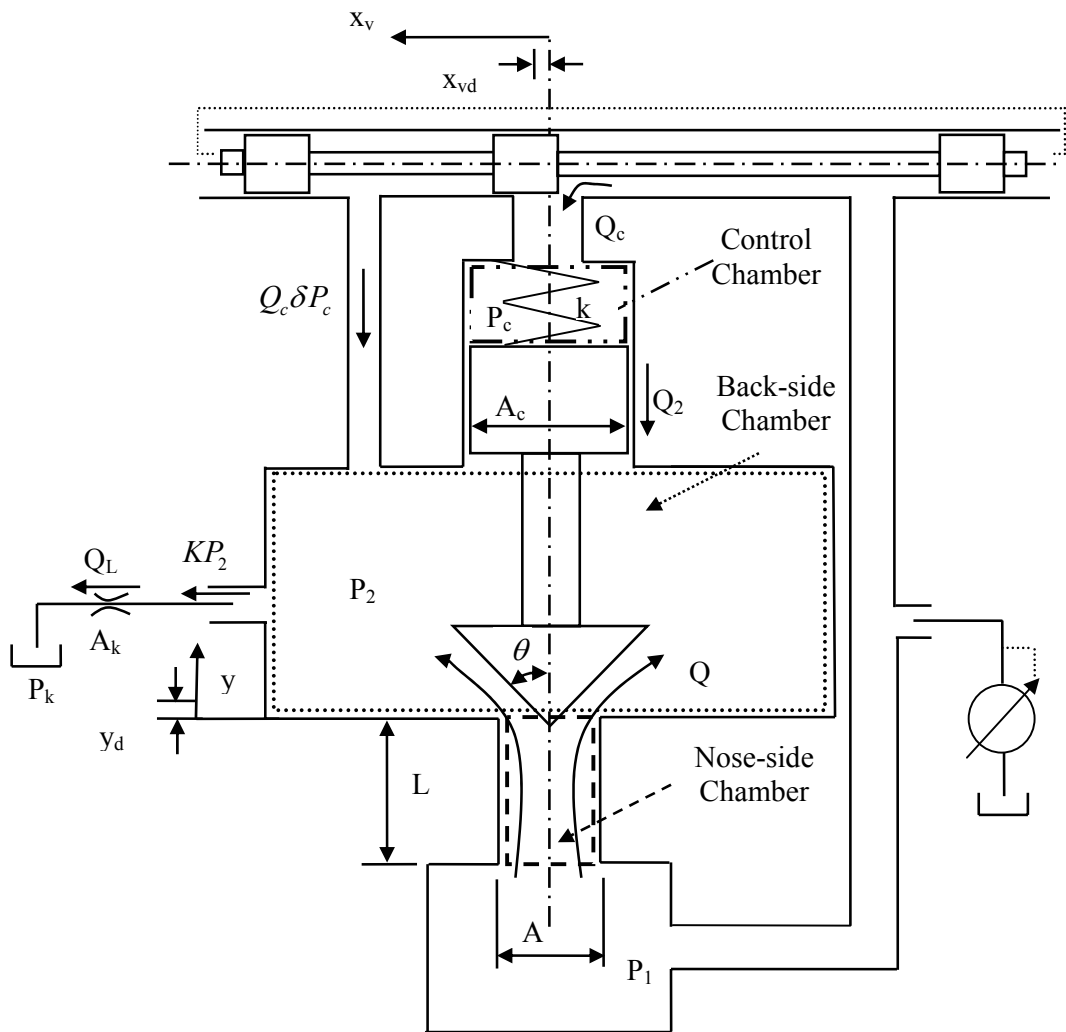


Figure 1-2. A two-stage poppet valve system structure

The second stage is a common poppet valve that connects with a cartridge by a spring, though the spring is very weak here. The fluid damping influence is considered to be linearly proportional to the poppet velocity in this two-stage valve system. The fluid can move either from the nose side to the back side or inversely depending on the resultant force of the mass inertia, the damping force, the spring force, the static pressure forces and the flow force. The size of the poppet opening and the pressure drop across the poppet head determines the amount of the load that the system can be taken.

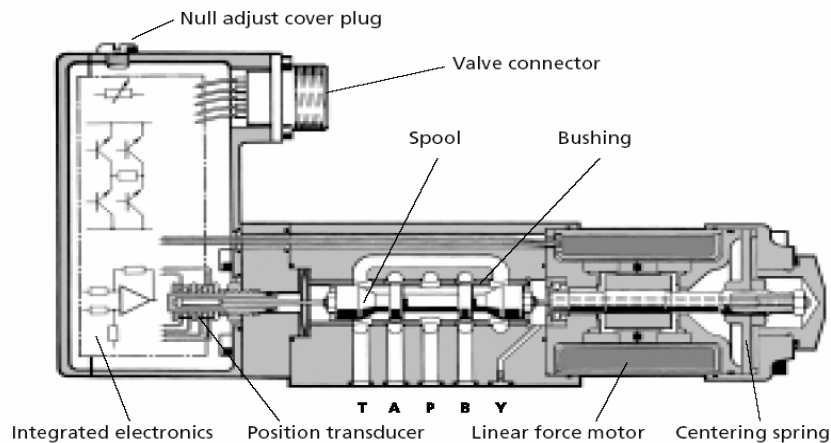


Figure 1-3. Sectional view of a MOOG D633/D634 direct drive servo-proportional control valve

The operation of the system can be explained by taking the case that the nose-side pressure is higher than the back-side pressure. In this case, the back-side part can be regarded as the load side. Assume that a variable displacement pump is used to keep the pressure drop crossing the poppet head constant. When the load is slowing down, the requirement of the metering flow goes down. Therefore the spool valve is required to move to the left side. The opening of the control port that connects the poppet nose side with the control chamber increases. More fluid allows entering the poppet control chamber. More fluid pressure force is produced to break the force balance and push the poppet towards the fixed seat to make the smaller poppet opening. The fluid flowing from the high-pressure supply end to the low-pressure exhaust port decreases. The increasing control chamber in turn contributes to make the control pressure down till it reaches a new equilibrium status with other forces on the poppet. Therefore, when the poppet is reaching the desired position, the control opening becomes to reduce till it is small enough to compensate the leakage exiting the control chamber. When more flow is

needed, the movement of the spool valve is going to be on-the-right-side. The opening of the control port that connects the poppet back side with the control chamber increases. Fluid is allowed to flow from the poppet control chamber to the back-side chamber. Decreasing the fluid pressure force allows the poppet land to move away from the fixed seat to make the bigger poppet opening. Then the poppet is lifted farther from the seat to allow more fluid metering from the high-pressure supply end to the low-pressure exhaust port to provide more energy to endure more loading. The movement of the poppet stops when the control pressure increases to a certain degree to make the new force balance on the poppet. The opening of the control port drops till it is small enough to balance the leakage loss in the control chamber. Note that at any equilibrium point, the spool opening is small and opens to connect the nose side chamber with the control chamber. Pressures acting on the poppet can keep roughly fixed relationships.

### 1.3 Literature Review

#### 1.3.1 Poppet Valve Research

The greatest disadvantage of the poppet valve is that this type of valve often endures self-excited oscillation which is unstable. Therefore many basic works have been focused on poppet stability problems. In the early 1960's, J.A. Stone's work [3] showed that the downstream configuration (e.g., the length and diameter of the chamber) had a strong influence on the system stability. The smaller the chamber is, the higher the flow forces are. The steady-state flow force was mathematically modeled and experimentally shown to roughly match with the theoretical values, though test data were about 20 percent below the theoretical values. Experiments were also carried out on the discharge

coefficient with the changes of the poppet angles and shapes, and poppet flow characteristics with various exhaust conditions that contains different liquids. In 1964, James E. Funk [4] analytically proved that interaction of the fluid delivery line dynamics and the spring mass dynamics of the poppet valve could cause poppet-valve instability. In this work, it is shown that if the valve natural frequency is equal to one of the harmonics of the delivery line, the system will become very unstable. The fluid flows from the upstream volume that contains the spring to the downstream volume that connects with a constant pressure reservoir, which moves in an opposite direction compared to the common use. The effect of the flow force on the poppet dynamics was neglected. The pipeline dynamics that was described by the momentum equation neglecting the viscous force, kinetic energy and the body force was included in the open loop system. A stability criterion that is related to the poppet parameters and the operating conditions was derived. Funk pointed out the valve should be designed to make a quick lift especially at the moment of moving from the fixed seat. After that, many works were carried out based on Funk's model and results. In Kohji Kasai's work [5], a mathematical model was developed for the system which involves the inlet and outlet piping and a theoretical stability criterion was derived by not including outlet piping. Kasai also obtained the relationship of the length of inlet piping, spring rate, inlet pressure, valve lift, valve shape and Reynolds number to describe the range of the disturbance frequency in which instability occurs. In 1972, Wandling and Johnson [6] published a paper that was an extension of Funk' work. More elements including the downstream pipeline, steady-state fluid force and spring-mass effects were added to the model. The poppet valve spring was doubted to be an important factor of the higher-frequency system stability. The coupling

effects between the downstream and upstream delivery lines were verified to be negative influences on the system stability. Brian Roberts [7] presented a system that contains four poppet valves controlled by pilot directional valves to fulfill elaborate flow control functions in 1988. A full account of the abundant and distinct benefits of this system is given in his work. In 1991, Johnson and Edge [8] conducted a series of experiments to explore the flow coefficients and steady-state flow force for poppet and disc valves with different geometries under the assumption that there are no cavitations in the chambers and the fluid has a high Reynolds number property (greater than 2500). A conclusion was drawn from their research that the flow force is an undesirable factor leading to the instability problems for the flow control of poppet. And especially at the small opening, the fluid characteristics of the poppet and disc valves with angled seats has much more intense relationship with the reattachment of the flow jet to the valve seat than that of those with sharp-edged seats. The above reattachment leads to the higher flow coefficient, which appears as the pressure drop across the poppet opening increases. A computational method was used in the work of Kazumi Ito, Koji Takahashi and Kiyoshi Inou [9] to apply to the steady, axisymmetric, laminar flow in a poppet without consideration of fluid compressibility in 1993. The numerical results of pressure distribution that tallied closely with the measured ones showed that the pressure on the body wall of a poppet with diverge fluid jet drops promptly with the poppet restriction as Reynolds number increases or valve displacement decreases.

So far, although many studies have been carried out on one-stage poppet valves as relief valves, there is relatively little effort in the literature on the two-stage poppet valve systems. In 1991, Yung C. Shin's work [10] mathematically modeled and experimentally

analyzed the stability of a two-stage pilot relief valve system that comprises two poppet valves based on neglecting the transient flow force. Factors affecting the stability most were discussed to improve the dynamic characteristic of the valve. A two-stage electro-hydraulic flow control valve system, called a “Valvistor” was investigated by Rong Zhang [11] in 2002. Both the five-state nonlinear model and the four-state second-order linear model were presented to examine the validation of the model and to address the performance limitations that are the outcome of the physical structure of the valve system. This work showed that two inherent zeros in the open-loop transfer function, even though one of them might be cancelled by the low frequency pole, might bring a significant limitation on the closed-loop bandwidth. Du [1] in 2002, presented his work about an E/H (electro-hydraulic) poppet system that has the very similar physical structure with the system in this dissertation. He derived a nonlinear controller for flow control in both directions with certain limitations on the pressure difference between the input and output ports as the flow is reversed. The work done in this dissertation is an extension of Du’s study. There are six main differences between them as follows. Firstly, the structure difference is that Du did not consider any downstream or upstream condition. Here a fixed area orifice and a fluid reservoir with a constant pressure are chosen as back-side pipeline components to constitute the poppet valve system. The spool dynamics is ignored in this research by using a spool with a very fast response. However, the back-side pipeline is an important part of system modeling here. Secondly, Du presented a nonlinear system, while this study contains both nonlinear and linear models. The linear models can help the engineers to understand the system more and to get the basic restrictions of gains in PI control and nonlinear control. Thirdly, a complete linear flow



force that includes the steady and transient flow forces caused by both random and ordered motions of the flow across the poppet opening is derived in this work. The time-rate-change of pressures  $P_2$  was not taken into consideration by Du in the transient flow force. The steady-state flow force in Du's paper was in nonlinear formation, which is hard to be investigated. Fourthly, besides nonlinear control that is the only control approach in Du's paper, three other control methods are used in this work: modified PI control, LQG control and  $H_\infty$  control, though there are some limitations of them. Fifthly, even for the nonlinear control, one integral item of the poppet displacement error is added to the nonlinear controller to cancel the steady-state error in this work. And the system is proved to be globally asymptotically stable by Lyapunov theorem, which was not done by Du. The last difference is that the design in this work is checked by tracking a sine wave of 10 HZ, instead of 2 HZ frequency. Patrick Opdenbosch [12] at the Georgia Institute of Technology made a study on a two-stage poppet valve system with a Nodal Link Perceptron Network (NLPN) control scheme in 2004. A nonlinear analytical model was derived to describe the dynamic behavior of the poppet. It was noticed that the flow forces were treated as disturbances and the flow coefficient for the orifice flow passages were experimentally obtained from the steady-state flow, which might not tally with the real conditions.

All research mentioned above has the same assumption that the poppet moves exactly along its symmetrical central line, i.e. the transverse flow force and torsion moment on the poppet are negligible. Hayashi [13] pointed out in his review that T. Maeda demonstrated that the momentum change of the unsteady flow around the poppet can induce to the appearance of the self-excited oscillation. He also made a claim that the

source of this instability comes from the internal flow dynamic that the poppet suffers, instead of coupling effects caused by the interaction between the poppet and other line components.

### 1.3.2 Automatic Control History

Generally speaking, the evolution history of automatic control can be roughly divided into 3 main periods as follows: pre-classical control period (to 1900), classical control period (1900-1950) and modern control period (1950-present). Actually, the time duration of these periods overlap. Some important review papers, including [14], [15], [16], [17] and [18], are used in presenting this section.

The seeds of automatic feedback control began to sprout about 2000 years ago for the needs of precise measurement of time in the Greek and Arab societies [15]. The first milestone of automatic control history was, in 1788, with the invention of the centrifugal governor that was utilized to control the rotation speeds of a steam engine shaft designed by James Watt. In the mid-1800's, mathematics came upon the stage to be used to analyze the stability of dynamic motions of control systems [15]. In that period, J.V. Poncelet and G.B. Airy implemented differential equations in the discussion of the governor dynamics. However, they could not find the conditions that stable system behavior appears [16]. This problem was solved by J.C. Maxwell when he published the paper titled, "On Governor" [16]. This significant contribution was to show that the system is stable if all roots of its characteristic equation obtained by linearizing the differential equations are located on the left-half plane. In 1874 Edward J. Routh gave the mathematical expression of how to determine system stability, known as the Routh-

Hurwitz stability criteria, which also was independently derived by Adolf Hurwitz in 1895 [15]. The work done by A.M. Lyapunov in 1892 deserved great attention. He studied the behavior of dynamic system expressed by nonlinear differential equations from the view of energy [15]. Lyapunov stability theorems based on the above study provided sufficient conditions for system asymptotic stability that plays a crucial role in nonlinear analysis.

In the classical control period, with development of mass communication and the requirements of World War II, the frequency domain techniques for control design thrived. In 1922, Nicholas Minorsky first used a PID (proportional-integral-derivative) controller in his position control for a ship steering system [15]. A critical achievement of numerical analysis of control system in paper titled “Regeneration Theory”, lately developed to become Nyquist stability criterion, was published by Harry Nyquist in 1932. The concept of phase and gain margins, frequency response plots of a complex function was put forwarded by H.W. Bode in 1940. The work, summarized in the book “Theory of Servomechanisms”, in the Radiation Laboratory in Massachusetts Institute of Technology was highly successful during 1940’s: Nichols chart by N.B. Nichols in 1947, root locus method by W.R. Evan in 1948, and so on [16].

The techniques about the state-space approach and optimal control caught the public’s attention back to time-domain analysis. The work of Richard Bellman from 1948 to 1962 and L.S. Pontryagin around 1960 laid the groundwork for optimal control theory that is an extension of the calculus of variations [16]. The previous one initiated the study of the principle of optimality and dynamics programming, while the latter one formulated his “maximum principle” based on the calculus of variations method. R. Kalman was

noted for his contribution to the linear quadratic regulator (LQR), optimal filtering problem and estimation theory around 1960. His research results achieved a considerable application in time-varying linear systems and multi-input/multi-output (MIMO) systems. The mature exposition of linear quadratic gaussian (LQG) can be found in, [19], [20] and [21]. The first one in 1979 provides a profitable method to adjust the estimated-state-observer controller with the use of Kalman filter to obtain the same system performance as that having a full-state feedback controller. The second one in 1981 stated a practical design procedure of LQG for MIMO systems. The last one in 1986 made a concluding speech on introducing LQG and utilizing the particular skills when executing it on certain projects. However, LQG has internal shortcomings: the plant mathematics could have a significant discrepancy with the actual one and the forms of disturbance are not limited to be white noises. Therefore, new concepts, such as  $H_2$  and  $H_\infty$  norm, to define the integral quadratic restriction for system performances rose into the engineers' view in the optimal control area. G. Zames, in 1981 [22] and 1983 [23], took consideration into a weighted  $H_\infty$  norm to be a mathematical indication of system behavior and put forward studies of this fresh approach on multivariable systems without right half-plane zeros (RHP), single variable stable systems with a single RHP zero and single variable unstable systems in the servo-industry. The general formulas for systems with a finite number of RHP zeros or poles were also derived. Doyle and Glover [24] made an exposition about how to get all state-space controllers for a standard  $H_2$  or  $H_\infty$  problem by solving two Riccati equations in 1989.

In a general way, the classical control techniques are not manageable ways to deal with the control problems of the MIMO systems. However modern control techniques

display their advantages with the fact that they basically are time-domain methods that use space-state models to describe system behaviors for both MIMO systems and single-input/single-output (SISO) systems.

The development of nonlinear control technology was not as flourishing as that of linear control methodology. However, several useful theoretical approaches were uncovered as follows: phase plane, describing function, feedback linearization, sliding control and adaptive control, and so on. These topics can be found in books [25], [26], [27]. In 1996 Atherton [18] investigated the achievement of nonlinear control from its very first beginning to approximately 1960. In Astrom's journal paper [28] of 1996, the important productions of adaptive control from the mid-1950s to the mid-1960s were presented.

Some advanced control methods have been applied to hydraulic systems. An adaptive robust control (ARC) was presented in Yao's work [29] of 2001. A discontinuous projection based ARC controller is created to provide the high performance robust motion control of electro-hydraulic servo-systems driven by double-rod hydraulic actuators with the consideration of parameter uncertainty and certain non-linearity uncertainty.  $H_2/H_\infty$  MIMO controllers were developed to electronically coordinate the power distribution for an earthmoving vehicle's powertrain transmission in Zhang's paper [30]. The  $H_\infty$  controller exhibits better nominal performance and robust performance than the  $H_2$  controller, which is represented by that the system with the  $H_\infty$  controller demonstrates quicker response, wider tracking range and better disturbance rejection. Fales [31] used a LQG controller in a wheel loader control system to achieve the motion control for the bucket leveling.

## 1.4 Thesis Objective and Organization

The objective of this work is to develop mathematical models, stability criteria and control designs for a two-stage metering poppet valve system that may be used in a valve stack to create an independent metering function for the hydraulic system (shown in Figure 1-2). The poppet system is asked to have the ability to meter a certain amount of flow that can take the required load under given working conditions. Since it is assumed that the nominal nose-side pressure  $P_1$ , the nominal back-side pressure  $P_{2d}$  and the nominal piping pressure  $P_k$  are known, this task becomes to make the poppet move to the desirable position when the spool actuator is operated according to the desirable command which is obtained from the load and system information. The poppet must respond quickly enough with the acceptable steady-state error to track a 10 HZ sine wave that is a reference poppet displacement. The steady-state error must be less than 10% of the desired poppet displacement. In practice, if a poppet can exhibit a frequency response of 5 HZ or 6 HZ, it is quick enough to meet the flow metering requirement in the hydraulic circuit. However, according to engineer's experience, when the controller is applied to the real physical system, the response speed of a hydraulic component, for example a poppet valve, usually slows down to about 50% of the one in simulation. The phase lag can not be bigger than 90 degree for this research. The settling time of about 30 ms for the step response is a goal for the speed of response.

This study begins by formulating the mathematical models that are basically third-order systems, including linear and nonlinear expressions, for this two-stage open-loop poppet-valve system. Using non-dimension analysis, the poppet inertia and the

influence of the change of control pressure in the back-side chamber are neglected to produce a reduced-order analytical form that is a second-order linear system. In Chapter 3, four control methods are applied to accomplish the closed-loop systems: modified PI control, LQG control,  $H_\infty$  control and nonlinear feedback control. The first three ones are not only implemented on linear systems, but also verified by being combined with the nonlinear models. The last one is specially assigned to the nonlinear system. Stability criteria and the ranges of control gains for the reduced-order linear closed-loop system with the PI controller are solved according to the Routh-Hurwitz method. The nonlinear system with the nonlinear controller is proved to have globally asymptotical stability. In the simulation Chapter 4, discussions are focused on how key parameters affect the system stability behavior by measuring their costs to the open-loop stability criteria. Nominal system pressures (nose-side pressure  $P_1$  and back-side pressure  $P_{2d}$ ), leak coefficients, system structure geometries (back-side volume  $V_L$  and the ratio of the poppet land area and the nose-side port area  $rA_c$ ), fluid properties (fluid bulk modulus  $\beta$  and orifice coefficient  $C_d$ ) and spring rate  $k$  are taken into consideration in this investigation. The system is simulated to examine its regulating and tracking ability of the desired poppet displacement. The reference poppet displacement of the step response is given to investigate the system regulation ability, while the desired poppet displacement of the sine wave with 10 HZ frequency is used for the tracking problem. Simulink results are discussed and compared for the two groups of closed-loop systems. The first group includes the full-model linear system with the modified PI controller, the reduced-order linear system with the modified PI controller, the full-model linear system with the LQG controller, the full-model linear system with the  $H_\infty$  controller and the

nonlinear system with the nonlinear controller. The second group contains the nonlinear system with the modified PI controller, the nonlinear system with the LQG controller, the nonlinear system with the  $H_\infty$  controller and the nonlinear system with the nonlinear controller. Subsequently, Chapter 5 states the finding conclusions and contributions of this work to the metering poppet system. Finally, Chapter 6 suggests possible work that can be done in future.



## CHAPTER 2. SYSTEM MODELING

### 2.1 Introduction

In this chapter, mathematical models are set up for describing main dynamic behaviors of the primary mechanical components within this two-stage metering poppet-valve system. The governing equations for the nonlinear and linear open-loop systems with 3 states are obtained. The second-order reduced-order linear open-loop system is derived from non-dimension analysis by neglecting the poppet inertia and the control pressure effect in the back-side chamber. The flow across the poppet orifice can move in two directions. Therefore, all linear analysis includes two cases: the nominal nose-side pressure of the poppet  $P_1$  is higher than the nominal back-side pressure of the poppet  $P_{2d}$  that is higher than the nominal load pressure  $P_k$ , i.e.  $P_1 > P_{2d} > P_k$ , and the nominal nose-side pressure of the poppet  $P_1$  is lower than the nominal back-side pressure of the poppet  $P_{2d}$  that is also lower than the nominal load pressure  $P_k$ , i.e.  $P_1 < P_{2d} < P_k$ . The linearization can not be performed when  $P_1$  is equal to  $P_{2d}$ , or  $P_{2d}$  is equal to  $P_k$ , because these differences of pressures will appear in the denominators of the flow gains. In the nonlinear model, the flow force is still treated as a linear force as well as that in the linear model. The model continuity may be guaranteed by adding saturation components in the simulation.

## 2.2 Poppet Analysis

Figure 2-1 shows the free-body diagram of the poppet valve. The following discussion assumes that the poppet only moves in the axial direction. The deviation from the center symmetrical position due to unsteady transverse flow force is ignored [2]. In practice, the rotating movement of the poppet can produce the small moment according to its central axis.

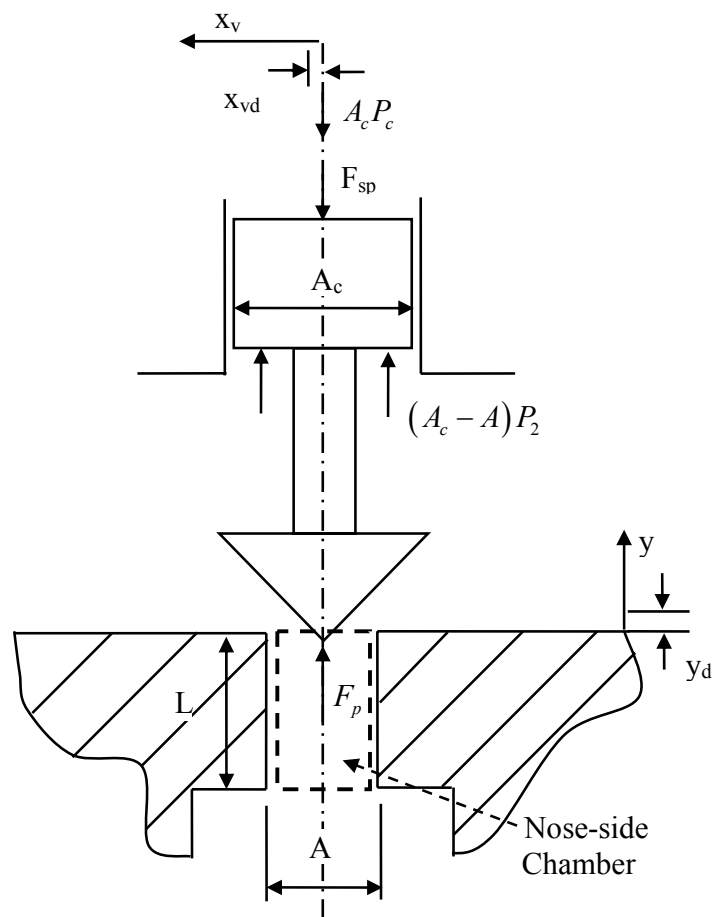


Figure 2-1. Forces acting on the poppet

The forces acting on the poppet come from four sources: the poppet-valve spring force  $F_{sp}$ , the control pressure force acting on the top face of the poppet land  $A_c P_c$ , the back-side pressure force  $(A_c - A)P_2$ , and the resultant flow force produced by the fluid passage across the nose-side chamber  $F_p$ . It is assumed that pressure forces act evenly on the contacting faces. Here, they are treated as concentrated forces that act on the centers of the faces. In this research, the nose-side pressure  $P_1$  is held constant by the variable displacement pump. It may be summarized that the forces on the poppet valve in the  $y$ -direction and set them equal to the valve's time rate of change of linear momentum to produce the following equation of motion for the poppet valve.

$$m\ddot{y} + c\dot{y} = F_p + (A_c - A)P_2 - A_c P_c - (F_{sp} + F_{spd}), \quad (2.1)$$

where  $y$  is the instantaneous vertical displacement referenced from the poppet seat (See Figure 2-1),  $P_c$  is the instantaneous control pressure acting on the top-side cross section of the poppet land,  $F_{sp}$  is the instantaneous spring force and  $F_{spd}$  is the nominal spring force on the poppet, which is chosen as zero. It will be reasonably illustrated in the next section that the force  $F_p$  includes the static pressure force on the poppet nose side  $AP_1$  produced by the random motion (diffusion) of molecules of the flow and the flow force  $F_f$  yielded by the ordered motion (convection) of the flow that introduces the linear momentum change of the flow passage across the poppet opening. The following equation maybe used to depict the flow force  $F_p$

$$F_p = AP_1 + F_f. \quad (2.2)$$

The following equation is used to describe the spring force when the poppet valve is at location  $y$

$$F_{sp} = ky, \quad (2.3)$$

where  $k$  is the spring rate. In this analysis, the spring force is so small that it can be considered to be zero. However, for the completeness of the analysis, it is included in this derivative process. Substituting Equation (2.3) into Equation (2.1) produces

$$m\ddot{y} + c\dot{y} + ky = F_p - AP_2 + A_c(P_2 - P_c). \quad (2.4)$$

### 2.2.1 Poppet Valve Flow Force

It is necessary to understand the detailed information of the poppet valve flow force  $F_p$  to complete Equation (2.4). The Navier-Stokes Equations are given in vector form to describe the force balance of the fluid in the given deformable nose-side control volume as follows [32]

$$\rho \left\{ \frac{\partial \vec{u}}{\partial t} + (\vec{u} \cdot \nabla) \vec{u} - \vec{f} \right\} = -\nabla p + \mu \nabla^2 \vec{u}, \quad (2.5)$$

where  $\rho$  is the fluid density,  $\vec{u}$  is the fluid velocity vector,  $\nabla$  is the gradient operator, and  $\nabla^2$  is the Laplacian operator,  $\vec{f}$  is the body force vector,  $\nabla p$  is the gradient of the fluid pressure and  $\mu$  is the fluid viscosity.

In absence of the body forces and viscosity effect, and considering that all vectors change only in  $y_1$  direction (shown in Figure 2-2), Navier-Stokes Equations can be simplified to

$$\rho \left\{ \frac{\partial \vec{u}_{y_1}}{\partial t} + (\vec{u}_{y_1} \cdot \nabla) \vec{u}_{y_1} \right\} = -\nabla p_{y_1}. \quad (2.6)$$

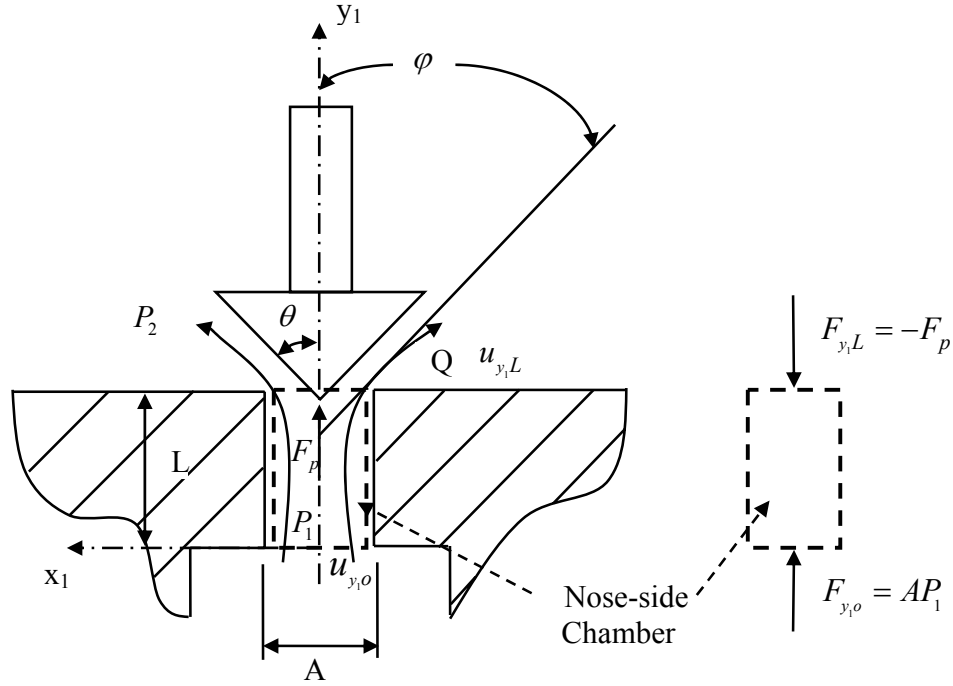


Figure 2-2. Poppet nose-side control volume for calculating the poppet flow force

The horizontal flow force which is perpendicular to the symmetrical line of the poppet is small enough to be neglected. The following force-balance equation within the poppet nose-side chamber is given by calculating the volume integral of the above equation

$$\int_{c.v.} \rho \frac{\partial \vec{u}_{y_1}}{\partial t} dV_m + \int_{c.v.} \rho \vec{u}_{y_1} \cdot \frac{\partial \vec{u}_{y_1}}{\partial y_1} dV_m = - \int_{c.v.} \frac{\partial p_{y_1}}{\partial y_1} dV_m, \quad (2.7)$$

where  $V_m = A_m y_1$  is the changeable nose-side control volume *c.v.* that is shown in Figure 2-2 with the maximum length  $L$ ,  $A_m = A$  is the cross-section area of a control volume

boundary surface *c.s.* and subscript  $y_1$  represents the sub-vectors in  $y_1$  direction. In this case, the Equation (2.7) can be rewritten as

$$\frac{\partial}{\partial t} \int_0^L \rho Q dy_1 + \int_{u_{y_1o}}^{u_{y_1L}} \rho Q d\vec{u}_{y_1} = - \int_{P_{y_1o}}^{P_{y_1L}} A_m dP_{y_1}, \quad (2.8)$$

where  $u_{y_1o} = \frac{Q}{A}$  is the fluid entering velocity,  $u_{y_1L} = \frac{Q}{A_p} \cos(\varphi)$  is the vertical vector of the fluid exiting velocity,  $Q$  is the main flow across the poppet opening,  $A_p$  is the instantaneous poppet opening area that is the function of poppet displacement  $y$  and the valve conical angle  $\theta$ ,  $A$  is the poppet inlet area,  $\varphi$  is the jet angle of the fluid flowing out of the poppet valve,  $P_{y_1o} = P_1$  and  $P_{y_1L}$  are the corresponding pressures related to the boundary condition of the control volume. The following equation can be obtained by evaluating the integral in Equation (2.8)

$$\rho L \frac{\partial Q}{\partial t} + \rho Q (u_{y_1L} - u_{y_1o}) = F_{y_1L} + AP_1, \quad (2.9)$$

where  $F_{y_1o} = AP_1$  is the pressure force acting on the bottom surface of the control volume,  $F_{y_1L} = -F_p$  is the resultant force acting on the top surface of the control volume by the poppet head. Then the following equation is summarized to depict the flow force on the top surface of the nose-side volume

$$F_{y_1L} = -AP_1 + \rho L \frac{\partial Q}{\partial t} + \rho Q^2 \left( \frac{\cos(\varphi)}{A_p} - \frac{1}{A} \right). \quad (2.10)$$

Subsequently, the flow force acting on the poppet head which is the counterforce of  $F_{y1L}$  may be represented as follows

$$F_p = -F_{y1L} = AP_1 - \rho L \frac{\partial Q}{\partial t} - \rho Q^2 \left( \frac{\cos(\varphi)}{A_p} - \frac{1}{A} \right). \quad (2.11)$$

The poppet instantaneous discharge area  $A_p$  is a nonlinear area which can be demonstrated by the following equation

$$A_p = \pi [Dy \sin(\theta) - y^2 \cos(\theta) \sin^2(\theta)], \quad (2.12)$$

where  $D$  is the diameter of the poppet nose-side inlet. A linear form of the above equation can be given by

$$A_p = \pi D y \sin(\theta) \quad (2.13)$$

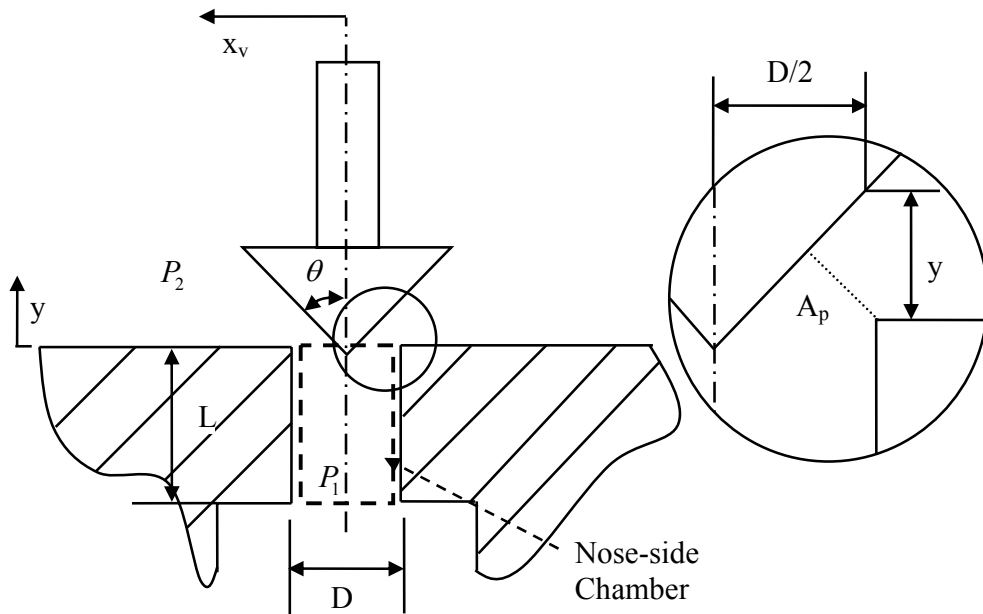


Figure 2-3. Poppet instantaneous discharging area

Therefore, the following scalar equation can be given to approximately describe the flow force acting on the poppet due to the change of the fluid momentum

$$F_f = -F_{ft} - F_{fs} = -\rho L \frac{\partial Q}{\partial t} - \rho Q^2 \left( \frac{\cos(\varphi)}{A_p} - \frac{1}{A} \right), \quad (2.14)$$

$$F_{ft} = \rho L \frac{\partial Q}{\partial t}, \quad (2.15)$$

$$F_{fs} = \rho Q^2 \left( \frac{\cos(\varphi)}{A_p} - \frac{1}{A} \right), \quad (2.16)$$

where  $F_{ft}$  is the transient flow force that may work to either open or close the valve which depends on the sign of  $\frac{\partial Q}{\partial t}$ , and  $F_{fs}$  is the steady flow force that always works to try to close the valve. There is an assumption for simplification of this problem that the jet angle  $\varphi$  is equal to the valve conical angle  $\theta$ .

The classical orifice equation [32] is used to describe the volumetric flow rate  $Q$  that goes through the small opening between the poppet head and the seat. This equation assumes that the fluid through the orifice is a steady, incompressible, high Reynolds number flow. It can be given by

$$Q = A_p C_d \sqrt{\frac{2}{\rho} |P_1 - P_2| \text{sign}(P_1 - P_2)}, \quad (2.17)$$

where  $C_d$  is the discharge coefficient that is usually obtained from experiments,  $\Delta P = P_1 - P_2$  is the instantaneous pressure drop across the poppet head,  $P_1$  is the constant



pressure in the nose-side chamber,  $P_2$  is the instantaneous pressure in the back-side chamber. The following equation can be defined by

$$\text{sign}(P_1 - P_2) = \begin{cases} 1 & P_1 > P_2 \\ 0 & P_1 = P_2 \\ -1 & P_1 < P_2 \end{cases} \quad (2.18)$$

The linearized orifice equation may be derived according to the nominal conditions as follows by using Taylor series expansion and neglecting the high-order items

$$Q = Q_d + \left( \frac{\partial Q}{\partial A_p} \frac{\partial A_p}{\partial y} \right)_d (y - y_d) + \left( \frac{\partial Q}{\partial (P_1 - P_2)} \right)_d [(P_1 - P_2) - (P_1 - P_{2d})], \quad (2.19)$$

where  $Q_d$  is the nominal flow rate across the poppet,  $\Delta y = y - y_d$  is the axial displacement derivation of the poppet from the nominal position, and  $\Delta P_d = P_1 - P_{2d}$  is the nominal pressure drop. The subscript “ $d$ ” is used to identify the nominal operation conditions of the system. It is needed to be noted that the linear expressions from Taylor series method are only valid when the derivations are not too far from the nominal conditions. And the linearization can not be performed when the desired back-side pressure  $P_{2d}$  is equal to the desired nose-side pressure  $P_1$ , because the pressure drop  $P_1 - P_{2d}$  appears in the denominator of  $K_{qt}, K_c$  known as the flow gain and the flow-pressure coefficient respectively [32] that will be defined later. Then this introduces the infinite values of the flow gains that are not acceptable. The flow gains can be derived as follows

$$K_{qt} = \left( \frac{\partial Q}{\partial A_p} \frac{\partial A_p}{\partial y} \right)_d = \pi DC_d \sin(\theta) \sqrt{\frac{2|P_1 - P_{2d}|}{\rho}} \text{sign}(P_1 - P_{2d}), \quad (2.20)$$

$$K_c = \left( \frac{\partial Q}{\partial (P_1 - P_2)} \right)_d = \frac{\pi D C_d y_d \sin(\theta)}{\sqrt{2\rho |P_1 - P_{2d}|}}. \quad (2.21)$$

By substituting Equations (2.20) and (2.21) into Equation (2.19) and rearranging items, the linearized form of the main flow  $Q$  can be given by

$$\begin{aligned} Q &= \frac{1}{2} Q_d + K_{qt} (y - y_d) + K_c (P_1 - P_2) \\ &= K_{qt} y - K_c (P_2 - P_{2d}) \end{aligned} \quad (2.22)$$

It is assumed that the time rate of change of the desired vectors is considered as zero. By substituting Equation (2.22) into Equation (2.15) and differentiate the main poppet flow  $Q$  with respect to time  $t$ , the transient flow force,  $F_{ft}$  can be linearly represented by

$$F_{ft} = \rho L K_{qt} \dot{y} - \rho L K_c \dot{P}_2. \quad (2.23)$$

Similarly, by using Taylor series expansion and neglecting the high-order items, the linearized form of the steady flow force  $F_{fs}$  can be represented by

$$F_{fs} = F_{fsd} + \left( \frac{\partial F_{fs}}{\partial A_p} \frac{\partial A_p}{\partial y} \right)_d (y - y_d) + \left( \frac{\partial F_{fs}}{\partial (P_1 - P_2)} \right)_d [(P_1 - P_2) - (P_1 - P_{2d})]. \quad (2.24)$$

where  $F_{fsd}$  is the nominal steady flow force.  $K_{fq}$  and  $K_{fct}$  [32] known as the flow force gain and the flow force pressure coefficient can be respectively given by

$$K_{fq} = \left( \frac{\partial F_{fs}}{\partial A_p} \frac{\partial A_p}{\partial y} \right)_d = \pi D C_d^2 \sin(2\theta) |P_1 - P_{2d}| - \frac{4\pi^2 D^2 C_d^2 \sin^2(\theta)}{A} y_d^2 |P_1 - P_{2d}|, \quad (2.25)$$

$$K_{fct} = \left( \frac{\partial F_{fs}}{\partial \Delta P} \right)_d = \left( \pi D C_d^2 \sin(2\theta) y_d - \frac{2\pi^2 D^2 C_d^2 \sin^2(\theta)}{A} y_d^2 \right) \text{sign}(P_1 - P_{2d}). \quad (2.26)$$

By substituting Equations (2.25) and (2.26) into Equation (2.24) and rearranging items, the linearized form of the steady flow force  $F_{fs}$  can be given by

$$F_{fs} = K_{fq} (y - y_d) + K_{fct} (P_1 - P_2). \quad (2.27)$$

By substituting Equations (2.23) and (2.27) into Equation (2.14), the linearized form of the flow force acting on the poppet due to the linear momentum change may be given by

$$F_f = \rho L K_{qt} \dot{y} - \rho L K_c \dot{P}_2 + K_{fq} (y - y_d) + K_{fct} (P_1 - P_2). \quad (2.28)$$

<sup>1</sup>Consequently, the linearized form of the flow force acting on the poppet may be demonstrated by

$$F_p = A P_1 - \rho L K_{qt} \dot{y} + \rho L K_c \dot{P}_2 - K_{fq} (y - y_d) - K_{fct} (P_1 - P_2). \quad (2.29)$$

Substituting Equation (2.29) into Equation (2.4) and rearranging terms produce the following motion equation of the poppet

$$m\ddot{y} + (c + \rho L K_{qt}) \dot{y} + (k + K_{fq}) y - K_{fq} y_d = (A - K_{fct}) P_1 + (A_c - A + K_{fct}) P_2 - A_c P_c + \rho L K_c \dot{P}_2. \quad (2.30)$$

## 2.2.2 Nominal Conditions

Under the steady-state conditions, the following equation can be used to describe the equilibrium of the poppet

---

<sup>1</sup> In the nonlinear model, the flow force is still treated as a linear force. The model continuity may be guaranteed by adding saturation components in simulation.

$$(A - K_{fct})P_1 = ky_d - (A_c - A + K_{fct})P_{2d} + A_c P_{cd}. \quad (2.31)$$

The desired control pressure can be derived from the above equation as follows

$$P_{cd} = \frac{(A - K_{fct})P_1 + (A_c - A + K_{fct})P_{2d} - ky_d}{A_c}. \quad (2.32)$$

The following equations are also given to describe the pressure relationships that control the poppet static behavior under the steady-state conditions

$$P_1 - P_{cd} = \frac{A_c - A + K_{fct}}{A_c}(P_1 - P_{2d}) + \frac{ky_d}{A_c}, \quad (2.33)$$

$$P_{cd} - P_{2d} = \frac{A - K_{fct}}{A_c}(P_1 - P_{2d}) - \frac{ky_d}{A_c}. \quad (2.34)$$

Note that the nominal conditions in which nose-side pressure  $P_1$  is equal to nominal back-side pressure  $P_{2d}$  are not involved in this analysis.

### 2.2.3 Equation of Motion for the Poppet Valve

Two different forms of the motion equation of the poppet valve are respectively used in the nonlinear system, in which the flow rates keep their nonlinear expressions, and the linear systems that do not contain any nonlinear item. The following equation is employed to describe the poppet dynamic behavior in the nonlinear system

$$m\ddot{y} + (c + \rho LK_{qt})\dot{y} + (k + K_{fq})y - K_{fq}y_d = (A - K_{fct})P_1 + (A_c - A + K_{fct})P_2 - A_c P_c + \rho LK_c \dot{P}_2. \quad (2.35)$$

By substituting Equation (2.31) into Equation (2.4) and rearranging the items, the following equation of motion of the poppet valve is given to express the poppet dynamic behavior in the linear systems

$$m\ddot{y} + (c + \rho LK_{qt})\dot{y} + (k + K_{fq})(y - y_d) = \rho LK_c \dot{P}_2 + (A_c - A + K_{fct})(P_2 - P_{2d}) - A_c(P_c - P_{cd}) \quad (2.36)$$

### 2.3 Back-side Pressure Analysis

The main objective of this work is to investigate the system stability behavior for the two-stage metering poppet valve design under various working load conditions. The simple back-side conditions are selected to include the back-side volume of the poppet house, a fixed-area orifice and a constant pressure reservoir. The following pressure rise-rate equation within the varying control volume is used to describe the fluid characteristics in the back-side chamber

$$\frac{V_L}{\beta} \dot{P}_2 = Q + Q_2 - Q_L - KP_2 - Q_c \delta P_c - \dot{V}_L, \quad (2.37)$$

where  $\beta$  is the flow bulk modulus,  $V_L$  is the back-side chamber volume,  $\dot{V}_L$  is the time-rate-of-change of the back-side volume that is so small that can be negligible,  $Q_2$  is the leakage from the control chamber to the back-side chamber through the gap between the poppet land and the hole that contains the poppet land due to pressure difference between the control pressure  $P_c$  and the load pressure  $P_2$ ,  $Q_L$  is the flow rate from the back-side chamber to the reservoir which has a constant pressure,  $Q_c$  is the flow rate entering or exiting the control chamber due to the pressure difference between the control pressure

and the pressure at the other side of the spool opening and  $K$  is the total leakage coefficient for the piping connecting the back-side chamber and the reservoir.

It is assumed that the pressure and fluid density within the back-side chamber is uniform throughout. That is, the fluid filling this chamber is homogeneous undergoing hydrostatic pressurization. There is an assumption that the piping leakage is proportional to the back-side pressure, which describes a low Reynolds number flow. The flow rate  $Q_c$  shows up in the back-side pressure equation only when the spool has a left-side opening. Note that the leakage that occurs between the spool land and the hole that contains it from the control chamber to the back-side chamber or the pump-side piping, or versus is so small that it is neglected. Then, the following equation of back-side pressure is obtained by

$$\frac{V_L}{\beta} \dot{P}_2 = Q + Q_2 - Q_L - KP_2 - Q_c \delta P_c \quad (2.38)$$

where

$$\delta P_c = \begin{cases} 0 & x_v \geq 0 \\ 1 & x_v < 0 \end{cases} \quad (2.39)$$

The left side of the above equation is the volume change of the back-side chamber due to the compressible flow in terms of time. The flow rates on its right side are caused by flows either entering or exiting the back-side chamber due to its pressure drop effect. The volume change of the back-side chamber due to boundary change is so small to be neglected.

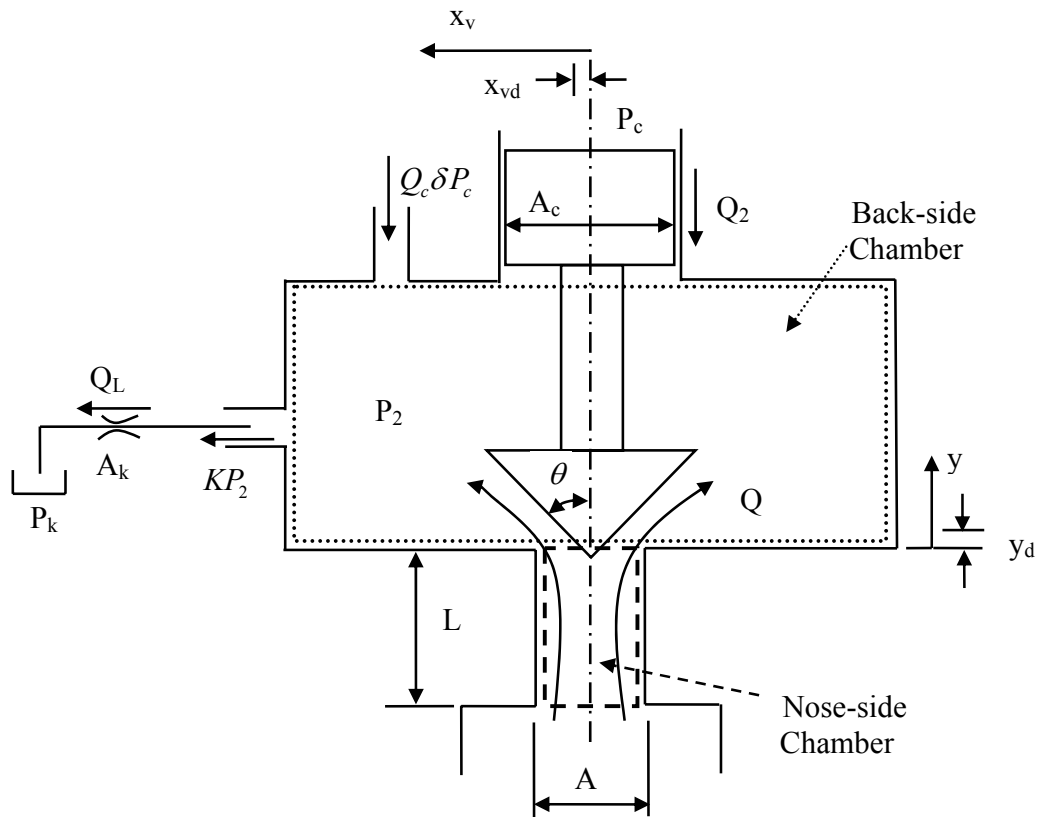


Figure 2-4. Flows entering or exiting the back-side chamber

### 2.3.1 Flow Rates in Back-side Chamber

Equations (2.17) and (2.22) can be respectively utilized as the nonlinear mathematical expression and linear mathematical expression for the flow rate  $Q$  across the poppet main opening.

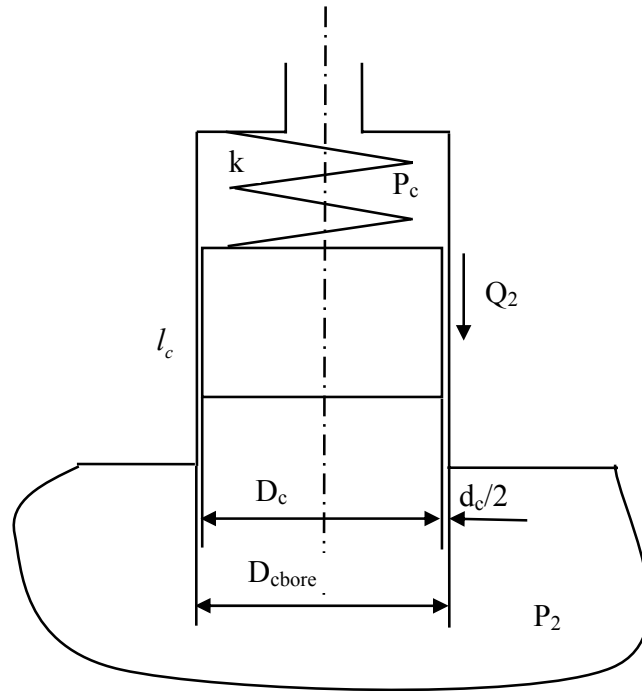


Figure 2-5. Leakage between the poppet land and its containing bore

The following equation is used to describe the leakage  $Q_2$

$$Q_2 = K_2 (P_c - P_2), \quad (2.40)$$

where  $K_2$  is the leakage coefficient of the leakage between the poppet land and the hole that contains it due to the pressure drop between the control chamber and the back-side chamber. This leakage can be considered as an annular leakage between the round substance and outside tube that contains it (See Figures 2-5). Therefore, the classical annular leakage equation is used to explicitly describe it. The circular flow passage here is assumed as a Poiseuille flow in which the viscous shear force is the dominating effect. Consequently, the following equation [52] based on Poiseuille flow can be used to describe leakage coefficients by considering the worst eccentricity cases when  $\varepsilon=1$



$$K_2 = \frac{\left(1 + \frac{3}{2}\varepsilon^2\right)\pi D_{cbore} d_c^2}{96\mu l_c} = \frac{5\pi D_{cbore} d_c^2}{192\mu l_c}, \quad \varepsilon=1, \quad (2.41)$$

where  $D_{cbore}$  is the diameter of the hole that holds the poppet land,  $d_c$  is the diameter clearance between the poppet land and the hole that contains it,  $l_c$  is the metering length of the poppet land,  $\mu$  is the fluid viscosity and  $\varepsilon$  is the eccentricity ratio. It can be defined as

$$\varepsilon = \frac{e}{h_o}, \quad (2.42)$$

where  $e$  is the eccentricity dimension between the center of the inside cylinder and the center of the outside tube,  $h_o$  is the clearance of the circular walls between the inside insert and the outside tube. It is assumed that the metering length of the poppet land  $l_c$  is kept as constant.

The load flow  $Q_L$  is expressed by classical orifice equation considering to the small fixed-area orifice in the back-side piping channel as follows

$$Q_L = A_k C_d \sqrt{\frac{2}{\rho} |P_2 - P_k| \text{sign}(P_2 - P_k)}, \quad (2.43)$$

where  $P_k$  is a constant pressure representing the fictitious working environment. The linearized piping flow rate may be derived according to the nominal conditions as follows by using Taylor series expansion and neglecting the high-order items

$$Q_L = Q_{Ld} + \left( \frac{\partial Q}{\partial (P_2 - P_k)} \right)_d [(P_2 - P_k) - (P_2d - P_k)], \quad (2.44)$$

where  $Q_{Ld}$  is the nominal piping flow rate across the fixed-area orifice from the back-side chamber to the reservoir. Note that the linearization can not be performed when the desired back-side pressure  $P_{2d}$  is equal to the desired load pressure  $P_k$ , because the pressure drop  $P_{2d} - P_k$  appears in the denominator of  $K_{cL}$  known as the flow-pressure coefficient of the back-side pipeline flow that will be defined later. Then this introduces the infinite values of the flow gains that are not acceptable. The dynamics of the pipeline is neglected in this study. The load flow-pressure gains can be derived as follows

$$K_{cL} = \left( \frac{\partial Q_L}{\partial (P_2 - P_k)} \right)_d \text{sign}(P_{2d} - P_k) = \frac{A_k C_d}{\sqrt{2\rho |P_{2d} - P_k|}}. \quad (2.45)$$

By substituting Equation (2.45) into Equation (2.44) and rearranging items, the following load flow rate equation might be given by

$$Q_L = \frac{1}{2} Q_{Ld} + K_{cL} (P_2 - P_k) = K_{cL} (P_{2d} - P_k) + K_{cL} (P_2 - P_k). \quad (2.46)$$

The spool can only travel from -1mm to 1mm in the channel, which leads to a small opening orifice. Therefore, the control flow  $Q_c$  can be expressed by classical orifice equation as follows

$$Q_c = hx_v C_d \sqrt{\frac{2}{\rho} |\delta P|} \text{sign}(\delta P), \quad (2.47)$$

where  $x_v$  is the instantaneous spool displacement,  $h$  is the rectangular height, and

$$\delta P = \begin{cases} P_1 - P_c & x_v \geq 0 \\ P_c - P_2 & x_v < 0 \end{cases}. \quad (2.48)$$

The spool-valve port with rectangular geometry is used and shown in Figure 2-6.  $w$  is the rectangular width. It is clear that the instantaneous discharge opening area  $A_1$  of the spool can be given by

$$A_1 = hx_v \quad \text{and} \quad \frac{\partial A_1}{\partial x} = h \quad (2.49)$$

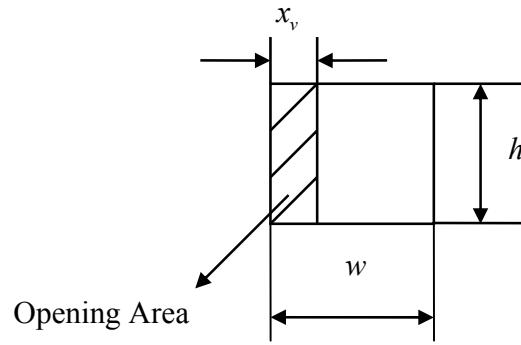


Figure 2-6. Spool valve rectangular port geometry

At the equilibrium position, the control orifice that is formed by the spool land and the control chamber always opens on the right of the poppet symmetrical center line. Therefore, the control flow rate for the linear analysis can be given by

$$Q_c = hx_v C_d \sqrt{\frac{2}{\rho} |P_1 - P_c|} \text{sign}(P_1 - P_c). \quad (2.50)$$

Similar as the linearized orifice Equation (2.19), the following control flow rate equation can be given by utilizing Taylor series method and omitting high-order items

$$Q_c = Q_{cd} + \left( \frac{\partial Q_c}{\partial x_v} \right)_d (x_v - x_{vd}) + \left( \frac{\partial Q_c}{\partial (P_1 - P_c)} \right)_d [(P_1 - P_c) - (P_1 - P_{cd})], \quad (2.51)$$

where  $Q_{cd}$  is the nominal control pressure.  $K_{q1t}, K_{c1}$  known respectively as the control flow force gain and the control flow force pressure coefficient can be given by

$$K_{q1t} = \left( \frac{\partial Q_c}{\partial x_v} \right)_d = hC_d \sqrt{\frac{2|P_1 - P_{cd}|}{\rho}} \text{sign}(P_1 - P_{cd}), \quad (2.52)$$

$$K_{c1} = \left( \frac{\partial Q_c}{\partial (P_1 - P_c)} \right)_d = \frac{hC_d x_{vd}}{\sqrt{2\rho|P_1 - P_{cd}|}}. \quad (2.53)$$

By substituting Equations (2.52) and (2.53) into Equation (2.51) and rearranging items, the linearized form of the steady-state flow force  $F_{fs}$  can be given by

$$\begin{aligned} Q_c &= \frac{1}{2} Q_{cd} + K_{q1t} (x_v - x_{vd}) + K_{c1} (P_1 - P_c) \\ &= K_{q1t} x_v - K_{c1} (P_c - P_{cd}) \end{aligned} \quad (2.54)$$

### 2.3.2 Nominal Conditions

Under the steady-state conditions, the nonlinear expressions of the nominal poppet main flow rate and the nominal pipeline flow rate are respectively given by

$$Q_d = Dy_d C_d \sin(\theta) \sqrt{\frac{2}{\rho} |P_1 - P_{2d}|} \text{sign}(P_1 - P_{2d}), \quad (2.55)$$

$$Q_{Ld} = A_k C_d \sqrt{\frac{2}{\rho} |P_{2d} - P_k|} \text{sign}(P_{2d} - P_k). \quad (2.56)$$

Also, the linear expressions of the nominal poppet main flow rate, the nominal pipeline flow rate and the nominal leakage flow rate are respectively given by

$$Q_d = \frac{1}{2} Q_d + K_c (P_1 - P_{2d}) = 2K_c (P_1 - P_{2d}), \quad (2.57)$$

$$Q_{Ld} = \frac{1}{2}Q_{Ld} + K_{cL}(P_{2d} - P_k) = 2K_{cL}(P_{2d} - P_k), \quad (2.58)$$

$$Q_{2d} = K_2(P_{cd} - P_{2d}). \quad (2.59)$$

The steady-state flow rate balance in the back-side chamber can be depicted as

$$Q_d - Q_{Ld} - KP_{2d} + K_2(P_{cd} - P_{2d}) = 0. \quad (2.60)$$

For calculating the nominal poppet displacement, the poppet flow force pressure coefficient  $K_{fct}$  in Equation (2.26) can be simplified by neglecting the high-order item as follows

$$K_{fct} = \pi DC_d^2 \sin(2\theta) y_d \text{sign}(P_1 - P_{2d}), \quad (2.61)$$

From Simultaneous Equations (2.32), (2.61), (2.55), (2.56) and (2.60), the following equation of the nominal displacement of the poppet valve can be given by

$$y_d = \frac{A_k C_d \sqrt{\frac{2}{\rho} |P_{2d} - P_k| \text{sign}(P_{2d} - P_k) - \frac{K_2 A}{A_c} (P_1 - P_{2d}) + KP_{2d}}}{\pi DC_d \sin(\theta) \sqrt{\frac{2}{\rho} |P_1 - P_{2d}| \text{sign}(P_1 - P_{2d}) - \frac{K_2}{A_c} \pi DC_d^2 \sin(2\theta) (P_1 - P_{2d}) \text{sign}(P_1 - P_{2d}) - \frac{K_2 k}{A_c}}}. \quad (2.62)$$

This static displacement combining with stable system pressures decides how much flow is metered into or out of the back-side chamber, which represents the poppet responses for corresponding external loads. Note that the nominal condition under the case in which the desired nose-side pressure  $P_1$  is equal to the desired back-side pressure  $P_{2d}$  or/and the desired back-side pressure  $P_{2d}$  is equal to the desired reservoir pressure  $P_k$  is not included in this analysis. Substituting Equations (2.57) and (2.58) into Equation (2.60), and rearranging items produce

$$2K_{cL}(P_{2d} - P_k) = K_{qt}y_d + K_2(P_{cd} - P_{2d}) - KP_{2d}. \quad (2.63)$$

### 2.3.3 Back-side Pressure Equation

Two different forms of the back-side pressure equation are depicted for the nonlinear system and the linear systems. The following equations are employed to represent the back-side chamber fluid characteristics for the nonlinear system

$$\frac{V_L}{\beta} \dot{P}_2 = Q + K_2(P_c - P_2) - Q_L - KP_2 - Q_c \delta P_c, \quad (2.64)$$

$$\delta P_c = \begin{cases} 0 & x \geq 0 \\ 1 & x < 0 \end{cases}, \quad (2.65)$$

$$Q = \pi D y \sin(\theta) C_d \sqrt{\frac{2}{\rho}} |P_1 - P_2| \text{sign}(P_1 - P_2), \quad (2.66)$$

$$Q_L = A_k C_d \sqrt{\frac{2}{\rho}} |P_2 - P_k| \text{sign}(P_2 - P_k), \quad (2.67)$$

$$Q_c = h x_v C_d \sqrt{\frac{2}{\rho}} |\delta P| \text{sign}(\delta P), \quad (2.68)$$

$$\delta P = \begin{cases} P_1 - P_c & x_v \geq 0 \\ P_c - P_2 & x_v < 0 \end{cases}. \quad (2.69)$$

The following analysis is carried out for linear systems. Flow rate  $Q_c$  is not considered in linear analysis, because linearization is carried out only at equilibrium position. No matter the back-side pressure  $P_2$  is higher or lower than the nose-side pressure  $P_1$ , for keeping its balance, the spool actuator only can have a tiny opening on its

right side of the control port. Therefore, for any linearization  $\delta P_c$  is always equal to zero.

The following pressure rise-rate equation within the varying control volume is used to describe the fluid characteristics in the back-side volume for the linear systems

$$\dot{P}_2 = \frac{\beta}{V_L}(Q + Q_2 - Q_L - KP_2). \quad (2.70)$$

Substituting Equations (2.22), (2.40), (2.46), and (2.63) into Equation (2.70), and arranging similar items produce the following equation to describe the pressure dynamic behavior in the back-side volume in linear analysis

$$\frac{V_L}{\beta}\dot{P}_2 + (K + K_c + K_2 + K_{cl})(P_2 - P_{2d}) = K_{qt}(y - y_d) + K_2(P_c - P_{cd}). \quad (2.71)$$

#### 2.4 Control Pressure Analysis

The spool valve acts as the pilot valve to control the poppet valve displacement. The following pressure rise-rate equation within the varying control volume (shown in Figure 2-7) is used to describe the fluid characteristics in the control chamber

$$\frac{V_{co}}{\beta}\dot{P}_c = Q_c - K_2(P_c - P_2) + A_c\dot{y}, \quad (2.72)$$

where  $V_{co}$  is the control chamber volume, which is assumed as constant by ignoring the volume change caused by the movement of the poppet.

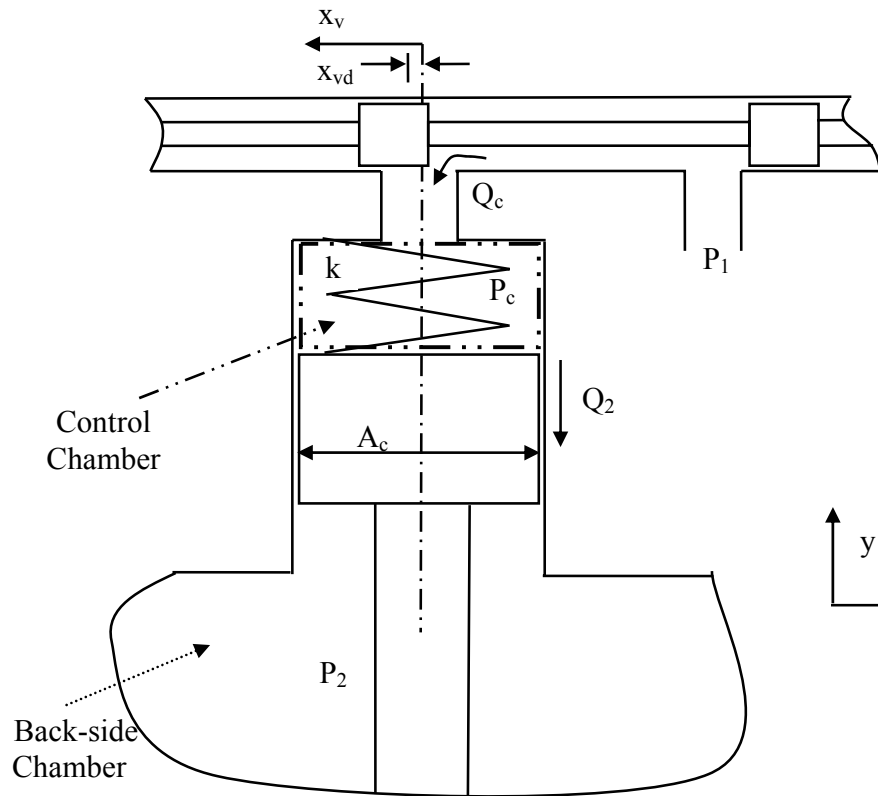


Figure 2-7. Control pressure analysis

The nonlinear fluid characteristics of the control flow rate  $Q_c$  is expressed in Equations (2.47) and (2.48). And the linear mathematical statement of the control flow rate  $Q_c$  is depicted in Equation (2.54). The left side of the above equation is the volume change of the control chamber due to compressible flow in terms of time. The flow rates on its right side are caused by flows either entering or exiting the control chamber due to its pressure drop effect. The last item on the right side is the volume change of the control chamber due to boundary change.



#### 2.4.1 Nominal Conditions

Under the steady-state conditions, the nominal control flow rate is given by

$$\begin{aligned} Q_{cd} &= hx_{vd}C_d\sqrt{\frac{2}{\rho}|P_1-P_{cd}|}\text{sign}(P_1-P_{cd}) \\ &= \frac{1}{2}Q_{cd} + K_{c1}(P_1-P_{cd}) = 2K_{c1}(P_1-P_{cd}) \end{aligned} \quad (2.73)$$

The static flow rate relationship under the nominal conditions in the control chamber can be expressed as

$$Q_{cd} = K_2(P_{cd} - P_{2d}). \quad (2.74)$$

From simultaneous Equations (2.33), (2.34), (2.73) and (2.74), the following equation of the nominal opening of the spool valve can be given by

$$\begin{aligned} x_{vd} &= \frac{K_2(P_{cd} - P_{2d})}{hC_d\sqrt{\frac{2}{\rho}|P_1-P_{cd}|}\text{sign}(P_1-P_{cd})} \\ &= \frac{K_2\frac{A-K_{fet}}{A_c}(P_1-P_{2d}) - \frac{K_2ky_d}{A_c}}{hC_d\sqrt{\frac{2}{\rho}\left|\frac{A_c-A+K_{fc}}{A_c}(P_1-P_{2d}) + \frac{K_2ky_d}{A_c}\right|}\text{sign}(P_1-P_{cd})} \end{aligned} \quad (2.75)$$

Considering that the spring force effect is negligible in the design and making an assumption that  $\text{sign}(P_1 - P_{cd}) = \text{sign}(P_1 - P_{2d})$ , the following equation can be derived to obtaining the nominal spool position

$$x_{vd} = \frac{K_2\frac{A-K_{fet}}{A_c}}{hC_d\sqrt{\frac{2}{\rho}\frac{A_c-A+K_{fet}}{A_c}}}\sqrt{|P_1-P_{2d}|}. \quad (2.76)$$

Similar as before, note that the nominal condition in which the desired nose-side pressure  $P_1$  is equal to the desired back-side pressure  $P_{2d}$  or/ and the desired nose-side pressure  $P_1$  does not equal to the desired control pressure  $P_{cd}$  is not included in this analysis.

By substituting Equation (2.73) into Equation(2.74), and rearranging items, the following nominal pressure relation can be given by

$$2K_{c1}P_1 = 2K_{c1}P_{cd} + K_2(P_{cd} - P_{2d}). \quad (2.77)$$

#### 2.4.2 Control Pressure Equation

Two different forms of the control pressure equation are depicted for the nonlinear system and the linear systems. The following equations are employed to represent the control chamber fluid characteristics for the nonlinear system

$$\frac{V_{co}}{\beta} \dot{P}_c = Q_c - K_2(P_c - P_2) + A_c \dot{y}, \quad (2.78)$$

$$Q_c = hx_v C_d \sqrt{\frac{2}{\rho} |\delta P|} \text{sign}(\delta P), \quad (2.79)$$

$$\delta P = \begin{cases} P_1 - P_c & x_v \geq 0 \\ P_c - P_2 & x_v < 0 \end{cases}. \quad (2.80)$$

Substituting Equations(2.40), (2.54) and (2.77) into Equation (2.70), and arranging items produce the following equation to describe the pressure dynamic behavior in the back-side volume in linear analysis

$$(K_3 + K_{c1})(P_c - P_{cd}) = A_c \dot{y} + K_2(P_2 - P_{2d}) + K_{qlr}(x_v - x_{vd}). \quad (2.81)$$

Note that the time-change rate of the control pressure is very small so that it is negligible in the linear analysis, though it is involved in the nonlinear analysis.

## 2.5 Nonlinear Governing Equations for the Open-loop System

The nonlinear governing equations for the open-loop poppet-valve system can be summarized as follows

$$m\ddot{y} + C_{eff}\dot{y} + K_{eff}y - K_{fq}y_d = (A - K_{fct})P_1 + A_{eff}P_2 - A_cP_c + \rho LK_c\dot{P}_2, \quad (2.82)$$

where  $K_{eff}$ ,  $C_{eff}$  and  $A_{eff}$  are constants as follows

$$K_{eff} = k + K_{fq}, \quad (2.83)$$

$$C_{eff} = c + \rho LK_{qt}, \quad (2.84)$$

$$A_{eff} = A_c - A + K_{fct}, \quad (2.85)$$

$$\frac{V_L}{\beta}\dot{P}_2 = Q + K_2(P_c - P_2) - Q_L - KP_2 - Q_c\delta P_c, \quad (2.86)$$

where

$$\delta P_c = \begin{cases} 0 & x_v \geq 0 \\ 1 & x_v < 0 \end{cases}, \quad (2.87)$$

$$Q = \pi D y \sin(\theta) C_d \sqrt{\frac{2}{\rho} |P_1 - P_2| \text{sign}(P_1 - P_2)}, \quad (2.88)$$

$$Q_L = A_k C_d \sqrt{\frac{2}{\rho} |P_2 - P_k| \text{sign}(P_2 - P_k)}, \quad (2.89)$$

$$Q_c = hx_v C_d \sqrt{\frac{2}{\rho}} |\delta P| \text{sign}(\delta P), \quad (2.90)$$

$$\delta P = \begin{cases} P_1 - P_c & x_v \geq 0 \\ P_c - P_2 & x_v < 0 \end{cases}, \quad (2.91)$$

$$\frac{V_{co}}{\beta} \dot{P}_c = Q_c - K_2 (P_c - P_2) + A_c \dot{y}. \quad (2.92)$$

Figure 2-8 shows the block diagram for the open-loop poppet-valve system.

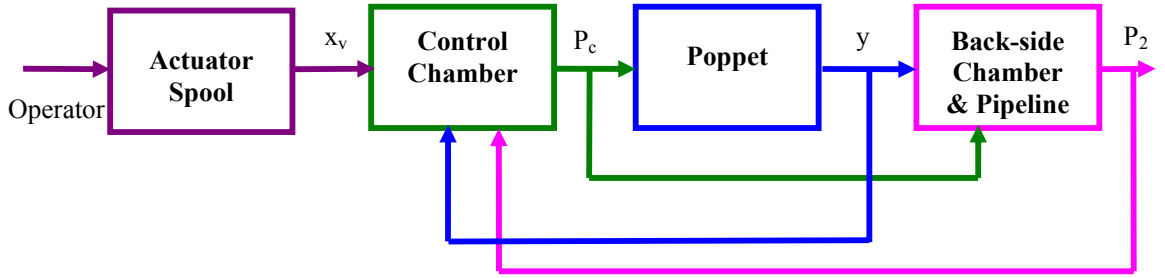


Figure 2-8. Block diagram for the open-loop poppet-valve system

## 2.6 Linear Governing Equations for the Full-model Open-loop System

The linear governing equations for the open-loop poppet-valve system can be summarized as follows

$$m\ddot{y} + C_{eff}\dot{y} + K_{eff}(y - y_d) = \rho L K_c \dot{P}_2 + A_{eff}(P_2 - P_{2d}) - A_c(P_c - P_{cd}), \quad (2.93)$$

$$\frac{V_L}{\beta} \dot{P}_2 + K_v(P_2 - P_{2d}) = K_{qt}(y - y_d) + K_2(P_c - P_{cd}), \quad (2.94)$$

$$K_s(P_c - P_{cd}) = A_c \dot{y} + K_2(P_2 - P_{2d}) + K_{qlt}(x_v - x_{vd}), \quad (2.95)$$

where  $K_v$  and  $K_s$  are constants as follows

$$K_v = K + K_c + K_2 + K_{cl}, \quad (2.96)$$

$$K_s = K_2 + K_{c1}. \quad (2.97)$$

In linear analysis, the system analysis under special conditions (when the nose-side pressure  $P_1$  and the nominal back-side pressure  $P_{2d}$  equals or/and the back-side pressure  $P_{2d}$  and the load pressure  $P_k$  equals) is not taken into consideration.

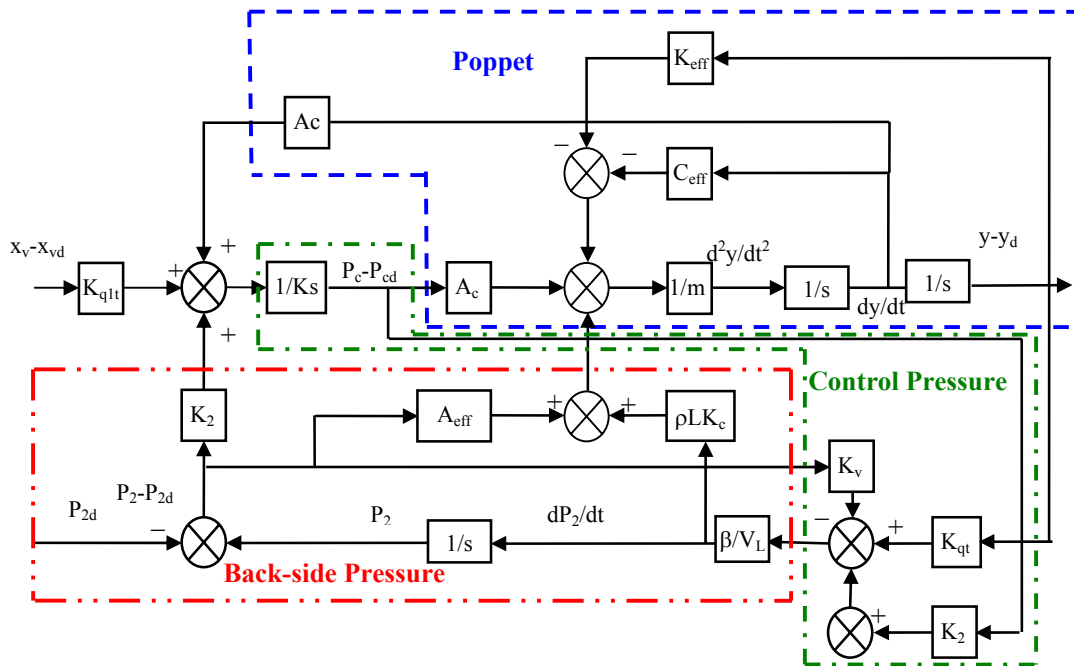


Figure 2-9. Block diagram for the full-model linear open-loop poppet-valve system

Figure 2-9 shows the block diagram for the full-model linear open-loop poppet-valve system. It is assumed the nominal pressure drop across the poppet is known. Therefore, for taking the desired external load under certain power supply that drives the

fluid to flow through the poppet, an operator can give the spool valve displacement  $x_{vd}$  to make the poppet valve move upward or downward its seat to reach position  $y_d$ .

## 2.7 Steady-State Solution

The mathematical expressions of state equilibrium relations between the system variables are given by removing the time-rate-of-change items as follow

$$K_{eff}(y - y_d) = A_{eff}(P_2 - P_{2d}) - A_c(P_c - P_{cd}), \quad (2.98)$$

$$K_v(P_2 - P_{2d}) = K_{qt}(y - y_d) + K_2(P_c - P_{cd}), \quad (2.99)$$

$$K_s(P_c - P_{cd}) = K_2(P_2 - P_{2d}) + K_{qlt}(x_v - x_{vd}). \quad (2.100)$$

The first equation depicts the force balance on the poppet under steady-state condition. The second and third equations represent respectively the static fluid behavior in the back-side chamber and the control chamber.

## 2.8 Linear Governing Equations for the Reduced-order Open-loop System

### 2.8.1 Non-Dimensional Governing Equations for the Full-model Linear Open-loop System

It can be illustrated from the above linear system equations that this is a 3<sup>rd</sup> order system with very complex parameters. It is necessary to perform non-dimensionalization to obtain a more clear view about how system variables and parameters act in practice. Some definitions are given by

$$\begin{aligned}
y &= y_d \hat{y}, & x_v &= x_{vd} \hat{x}_v, \\
t &= \tau \hat{t}, & P_c &= P_{cd} \hat{P}_c, & P_2 &= P_{2d} \hat{P}_2,
\end{aligned} \tag{2.101}$$

where the carets denote dimensionless quantities,  $\tau$  is a characteristic time in which the main dynamic behavior of the system may occur.  $y_d, x_{vd}, P_{cd}, P_{2d}$  are all desired values.

Substituting Equation (2.101) into Equations (2.93), (2.94) and (2.95), and rearranging items yield the three non-dimension system equations for the full-model linear open-loop poppet-valve system. The first equation describes the force balance on the poppet as follows

$$\Psi_1 \frac{d^2 \hat{y}}{d\hat{t}^2} + \Psi_2 \frac{d\hat{y}}{d\hat{t}} + \Psi_3 (\hat{y} - 1) = \Psi_4 \frac{d\hat{P}_2}{d\hat{t}} + \Psi_5 (\hat{P}_2 - 1) - (\hat{P}_c - 1), \tag{2.102}$$

where  $\Psi_1, \Psi_2, \Psi_3, \Psi_4, \Psi_5$  are all constant coefficients that change according to nominal conditions

$$\begin{aligned}
\Psi_1 &= \frac{m y_d}{\tau^2 A_c P_{cd}}, & \Psi_2 &= \frac{C_{eff} y_d}{\tau A_c P_{cd}} \\
\Psi_3 &= \frac{K_{eff} y_d}{A_c P_{cd}}, & \Psi_4 &= \frac{\rho L K_c P_{2d}}{\tau A_c P_{cd}}. \\
\Psi_5 &= \frac{A_{eff} P_{2d}}{A_c P_{cd}}.
\end{aligned} \tag{2.103}$$

The second one is the non-dimension mathematical description of the fluid characteristics in the back-side chamber as follows

$$\Xi_1 \frac{d\hat{P}_2}{d\hat{t}} = (\hat{y} - 1) - \Xi_2 (\hat{P}_2 - 1) + \Xi_3 (\hat{P}_c - 1), \tag{2.104}$$

where  $\Xi_1, \Xi_2, \Xi_3$  are all constant coefficients that change according to nominal conditions

$$\begin{aligned}\Xi_1 &= \frac{V_L P_{2d}}{\beta \tau K_{qt} \mathcal{Y}_d}, & \Xi_2 &= \frac{K_v P_{2d}}{K_{qt} \mathcal{Y}_d} \\ \Xi_3 &= \frac{K_2 P_{cd}}{K_{qt} \mathcal{Y}_d}\end{aligned}\quad (2.105)$$

The third one is the non-dimension mathematical description of the fluid characteristics in the control chamber as follows

$$\hat{x}_v - 1 = -Z_1 \frac{d\hat{y}}{dt} + Z_2 (\hat{P}_c - 1) - Z_3 (\hat{P}_2 - 1), \quad (2.106)$$

where  $Z_1, Z_2, Z_3$  are all constants that change according to nominal conditions

$$\begin{aligned}Z_1 &= \frac{A_c \mathcal{Y}_d}{\tau K_{q1r} x_{vd}}, & Z_2 &= \frac{K_c P_{cd}}{K_{q1r} x_{vd}} \\ Z_3 &= \frac{K_2 P_{2d}}{K_{q1r} x_{vd}}\end{aligned}\quad (2.107)$$

## 2.8.2 Linear Governing Equations for the Reduced-order Linear Open-loop System

The unimportant items in the governing equations can be detected from the non-dimension calculation. The reduced-order linear open-loop system can be obtained by ignoring the trivial effects and maintaining the primary factors for the stability criterion analysis of the PI control design in the next chapter. One set of typical known pressure conditions is introduced to investigate the quantity comparison for the non-dimension constant coefficients. The actual operating conditions will be given in Chapter 4 (See Tables 4-1 and 4-2). It is noted that the time constant  $\tau$  is set as 0.03 seconds in which



period the system is expected to fulfill main performance requirements. The following equation represents the set of pressure condition (Shown in Figure 2-10)

$$\begin{aligned}
 P_1 &= 22(10^6) + 5(10^6) \sin(62.8t) \text{ Pa} \\
 P_{2d} &= 20(10^6) + 5(10^6) \sin(62.8t) \text{ Pa} . \\
 P_k &= 5(10^6) \text{ Pa}
 \end{aligned}
 \tag{2.108}$$

It is obvious that the constant pressure drop, i.e. 2 MP<sub>a</sub>, exists between the two sides of the poppet opening. The desired nose-side pressure  $P_1$  is a sine wave with 10 HZ frequency as well as the desired back-side pressure  $P_{2d}$ . The amplitudes for  $P_1$  and  $P_{2d}$  are respectively 22 MP<sub>a</sub> and 20 MP<sub>a</sub>. The nominal load pressure  $P_k$  is a constant with the value of 5 MP<sub>a</sub>.

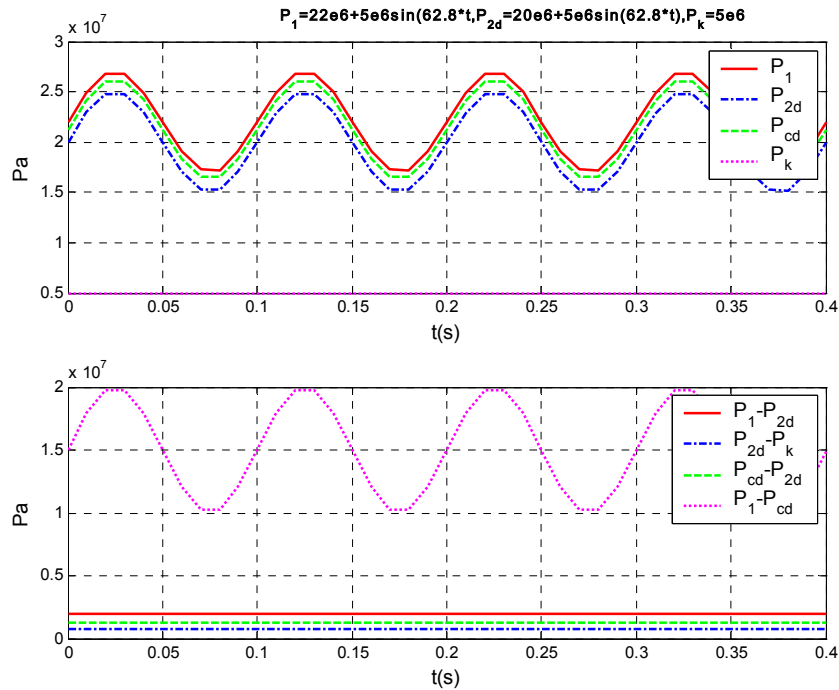


Figure 2-10. Pressures for calculating non-dimension governing equation coefficients

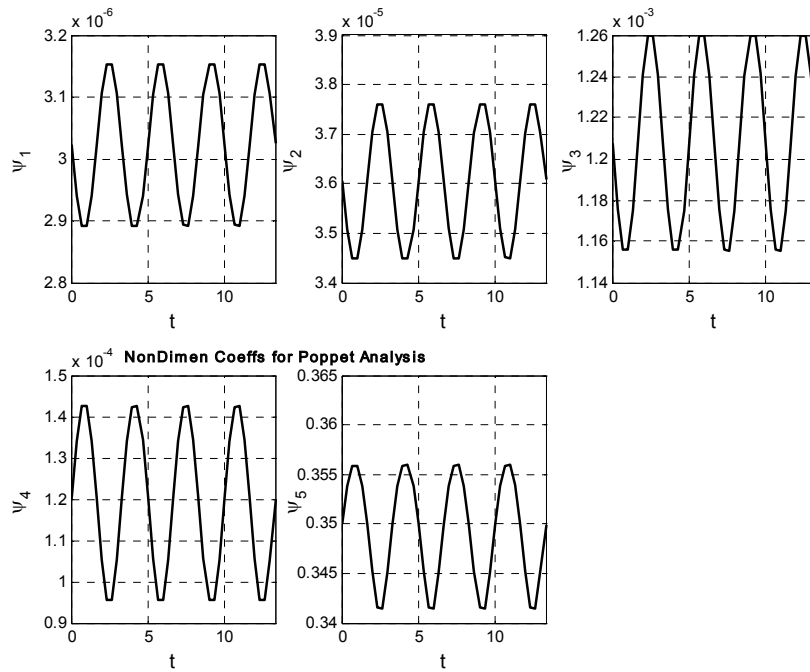


Figure 2-11. Non-dimension equation coefficients for the poppet analysis

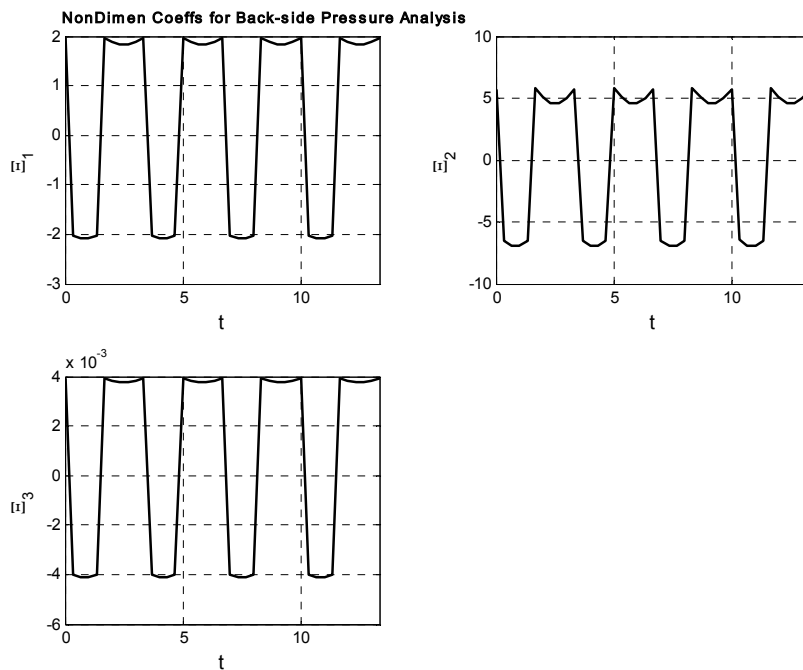


Figure 2-12. Non-dimension equation coefficients for the back-side pressure analysis

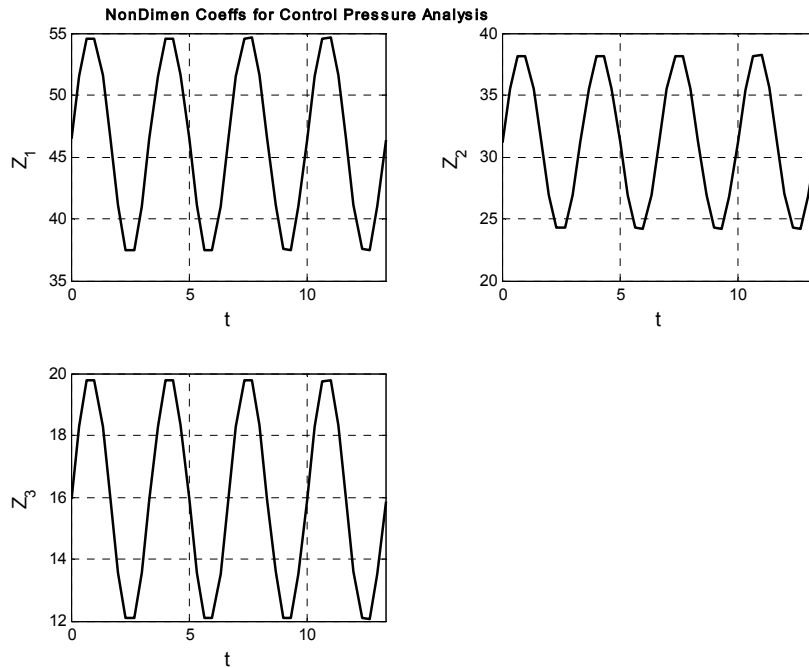


Figure 2-13. Non-dimension equation coefficients for the control pressure analysis

The calculating results for coefficients are shown in Figure 2-11 through Figure 2-13. Both x coordinate (time) and y coordinate (coefficients) are non-dimension values. Therefore there is no label to indicate their units. It is illustrated from Figure 2-11 that the order of magnitude of the first coefficient  $\Psi_1$  related to the mass inertia is at least 1 less than those of the rest coefficients in the poppet equation. Figure 2-12 shows that the values of the first and second  $\Xi_1$  and  $\Xi_2$  are respectively about 100 times and 10000 times of the value of the third coefficient  $\Xi_3$  related to the control pressure change in the back-side chamber. In Figure 2-13, it can tell us that all coefficients have obviously unavoidable influence on the control pressure. The values of coefficients  $Z_1$ ,  $Z_2$  and  $Z_3$  are at the same order magnitude level.

It is easy to make a conclusion that the values of  $\Psi_1$  in poppet analysis and  $\Xi_3$  in back-side pressure analysis are at least 10 times less than other corresponding coefficients. It is reasonable to consider to removing  $\Psi_1$  and  $\Xi_3$  to simplify the system and keep enough system information. Therefore, the poppet inertia and the change of control pressure in the back-side pressure analysis are not considered in the reduced-order linear system. The following equations are given to describe the reduce-order linear open-loop poppet-valve system

$$C_{eff}\dot{y} + K_{eff}(y - y_d) = \rho L K_c \dot{P}_2 + A_{eff}(P_2 - P_{2d}) - A_c(P_c - P_{cd}), \quad (2.109)$$

$$\frac{V_L}{\beta} \dot{P}_2 + K_v(P_2 - P_{2d}) = K_{qt}(y - y_d), \quad (2.110)$$

$$K_s(P_c - P_{cd}) = A_c \dot{y} + K_2(P_2 - P_{2d}) + K_{q1t}(x_v - x_{vd}). \quad (2.111)$$

## 2.9 Summary

In this chapter, three main mathematical models for both nonlinear and linear open-loop systems are presented: governing equations for the nonlinear system, governing equations for the full-model linear system and governing equations for the reduced-order linear system. With the help of dimensionless analysis, the reduced-order linear open-loop system is derived by neglecting the poppet mass and the change of the control pressure in the back-side chamber. The complete linear formation of the flow force acting on the poppet head is derived from the simplified Navier-Stoke Equations. The controller design, stability criterion analysis and model simulation in the subsequent chapters will be performed based on the open-loop systems established here.

## CHAPTER 3. CONTROL DESIGN

### 3.1 Introduction

There are two main difficulties existing in poppet control. One is that the poppet itself is pressure imbalanced due to its geometry. Another is that the system containing poppets is always undergoing a wide variation in pressure conditions. Therefore, poppet systems are easy to experience instability, normally distinguished by oscillation that can damage the component and make big noise. It is necessary to fall back on measures to control the poppet dynamic behavior. The controller design for this system is presented in this chapter. Four control methods are included: proportional-integral (PI) control, linear quadratic gaussian (LQG) control,  $H_\infty$  control and nonlinear feedback control. The analysis of the first three methods is based on the linear systems that are obtained from linearizing the nonlinear poppet system, while the fourth one is performed on the nonlinear poppet system. The validity of the linear controllers is checked by combining them with both the linear system and the nonlinear system in simulation chapter. A modified PI controller with changing gains is introduced to overcome the shortcoming of the PI controller with constant gains that can not adapt well to the diversity of system pressures. LQG is carried out on a single-input-multiple-output (SIMO) system which has one input of the spool displacement error  $x_v - x_{vd}$  and two outputs of the poppet displacement error  $y - y_d$  and the back-side pressure error  $P_2 - P_{2d}$ , while  $H_\infty$  control is fulfilled only for a SISO system which does not have  $P_2 - P_{2d}$ . The stability of the global

nonlinear linear system with the nonlinear controller is proved by utilizing Lyapunov stability theory.

The purpose of the control design is to make the poppet have the ability to meter a certain amount of flow that can take the required load under working conditions given. Since it is assumed that the nominal nose-side pressure  $P_1$ , the nominal back-side pressure  $P_{2d}$  and the nominal piping pressure  $P_k$  are known, this task becomes to make the poppet move to the desirable position when the spool actuator is operated by the desirable command which is obtained from the load and system information. The poppet must respond quickly enough with the acceptable steady-state error to track a 10 HZ sine wave that is a desired poppet displacement. The steady-state error must be less than 10% of the nominal poppet displacement. In practice, if a poppet can exhibit a frequency response of 5 HZ or 6 HZ, it is quick enough to meet the flow metering requirement in the hydraulic circuit. However, according to engineer's experience, when the controller is applied to the real physical system, the response speed of a hydraulic component, for example a poppet valve, usually slows down to about 50% of the one in simulation. The phase lag can not be bigger than 90 degree for this research. The settling time of about 30 ms for the step response is a goal for the speed of response.

## 3.2 Modified PI Control

### 3.2.1 Control Law

The PID (proportional-integral-derivative) controller is widely used in industry due to its simplicity and practicability. The proportional part can only proportionally increase or reduce the control error. Therefore, its control ability is limited and it has

nonzero steady-state error. The integral part has a low-pass frequency characteristic. It contributes to eliminate the steady-state error. However, its pole at the origin does add additional phase lag to the loop and could create system instability and make it slow as well. The phenomenon of “wind up” probably appears to reach physical saturation, which will prevent the controller from practical application. Limits of upper and lower integral saturation can be activated to avoid “wind up”. The derivative part can predict the future tendency of the control error. It will generate a large control signal, which might harm the system. In this research, only a PI controller is used to achieve the control goal.

The difficulty in this system is to control the poppet under a wide range of system pressures. Therefore, pressure control needs to be considered in PI design. Clues can be found by examining two important pressure relationships of the equilibrium position (shown in Figure 2-1) that appear in Equations (2.33) and (2.34). The following pressure relationships might be presented to develop a new PI controller

$$P_1 - P_c = \frac{A_c - A + K_{fct}}{A_c} (P_1 - P_2) + \frac{ky}{A_c}, \quad (3.1)$$

$$P_c - P_2 = \frac{A - K_{fct}}{A_c} (P_1 - P_2) - \frac{ky}{A_c}, \quad (3.2)$$

where  $y$  is the instantaneous poppet position,  $P_1$  is known poppet nose-side pressure,  $P_c$  is the instantaneous control pressure in the control chamber,  $P_2$  is the instantaneous poppet back-side pressure,  $A_c$  and  $A$  are respectively the cross section area of the poppet land and the poppet port,  $K_{fct}$  is the poppet flow force pressure coefficient and  $k$  is the

spring rate. Rearranging items in the steady-state Equation (2.100) produces the rudiment of the control law as follows

$$x_v - x_{vd} = \frac{1}{K_{q1t}} \left\{ K_2 [(P_c - P_2) - (P_{cd} - P_{2d})] - K_{c1} [(P_1 - P_c) - (P_1 - P_{cd})] \right\}. \quad (3.3)$$

By substituting Equations (3.1) and (3.2) into Equation (3.3) and rearranging items, the following static relationship between the spool displacement and pressures can be given to be the pre-expression of the control law

$$x_v - x_{vd} = -\frac{K_2 (A - K_{fct}) - K_{c1} A_{eff}}{K_{q1t}} (P_2 - P_{2d}) - \frac{kK_s}{A_c K_{q1t}} (y - y_d). \quad (3.4)$$

The above item and the common PI items constitute the final version of the PI controller that is used as the control law in this research as follows

$$x_v - x_{vd} = K_{p2} (y - y_d) + K_{I2} \int (y - y_d) dt - K_{pp} (P_2 - P_{2d}), \quad (3.5)$$

where  $K_{p2}$ ,  $K_{I2}$  and  $K_{pp}$  are respectively the proportional gain, the integral gain and the pressure gain as follows that are changing according to the nominal pressure conditions

$$\begin{aligned} K_{p2} &= \frac{K_p}{K_{q1t}} - \frac{kK_s}{A_c K_{q1t}} \\ K_{I2} &= \frac{K_I}{K_{q1t}} \\ K_{pp} &= \frac{K_2 (A - K_{fct}) - K_{c1} A_{eff}}{A_c K_{q1t}} \end{aligned}, \quad (3.6)$$



where  $K_p$  and  $K_I$  are respectively constant proportional gain and integral gain. Figure 3-1 shows the block diagram of the closed-loop poppet-valve system.

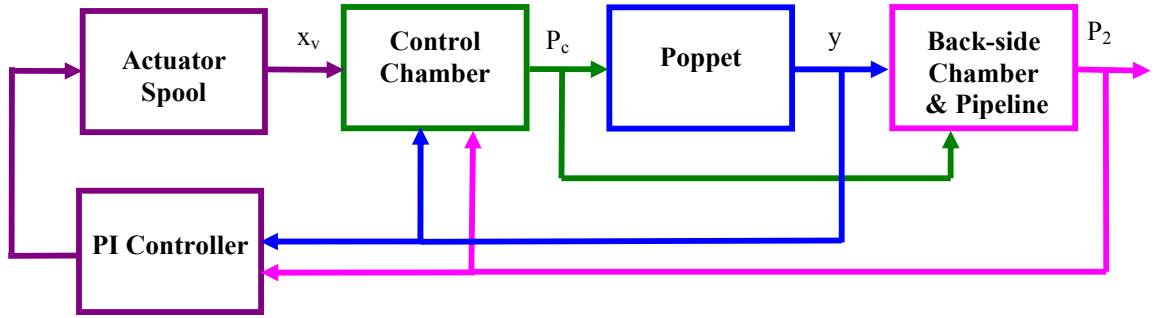


Figure 3-1. Block diagram for the closed-loop poppet-valve system

### 3.2.2 Characteristic Equation of the Reduced-order Linear Closed-loop System

The subsection implements the analysis about how to choose constant  $K_p, K_I$  for the closed-loop system that combines the control law of Equation (3.5) with the reduced-order linear open-loop system described in Chapter 2 (shown in Equations (2.109), (2.110) and (2.111)). The following characteristic equation of the reduced-order linear closed-loop system can be given by

$$d_0 s^3 + d_1 s^2 + d_2 s + d_3 = 0, \quad (3.7)$$

where  $d_0, d_1, d_2, d_3$  are constant coefficients as follows

$$d_0 = \frac{V_L}{\beta} \left( C_{eff} + \frac{A_c^2}{K_s} \right), \quad (3.8)$$

$$d_1 = K_{eff} \frac{V_L}{\beta} - \rho L K_c K_{qt} + \frac{A_c K_{P2} K_{qt} V_L}{K_s \beta} + K_v \left( C_{eff} + \frac{A_c^2}{K_s} \right), \quad (3.9)$$

$$d_2 = K_{eff}K_v + \frac{A_c}{K_s} \left( K_{q1t}K_{p2}K_v + K_{I2}K_{q1t} \frac{V_L}{\beta} \right), \quad (3.10)$$

$$d_3 = \frac{A_c K_v K_{q1t} K_{I2}}{K_s} = \frac{A_c K_v K_I}{K_s}. \quad (3.11)$$

### 3.2.3 Control Gain Analysis

Routh-Hurwitz stability criterion [32] can be used to help determine the stability problem of this linear third-order system. It states that the roots of the characteristic equation that describes a system can indicate whether this system is stable or unstable. If all real parts of these eigenvalues are negative, that is all roots locate within the left-hand complex plane, it means that the system is stable. There are two rules for a stable system in Routh-Hurwitz stability criterion:

- 1) All coefficients in the characteristic equation are positive.
- 2) Each coefficient in the first column of the Routh array must have the same sign.

Therefore, two stability criteria of the third-order system are given as

$$d_0, d_1, d_2, d_3 > 0 \text{ and } d_1 d_2 > d_0 d_3. \quad (3.12)$$

It is obvious that if  $c + \rho L K_{qt} + \frac{A^2}{K_s} > 0$ , then  $d_0 > 0$  is guaranteed. By substituting

Equations (2.83), (2.84) and (3.6) into Equation (3.9), rearranging items and making reference from Equations (2.20), (2.21), (2.25), (2.96) and (2.25) the following equations can be given by

$$\begin{aligned}
d_1 &= \underbrace{K_{fq} \frac{V_L}{\beta}}_{>0} - \underbrace{\rho L K_c}_{>0} K_{qt} + \underbrace{K_v}_{>0} \left( \underbrace{c + \rho L K_{qt} + \frac{A_c^2}{K_s}}_{>0, \text{ due to the requirement of } d_0 > 0} \right) + \underbrace{\frac{A_c V_L}{K_s \beta}}_{>0} K_P \\
&= \underbrace{K_{fq} \frac{V_L}{\beta}}_{>0} + \underbrace{(K + K_2 + K_{cL}) \rho L K_{qt}}_{>0} + \underbrace{K_v \left( c + \frac{A_c^2}{K_s} \right)}_{>0} + \underbrace{\frac{A_c V_L}{K_s \beta}}_{>0} K_P
\end{aligned} \tag{3.13}$$

It is assumed that the nominal nose-side pressure  $P_1$ , the nominal back-side pressure  $P_{2d}$  and the nominal back-side pressure  $P_k$  are never equal to each other. On one hand, under the system pressure relationship of  $P_1 > P_{2d} > P_k$ ,  $K_P > 0$  can make  $d_1$  always positive according to the lower expression of Equation (3.13). On the other hand, under the system pressure relationship of  $P_1 < P_{2d} < P_k$ ,  $K_P > 0, c + \rho L K_{qt} + \frac{A_c^2}{K_s} > 0$  can always give a positive value of  $d_1$  in the upper expression of Equation (3.13). Therefore,  $d_1 > 0$  can be satisfied by  $K_P > 0, c + \rho L K_{qt} + \frac{A_c^2}{K_s} > 0$  under working conditions that are interested in this research. It can be shown from Equations (2.95) and (2.96) that  $K_I > 0$  can make sure the stability criterion  $d_3 > 0$  to be satisfied. By substituting Equations (2.83) and (3.6) into Equation (3.10), rearranging items and making reference from Equations (2.25), (2.96) and (2.25), the following equation can be given by

$$d_2 = \underbrace{K_{fq} K_v}_{>0} + \underbrace{\frac{A_c K_v}{K_s}}_{>0} K_P + \underbrace{\frac{A_c V_L}{K_s \beta}}_{>0} K_I. \tag{3.14}$$

Consequently,  $K_P > 0$  and  $K_I > 0$  can furnish security for this stability criterion  $d_2 > 0$ .

By substituting Equations (2.83), (2.84) and (3.6) into Equation (3.11), rearranging items and making reference from Equations (2.20), (2.21), (2.25), (2.96) and (2.25), the following equations can be given by

$$d_1 d_2 - d_0 d_3 = \left( \underbrace{\frac{K_{fq} K_v}{>0} + \frac{A_c K_v}{K_s}}_{>0} K_p \right) \left( \underbrace{C_{eff} + \frac{A_c^2}{K_s}}_{>0, \text{ due to the requirement } d_0 > 0} \right) \frac{K_v}{>0} + \left[ \frac{K_{fq} K_v}{>0} + \frac{A_c}{K_s} \left( \frac{K_v}{>0} K_p + K_I \frac{V_L}{\beta} \right) \right] \left[ \frac{K_{fq} \frac{V_L}{\beta} - \rho L K_c K_{qt}}{>0} + \frac{A_c V_L}{K_s \beta} K_p \right]. \quad (3.15)$$

From the above equation, a conclusion can be drawn that if  $K_p > 0, c + \rho L K_{qt} + \frac{A_c^2}{K_s} > 0$ ,

$K_I > 0$  and  $K_p > \frac{K_s \beta V_L}{A_c V} \left( \rho L K_c K_{qt} - K_{fq} \frac{V_L}{\beta} \right)$  exist, the last stability requirement,

$d_1 d_2 - d_0 d_3 > 0$ , can be obtained.

It can be summarized that the following rule is derived to give basic guide line of how to choose the proportional gain  $K_p$  and the integral gain  $K_I$  in PI control design.

$$c + \rho L K_{qt} + \frac{A_c^2}{K_s} > 0$$

$$K_p > \max \left[ 0, \frac{K_s \beta}{A_c V_L} \left( \rho L K_c K_{qt} - K_{fq} \frac{V_L}{\beta} \right) \right]. \quad (3.16)$$

$$K_I > 0$$

However, this rule can only assure the system stability. For good system performance, the correct gains need to be selected with caution.

### 3.3 LQG Control

As an important part of robust control methods, Linear-Quadratic-Gaussian (LQG) control is widely used in aerospace engineering. It is a modern state-space technique for designing optimal dynamic regulators by combining a Kalman estimator to get optimal estimated states with a full-state feedback controller to make the system approaches its equilibrium status from the initial deviation. It is assumed that the plant is known and linear, illustrated by transfer functions or state-space matrices and the process disturbance and measurement noise covariance data are known as white noises with known statistical properties. Figure 3-2 shows the structure of the closed-loop system with a LQG controller. It is obvious that a Kalman estimator represented by the blue dash-line rectangle and a LQ Regulator (LQR) constitute the LQG controller represented by the red dash-double-dot-line polygon. Both the Kalman estimator and the LQR can be obtained by respectively solving two Riccati equations. The variables  $\mathbf{y}_m, \tilde{\mathbf{x}}, \tilde{\mathbf{y}}$  are respectively the measured output vector, the internal Kalman state vector and the estimated full-state output vector. Matrices  $\mathbf{A}_{op}, \mathbf{B}_{op}, \mathbf{C}_{op}$  and  $\mathbf{D}_{op}$  are open-loop system matrices.  $\mathbf{C}_{KF}$ , a 3-by-3 identity matrix, is one of the Kalman filter matrix.  $\mathbf{M}_f, \mathbf{W}$  and  $\mathbf{V}_n$  are respectively the Kalman filter innovation gain matrix, the input disturbance matrix and the measurement noise matrix.

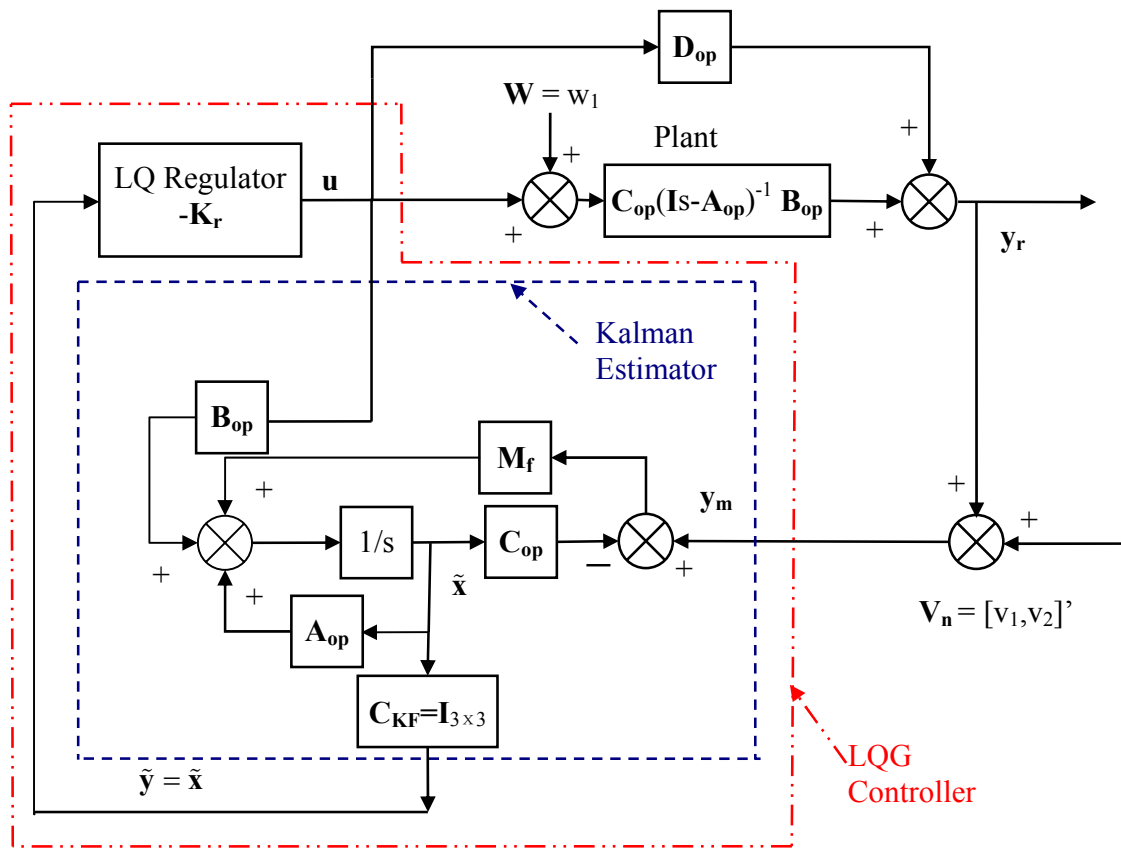


Figure 3-2. Structure of the linear closed-loop system with the LQG controller

### 3.3.1 State-Space Equations for the Full-model Linear Open-loop System

The states in this analysis are all errors between the instantaneous values and the nominal values. Thereby the tracking performance can also be performed by the regulation design. According to linear governing Equations (2.93) through (2.95), the states  $\mathbf{x}$ , input  $\mathbf{u}$  and output  $\mathbf{y}_r$  for the state-space plant that does not include disturbances can be chosen as

$$\mathbf{x} = \begin{bmatrix} x_1 \\ x_2 \\ x_3 \end{bmatrix} = \begin{bmatrix} y - y_d \\ \dot{y} \\ P_2 - P_{2d} \end{bmatrix}, \quad (3.17)$$

$$\mathbf{u} = [u] = [x_v - x_{vd}], \quad (3.18)$$

$$\mathbf{y}_r = \begin{bmatrix} y_{r1} \\ y_{r3} \end{bmatrix} = \begin{bmatrix} x_1 \\ x_3 \end{bmatrix} = \begin{bmatrix} y - y_d \\ P_2 - P_{2d} \end{bmatrix}. \quad (3.19)$$

where  $x_1, x_2$  and  $x_3$  are elements of the state vector  $\mathbf{x}$ ,  $y_{r1}$  and  $y_{r2}$  are elements of the output  $\mathbf{y}_r$ ,  $u$  is the control signal in error formation. They are all deviations from the desired position with assumption that the time rate of change of desired values is assumed as zero. Only instantaneous poppet position  $y$  and back-side pressure  $P_2$  are measured as outputs in LQG design.

It is assumed that there are two state measured noises  $v_1, v_2$  acting on the position sensor and the pressure sensor respectively and one process disturbance  $w_1$  acting on the spool displacement  $x_v$ . They can be expressed by

$$\mathbf{W} = [w_1], \mathbf{V}_n = \begin{bmatrix} v_1 \\ v_2 \end{bmatrix}. \quad (3.20)$$

The above process disturbance and sensor noise are defined as white noises which have flat constant power spectral density matrices  $\mathbf{Q}_n, \mathbf{R}_n$  respectively as follows

$$\begin{aligned}\mathbf{Q}_n &= [\sigma_w^2] \\ \mathbf{R}_n &= \begin{bmatrix} \sigma_{v_1}^2 & 0 \\ 0 & \sigma_{v_2}^2 \end{bmatrix},\end{aligned}\quad (3.21)$$

where  $\sigma_w$ ,  $\sigma_{v_1}$ ,  $\sigma_{v_2}$  are chosen constants related to the precision of measurement equipments and process disturbance. And  $\mathbf{W}, \mathbf{V}_n$  are matrices that must satisfy

$$\begin{aligned}E\{\mathbf{W}\mathbf{W}^T\} &= \mathbf{Q}_n \\ E\{\mathbf{V}_n\mathbf{V}_n^T\} &= \mathbf{R}_n \\ E\{\mathbf{W}\} &= E\{\mathbf{V}_n\} = 0, \\ E\{\mathbf{W}\mathbf{V}_n^T\} &= 0 \\ E\{\mathbf{V}_n\mathbf{W}^T\} &= 0\end{aligned}\quad (3.22)$$

where “E” is the expectation operator. The superscript “ $T$ ” means the transpose for a matrix. If the linear system is close to a singular system, it is probably hard to obtain the LQG robust feedback gains or Klamán estimator. This problem can be solved by fulfilling LQG control design on a non-dimension linear system to improve the design circumstance and solvability of this plant in Matlab. Non-dimension process disturbance and measurement noise can be separately expressed by

$$\mathbf{W}_{nd} = [w_{1nd}], \mathbf{V}_{nd} = \begin{bmatrix} v_{1nd} \\ v_{2nd} \end{bmatrix}, v_{1nd} = \frac{v_1}{y_d}, v_{2nd} = \frac{v_2}{P_{2d}}, w_{1nd} = \frac{w_1}{x_{vd}}. \quad (3.23)$$

The non-dimension flat constant power spectral density matrices  $\mathbf{Q}_{nND}$ ,  $\mathbf{R}_{nND}$  of the above non-dimension process disturbance and sensor noise can be respectively given by



$$\mathbf{Q}_{nND} = \begin{bmatrix} \sigma_{w_{nd}}^2 \end{bmatrix} = x_{vd}^2 \mathbf{Q}_n$$

$$\mathbf{R}_{nND} = \begin{bmatrix} \sigma_{v_{1nd}}^2 & 0 \\ 0 & \sigma_{v_{2nd}}^2 \end{bmatrix} = \begin{bmatrix} 1/y_d^2 & 0 \\ 0 & 1/P_{2d}^2 \end{bmatrix}^{-1} \mathbf{R}_n, \quad (3.24)$$

where  $\sigma_{w_{nd}}$ ,  $\sigma_{v_{1nd}}$ ,  $\sigma_{v_{2nd}}$  are dimensionless constant related to precision of measurement equipments and process disturbance as follows

$$\sigma_{w_{nd}} = \frac{\sigma_w}{x_{vd}}$$

$$\sigma_{v_{1nd}} = \frac{\sigma_{v_1}}{y_d}, \sigma_{v_{2nd}} = \frac{\sigma_{v_2}}{P_{2d}}$$

(3.25)

A matrix with the superscript “-1” indicates the inverse matrix for the original one.

The original open-loop plant model with process disturbance  $\mathbf{W}$  and measurement noise  $\mathbf{V}_n$  can be given as follows

$$\dot{\mathbf{x}} = \mathbf{A}_{op} \mathbf{x} + \mathbf{B}_{op} \mathbf{u} + \mathbf{F} \mathbf{W}$$

$$\mathbf{y}_m = \mathbf{C}_{op} \mathbf{x} + \mathbf{D}_{op} \mathbf{u} + \mathbf{H} \mathbf{W} + \mathbf{V}_n, \quad (3.26)$$

where  $\mathbf{y}_m$  is the measured output vector that contains disturbance,

$\mathbf{A}_{op}, \mathbf{B}_{op}, \mathbf{F}, \mathbf{C}_{op}, \mathbf{D}_{op}, \mathbf{H}$  are system matrices as follows

$$\mathbf{A}_{op} = \begin{bmatrix} 0 & 1 & 0 \\ \frac{1}{m} \left( -K_{eff} + \frac{K_c K_{qt} L \beta \rho}{V_L} \right) & \frac{1}{m} \left( -C_{eff} - \frac{A_c^2}{K_s} + \frac{A_c K_2 K_c L \beta \rho}{K_s V_L} \right) & \frac{1}{m} \left( A_{eff} - \frac{A_c K_2}{K_s} + \frac{K_c \left( \frac{K_2^2}{K_s} - K_v \right) L \beta \rho}{V_L} \right) \\ \frac{K_{qt} \beta}{V_L} & \frac{A_c K_2 \beta}{K_s V_L} & \frac{\left( \frac{K_2^2}{K_s} - K_v \right) \beta}{V_L} \end{bmatrix}, \quad (3.27)$$

$$\mathbf{B}_{op} = \begin{bmatrix} 0 \\ \frac{1}{K_s m} \left( -A_c K_{qt} + \frac{K_2 K_c K_{qt} L \beta \rho}{V_L} \right) \frac{1}{K_s m} \\ \frac{K_2 K_{qt} \beta}{K_s V_L} \end{bmatrix}, \quad (3.28)$$

$$\mathbf{F} = \mathbf{B}_{op}, \quad \mathbf{C}_{op} = \begin{bmatrix} 1 & 0 & 0 \\ 0 & 0 & 1 \end{bmatrix}, \quad \mathbf{D}_{op} = \begin{bmatrix} 0 \\ 0 \end{bmatrix}, \quad \mathbf{H} = \begin{bmatrix} 0 \\ 0 \end{bmatrix}. \quad (3.29)$$

Substituting Equation (3.29) into Equation (3.26) produces

$$\dot{\mathbf{x}} = \mathbf{A}_{op} \mathbf{x} + \begin{bmatrix} \mathbf{B}_{op} & \mathbf{B}_{op} \end{bmatrix} \begin{bmatrix} \mathbf{u} \\ \mathbf{W} \end{bmatrix}. \quad (3.30)$$

$$\mathbf{y}_m = \mathbf{C}_{op} \mathbf{x} + \mathbf{V}_n = \mathbf{y}_r + \mathbf{V}_n$$

where  $\mathbf{y}_m$  can be expressed as

$$\mathbf{y}_m = \begin{bmatrix} y_{m1} \\ y_{m3} \end{bmatrix} = \begin{bmatrix} y - y_d + v_1 \\ P_2 - P_{2d} + v_2 \end{bmatrix}, \quad (3.31)$$

where  $y_{m1}$  and  $y_{m2}$  are elements of the measured outputs  $\mathbf{y}_m$  with disturbance effects.

### 3.3.2 Kalman Estimator

The purpose of Kalman filter is to estimate the state variables of this dynamic system from a series of incomplete measurements which have random sensor errors and the input information. Figure 3-3 shows the state-space structure of the linear closed-loop system with the LQG controller (shown by the dash-double-dot-line polygon) for Kalman filter calculation.

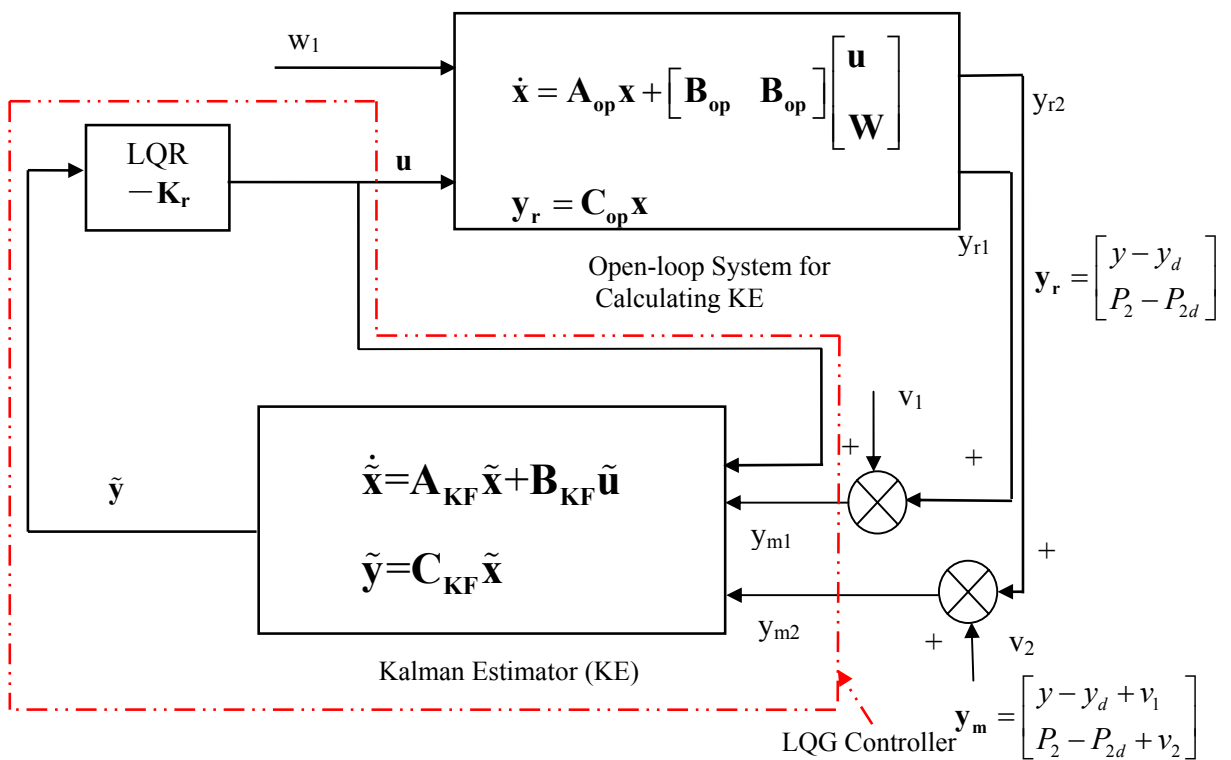


Figure 3-3. State-space structure of the linear closed-loop system with the LQG controller

The open-loop system that is used to get the Kalman estimator (as shown in Figure 3-3) can be given by

$$\begin{aligned}\dot{\mathbf{x}} &= \mathbf{A}_{op}\mathbf{x} + \begin{bmatrix} \mathbf{B}_{op} & \mathbf{F} \end{bmatrix} \begin{bmatrix} \mathbf{u} \\ \mathbf{W} \end{bmatrix} = \mathbf{A}_{op}\mathbf{x} + \begin{bmatrix} \mathbf{B}_{op} & \mathbf{B}_{op} \end{bmatrix} \begin{bmatrix} \mathbf{u} \\ \mathbf{W} \end{bmatrix} \\ \mathbf{y}_r &= \mathbf{C}_{op}\mathbf{x} + \begin{bmatrix} \mathbf{D}_{op} & \mathbf{H} \end{bmatrix} \begin{bmatrix} \mathbf{u} \\ \mathbf{W} \end{bmatrix} = \mathbf{C}_{op}\mathbf{x}\end{aligned}\quad (3.32)$$

The equation of the Kalman estimator might be given by (reference from Figure 3-2)

$$\begin{aligned}\dot{\tilde{\mathbf{x}}} &= \mathbf{A}_{op}\tilde{\mathbf{x}} + \mathbf{B}_{op}\mathbf{u} + \mathbf{M}_f(\mathbf{y}_m - \mathbf{C}_{op}\tilde{\mathbf{x}}) \\ \tilde{\mathbf{y}} &= \mathbf{C}_{KF}\tilde{\mathbf{x}} + \mathbf{D}_{KF}\tilde{\mathbf{u}} = \mathbf{C}_{KF}\tilde{\mathbf{x}} \\ \mathbf{y}_m &= \mathbf{C}_{op}\mathbf{x} + \mathbf{D}_{op}\mathbf{u} + \mathbf{V}_n = \mathbf{C}_{op}\mathbf{x} + \mathbf{V}_n\end{aligned}\quad (3.33)$$

The above equation can be rearranged as

$$\begin{aligned}\dot{\tilde{\mathbf{x}}} &= \mathbf{A}_{KF}\tilde{\mathbf{x}} + \mathbf{B}_{KF}\tilde{\mathbf{u}} \\ \tilde{\mathbf{y}} &= \mathbf{C}_{KF}\tilde{\mathbf{x}} + \mathbf{D}_{KF}\tilde{\mathbf{u}} = \mathbf{C}_{KF}\tilde{\mathbf{x}}\end{aligned}\quad (3.34)$$

where  $\mathbf{A}_{KF}$ ,  $\mathbf{B}_{KF}$ ,  $\mathbf{C}_{KF}$  and  $\mathbf{D}_{KF}$  are system matrices for the Kalman filter as follows

$$\begin{aligned}\mathbf{A}_{KF} &= \mathbf{A}_{op} - \mathbf{M}_f\mathbf{C}_{op}, \quad \mathbf{B}_{KF} = \begin{bmatrix} \mathbf{B}_{op} & \mathbf{M}_f \end{bmatrix} \\ \mathbf{C}_{KF} &= \begin{bmatrix} 1 & 0 & 0 \\ 0 & 1 & 0 \\ 0 & 0 & 1 \end{bmatrix}, \quad \mathbf{D}_{KF} = \begin{bmatrix} 0 & 0 & 0 \\ 0 & 0 & 0 \\ 0 & 0 & 0 \end{bmatrix}\end{aligned}\quad (3.35)$$

and  $\tilde{\mathbf{x}}$ ,  $\tilde{\mathbf{y}}$  and  $\tilde{\mathbf{u}}$  are respectively the internal states, outputs and inputs of the Kalman filter system as follows

$$\tilde{\mathbf{x}} = \begin{bmatrix} \tilde{x}_1 \\ \tilde{x}_2 \\ \tilde{x}_3 \end{bmatrix} = \begin{bmatrix} \tilde{y} - y_d \\ \dot{\tilde{y}} \\ \tilde{P}_2 - P_{2d} \end{bmatrix}, \quad (3.36)$$

$$\tilde{\mathbf{y}} = \begin{bmatrix} \tilde{y}_1 \\ \tilde{y}_2 \\ \tilde{y}_3 \end{bmatrix} = \begin{bmatrix} \tilde{x}_1 \\ \tilde{x}_2 \\ \tilde{x}_3 \end{bmatrix} = \begin{bmatrix} \tilde{y} - y_d \\ \dot{\tilde{y}} \\ \tilde{P}_2 - P_{2d} \end{bmatrix}, \quad (3.37)$$

$$\tilde{\mathbf{u}} = \begin{bmatrix} u \\ y_m \end{bmatrix} = \begin{bmatrix} x_v - x_{vd} \\ y_m \end{bmatrix}, \quad (3.38)$$

where  $\tilde{x}_1, \tilde{x}_2$  and  $\tilde{x}_3$  are elements of  $\tilde{\mathbf{x}}$  and  $\tilde{y}_1, \tilde{y}_2$  and  $\tilde{y}_3$  are elements of  $\tilde{\mathbf{y}}$ , the variable with “ $\sim$ ” denotes the variables which describe the dynamic behavior of the Kalman filter and the optimal matrix  $\mathbf{M}_f$ , which is used to minimize the steady-state error covariance

$\lim_{t \rightarrow \infty} E \left\{ (\mathbf{x} - \tilde{\mathbf{x}})(\mathbf{x} - \tilde{\mathbf{x}})^T \right\}$ , can be given by

$$\mathbf{M}_f = \mathbf{Y}_f \mathbf{C}_{op}^T \mathbf{R}_n^{-1}, \quad (3.39)$$

where  $\mathbf{Y}_f = \mathbf{Y}_f^T \geq 0$  is given by solving the following algebraic Riccati equation

$$\mathbf{Y}_f \mathbf{A}_{op}^T + \mathbf{A}_{op} \mathbf{Y}_f - \mathbf{Y}_f^T \mathbf{C}_{op}^T \mathbf{R}_n^{-1} \mathbf{C}_{op} \mathbf{Y}_f + \mathbf{Q}_n = 0. \quad (3.40)$$

Normally, the selection of  $\mathbf{M}_f$  needs to follow a principle that it can create a Kalman filter which has a faster response than those of the system.

### 3.3.3 Full-State Feedback LQR

The LQR problem is to find the control law  $\mathbf{u}$  containing full-state feedback to make all the system variables approach zero by the way of minimizing the quadratic cost function  $\mathbf{J}_r$  that can be described by the following equation

$$\mathbf{J}_r = \int_0^{\infty} \left( \tilde{\mathbf{x}}(t)^T \mathbf{Q} \tilde{\mathbf{x}}(t) + \mathbf{u}(t)^T \mathbf{R} \mathbf{u}(t) \right) dt, \quad (3.41)$$

where  $\mathbf{Q}$  and  $\mathbf{R}$  are weight matrices of the cost function that can be selected in this design as follows

$$\mathbf{Q} = \begin{bmatrix} 1/q_1^2 & 0 & 0 \\ 0 & 1/q_2^2 & 0 \\ 0 & 0 & 1/q_3^2 \end{bmatrix}, \quad (3.42)$$

$$\mathbf{R} = [1]$$

where  $q_1, q_2, q_3$  are constants that will be given to solve the Riccati equation for obtaining the LQR controller. The optimal control law can be given by

$$\mathbf{u} = -\mathbf{K}_r \tilde{\mathbf{x}}, \quad (3.43)$$

where,  $\mathbf{K}_r$  is the gain matrix that can be given by

$$\mathbf{K}_r = \mathbf{R}^{-1} \mathbf{B}_{op}^T \mathbf{Y}_r, \quad (3.44)$$

where  $\mathbf{Y}_r = \mathbf{Y}_r^T \geq 0$  is given by solving the following algebraic Riccati equation

$$\mathbf{A}_{op}^T \mathbf{Y}_r + \mathbf{Y}_r \mathbf{A}_{op} - \mathbf{Y}_r \mathbf{B}_{op} \mathbf{R}^{-1} \mathbf{B}_{op}^T \mathbf{Y}_r + \mathbf{Q} = 0. \quad (3.45)$$

In dimensionless analysis, the non-dimension weight matrices  $\mathbf{Q}_{ND}$  and  $\mathbf{R}_{ND}$  can be represented are selected as

$$\mathbf{Q}_{ND} = \begin{bmatrix} y_d & 0 & 0 \\ 0 & y_d / \tau & 0 \\ 0 & 0 & P_{2d} \end{bmatrix} \mathbf{Q} \begin{bmatrix} y_d & 0 & 0 \\ 0 & y_d / \tau & 0 \\ 0 & 0 & P_{2d} \end{bmatrix}^T. \quad (3.46)$$

$$\mathbf{R}_{ND} = x_{vd}^2 \mathbf{R}$$

### 3.3.4 Summary of the Closed-loop System with the LQG Controller

Combining Kalman filter design with LQ regulator design produces the following state-space equation for the closed-loop poppet system

$$\begin{aligned}\dot{\mathbf{x}}_g &= \mathbf{A}_{\text{clg}}\mathbf{x}_g + \mathbf{B}_{\text{clg}}\mathbf{u}_{\text{clg}}, \\ \mathbf{y}_g &= \mathbf{C}_{\text{clg}}\mathbf{x}_g + \mathbf{D}_{\text{clg}}\mathbf{u}_{\text{clg}},\end{aligned}\quad (3.47)$$

where  $\mathbf{x}_g$ ,  $\mathbf{y}_g$  and  $\mathbf{u}_{\text{clg}}$  are respectively states, outputs and inputs of the above closed-loop system as follows

$$\begin{aligned}\mathbf{x}_g &= \begin{bmatrix} \mathbf{x} \\ \tilde{\mathbf{x}} \end{bmatrix} = [x_1 \ x_2 \ x_3 \ \tilde{x}_1 \ \tilde{x}_2 \ \tilde{x}_3]^T, \\ &= [y - y_d \ \dot{y} \ P_2 - P_{2d} \ \tilde{y} - y_d \ \dot{\tilde{y}} \ \tilde{P}_2 - P_{2d}]^T\end{aligned}\quad (3.48)$$

$$\mathbf{y}_g = \tilde{\mathbf{y}} = \begin{bmatrix} \tilde{y}_1 \\ \tilde{y}_2 \\ \tilde{y}_3 \end{bmatrix} = \begin{bmatrix} \tilde{x}_1 \\ \tilde{x}_2 \\ \tilde{x}_3 \end{bmatrix} = \begin{bmatrix} \tilde{y} - y_d \\ \dot{\tilde{y}} \\ \tilde{P}_2 - P_{2d} \end{bmatrix},\quad (3.49)$$

$$\mathbf{u}_{\text{clg}} = \begin{bmatrix} w_1 \\ v_1 \\ v_2 \end{bmatrix},\quad (3.50)$$

$\mathbf{A}_{\text{clg}}$ ,  $\mathbf{B}_{\text{clg}}$ ,  $\mathbf{C}_{\text{clg}}$  and  $\mathbf{D}_{\text{clg}}$  are system matrices for the closed-loop system with the LQG controller as follows

$$\mathbf{A}_{\text{clg}} = \begin{bmatrix} \mathbf{A}_{\text{op}} & -\mathbf{B}_{\text{op}}\mathbf{K}_r \\ \mathbf{M}_f\mathbf{C}_{\text{op}} & \mathbf{A}_{\text{op}} - \mathbf{M}_f\mathbf{C}_{\text{op}} - \mathbf{B}_{\text{op}}\mathbf{K}_r \end{bmatrix}.\quad (3.51)$$

$$\mathbf{B}_{\text{clg}} = \begin{bmatrix} \mathbf{B}_{\text{op}} & \mathbf{0}_{3 \times 2} \\ \mathbf{0}_{3 \times 1} & \mathbf{M}_f \end{bmatrix}, \quad (3.52)$$

$$\mathbf{C}_{\text{clg}} = \begin{bmatrix} \mathbf{C}_{\text{op}} & \mathbf{0}_{2 \times 3} \end{bmatrix} = \begin{bmatrix} 1 & 0 & 0 & 0 & 0 & 0 \\ 0 & 0 & 1 & 0 & 0 & 0 \end{bmatrix}, \quad (3.53)$$

$$\mathbf{D}_{\text{clg}} = \begin{bmatrix} 0 & 1 & 0 \\ 0 & 0 & 1 \end{bmatrix}. \quad (3.54)$$

Substituting Equations (3.48) through (3.54) into Equation (3.47) produces

$$\dot{\mathbf{x}}_{\text{g}} = \begin{bmatrix} \mathbf{A}_{\text{op}} & -\mathbf{B}_{\text{op}}\mathbf{K}_r \\ \mathbf{M}_f\mathbf{C}_{\text{op}} & \mathbf{A}_{\text{op}} - \mathbf{M}_f\mathbf{C}_{\text{op}} - \mathbf{B}_{\text{op}}\mathbf{K}_r \end{bmatrix} \begin{bmatrix} \mathbf{x} \\ \tilde{\mathbf{x}} \end{bmatrix} + \mathbf{B}_{\text{clg}} \begin{bmatrix} w_1 \\ v_1 \\ v_2 \end{bmatrix}. \quad (3.55)$$

$$\mathbf{y}_{\text{g}} = \mathbf{C}_{\text{op}}\tilde{\mathbf{x}} + \begin{bmatrix} v_1 \\ v_2 \end{bmatrix}$$

### 3.4 $H_{\infty}$ Control

#### 3.4.1 System Uncertainty

The modeling errors, which can be defined as “uncertainty”, always exist between the mathematical model and the true physical system. There are two main types of system uncertainty: parametric uncertainty and unmodelled plant uncertainty. The correct value of many parameters is either hard to be measured, or very complex to get the numerical expression, or varies with the change of time and working condition. There is no doubt that any analytical model can not avoid unmodelled model uncertainty, which either comes from intended neglect or originates from human knowledge deficiency in



cognition of the real world. In this study, only parameter uncertainty is considered, i.e. assume that the mathematical models make a good agreement with the real system. Three key parameters (fluid bulk modulus  $\beta$ , orifice coefficient  $C_d$  and spring rate  $k$ ) with ranges are chosen to perform uncertainty analysis. Figure 3-4 shows the plant  $\mathbf{G}_p$  with the lumped multiplicative input uncertainty [30].  $\mathbf{G}_{\text{norm}}$  is the nominal plant without consideration of the uncertainty. The parameter uncertainties are depicted as the product of the uncertainty weight function  $\mathbf{W}_I$  and the lumped complex perturbation  $\Delta_I$  that is a stable transfer function and has a  $H_\infty$  norm less than 1, i.e.  $\|\Delta_I\|_\infty \leq 1$ .

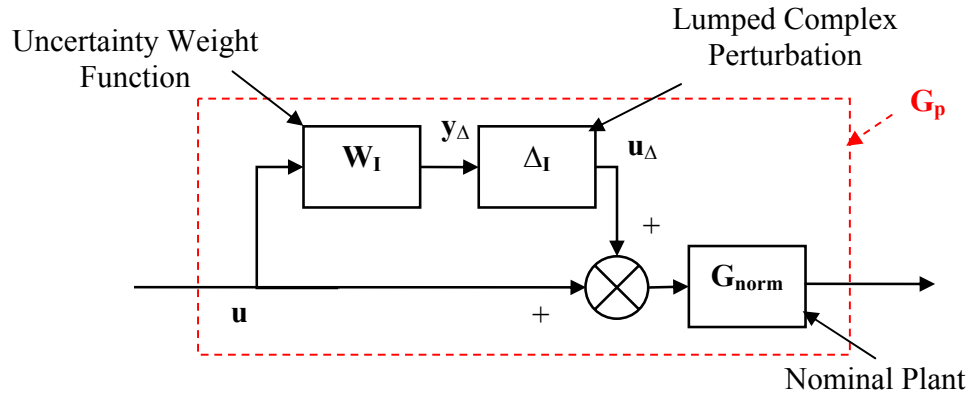


Figure 3-4. Plant with the lumped multiplicative uncertainty:  $\mathbf{G}_p$

Subsequently, the set of mathematical system plants with the multiplicative input uncertainty in transfer function is given by [30]

$$\Pi: \mathbf{G}_p(s) = \mathbf{G}(s)(\mathbf{I} + \mathbf{W}_I(s)\Delta_I(s)), \quad \underbrace{|\Delta_I(j\omega)| \leq 1}_{\|\Delta_I\|_\infty \leq 1} \quad \forall \omega. \quad (3.56)$$

The form of weight function  $\mathbf{W}_I$  of the multiplicative input uncertainty can be expressed by

$$|\mathbf{W}_I(j\omega)| \geq \max_{\mathbf{G}_p \in \Pi} \left| \frac{\mathbf{G}_p(j\omega) - \mathbf{G}_{\text{norm}}(j\omega)}{\mathbf{G}_{\text{norm}}(j\omega)} \right|, \quad \forall \omega, \quad (3.57)$$

where  $\omega$  is the frequency. Therefore, any  $\mathbf{W}_I$  whose magnitude is greater than the maximum value of the absolute ratio of the model error between the system with uncertainty  $\mathbf{G}_p$  and the nominal system  $\mathbf{G}_{\text{norm}}$  with respect to the nominal system  $\mathbf{G}_{\text{norm}}$ , can be chosen to symbolize the system multiplicative input uncertainty weight function.

### 3.4.2 Mixed Sensitivity $H_\infty$ Control Design

#### 3.4.2.1 Standard Control Configuration for a Common System with Uncertainty

Figure 3-5 demonstrates the standard control configuration that is used to solve control design problem (including  $H_\infty$  control design) and carry out robust analysis for a common system with uncertainty.  $\mathbf{P}_h$  is the generalized open-loop plant, while  $\mathbf{N}_h$  is the generalized closed-loop plant (the structure of dash-double-dot line that includes the controller  $\mathbf{K}_h$ ). The uncertainties represented as  $\Delta_I$  and  $\Delta_P$  are withdrawn from the nominal closed system  $\mathbf{N}_h$ . The block  $\Delta_I$  is a certain normalized form ( $\|\Delta_I\|_\infty \leq 1, \forall \omega$ ) of the real uncertainty. It may be a block-diagonal matrix [30]. Therefore, the system is designed to undergo a specific uncertainty that has no explicit mathematic form. In this study, it is chosen as a multiplicative input uncertainty expressed by Equation (3.57). The full complex matrix block  $\Delta_P$  ( $\|\Delta_P\|_\infty \leq 1, \forall \omega$ ) is specially stated to represent a fictitious

uncertainty coming from  $H_\infty$  performance specifications [30], for example, tracking requirement, noise truncation and control energy limitation.

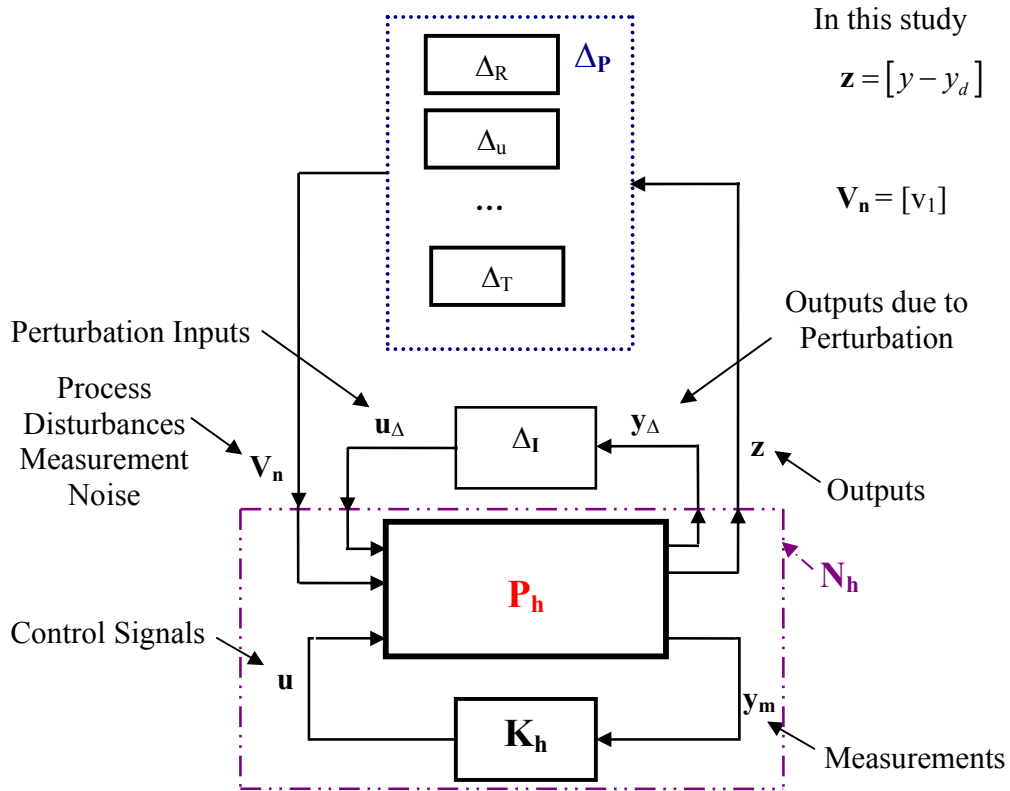


Figure 3-5. Standard system structure with uncertainty for control design and robust analysis

In the practical design process, the more useful configuration (shown in Figures 3-6) may be used to find out the stable controller  $K_h$  for the generalized plant  $P_h$ . The following relationship exists in Figure 3-6

$$\begin{bmatrix} \mathbf{y}_\Delta \\ \mathbf{z} \\ \mathbf{y}_m \end{bmatrix} = \mathbf{P}_h \begin{bmatrix} \mathbf{u}_\Delta \\ \mathbf{V}_n \\ \mathbf{u} \end{bmatrix}, \quad (3.58)$$

where  $\mathbf{z}$  is the system output vector that usually are errors needed to be small enough,  $\mathbf{y}_m$  is the measurable output vector,  $\mathbf{V}_n$  can be measurement noise or process disturbance or both,  $\mathbf{u}$  is the control law,  $\mathbf{y}_\Delta$  is the outputs due to system uncertainties and  $\mathbf{u}_\Delta$  is the inputs due to system uncertainties.

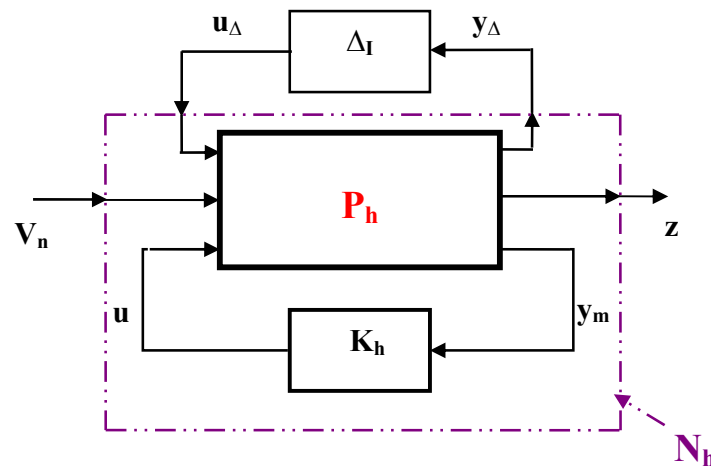


Figure 3-6. Standard control design configuration for a system with uncertainty

Note that in the process of obtaining the proper controller  $\mathbf{K}_h$  for this poppet system, only is the nominal plant utilized without consideration of the disturbance  $\mathbf{V}_n$ . Therefore the control design can be fulfilled accompanying with the assumption that the real uncertainty is not involved in the design process, although it plays an important role

for analyzing system robustness later. For the control design, the following input-output relationship can be given by

$$\begin{bmatrix} \mathbf{z} \\ \mathbf{y}_m \end{bmatrix} = \mathbf{P}_h \begin{bmatrix} \mathbf{V}_n \\ \mathbf{u} \end{bmatrix}. \quad (3.59)$$

The generalized open-loop plant  $\mathbf{P}_h$  (shown in Figures 3-5 and 3-6) can be denoted by partitioned transfer functions as follows.

$$\mathbf{P}_h = \begin{bmatrix} \mathbf{P}_{h11} & \mathbf{P}_{h12} \\ \mathbf{P}_{h21} & \mathbf{P}_{h22} \end{bmatrix}, \quad (3.60)$$

where  $\mathbf{P}_{h11}$ ,  $\mathbf{P}_{h12}$ ,  $\mathbf{P}_{h21}$  and  $\mathbf{P}_{h22}$  are all system transfer function matrices. Then the following relationship can be derived as

$$\begin{aligned} \mathbf{z} &= \mathbf{P}_{h11} \mathbf{V}_n + \mathbf{P}_{h12} \mathbf{u} \\ \mathbf{y}_m &= \mathbf{P}_{h21} \mathbf{V}_n + \mathbf{P}_{h22} \mathbf{u} \end{aligned} \quad (3.61)$$

Another configuration (shown in Figure 3-7) may be more valuable to perform the robust analysis for the system with uncertainty. This well-known framework is to be called  $N\Delta$ -structure [30]. Similarly, the relationship lying in Figure 3-7 can be given by

$$\begin{bmatrix} \mathbf{y}_\Delta \\ \mathbf{z} \end{bmatrix} = \mathbf{N}_h \begin{bmatrix} \mathbf{u}_\Delta \\ \mathbf{V}_n \end{bmatrix}. \quad (3.62)$$

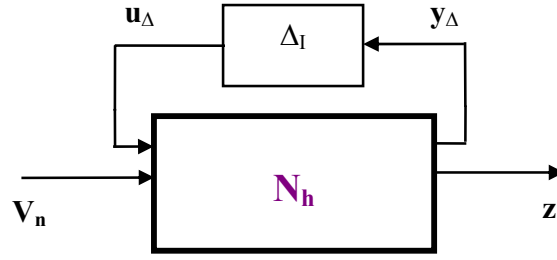


Figure 3-7.  $N\Delta$ -structure for analyzing robustness of a system with uncertainty

### 3.4.2.2 Common $H_\infty$ Control Design

$H_\infty$  control method is one of powerful ways of controller design for both SISO (single input and single output) and MIMO (multiple inputs and multiple outputs) linear systems. Especially for MIMO systems, instead of phase and gain margin, a new concept of singular value is introduced to be the stability criterion. The  $H$  stands for “Hardy Space”. The infinity norm is the peak value of a transfer function in all frequency ranges that can be expressed as follows

$$\|N_h(s)\| = \max_{\omega} |N_h(j\omega)| \quad (\text{for the SISO systems}), \quad (3.63)$$

$$\|N_h(s)\| = \max_{\omega} \bar{\sigma}(N_h(j\omega)) \quad (\text{for the MIMO systems}), \quad (3.64)$$

where  $\bar{\sigma}(\cdot)$  stands for the largest singular value of the matrix  $N_h$  at a certain frequency that represents the worst direction and the worst frequency. The singular values of the matrix  $N_h$  can be defined as

$$\sigma_i = \sqrt{\lambda_i(N_h^H N_h)} = \sqrt{\lambda_i(N_h N_h^H)} \quad i = 1 \cdots n, \quad (3.65)$$

where  $n$  is the number of all eigenvalues,  $\lambda_i$  is the  $i$ th eigenvalue, and the matrix with a superscript “ $H$ ” identifies a complex conjugate transpose matrix.

The optimal  $H_\infty$  control design for the common system aims at finding all stabilizing controllers  $\mathbf{K}_h$  to minimize the  $H_\infty$  norm of the matrix  $\mathbf{N}_h$  that can be expressed by the following equation

$$\mathbf{N}_h = F_{N_i}(\mathbf{P}_h, \mathbf{K}_h) = \mathbf{P}_{h11} + \mathbf{P}_{h12} \mathbf{K}_h [\mathbf{I} - \mathbf{P}_{h22} \mathbf{K}_h]^{-1} \mathbf{P}_{h21}, \quad (3.66)$$

where  $F_{N_i}(\mathbf{P}_h, \mathbf{K}_h)$  is the lower linear fractional transformation (LFT) in which the generalized plant  $\mathbf{P}_h$  and a stable controller  $\mathbf{K}_h$  are parameters. It is necessary to require that the final closed-loop system should be internally stable. The essence of the control task is to make the influence of the disturbances  $\mathbf{V}_n$  on the output  $\mathbf{z}$  as small as possible.

However, Glover and Doyle [24] showed that the process of finding the optimal  $H_\infty$  solution is numerically and theoretically complicated. Therefore the main task becomes to find all stabilizing controllers  $\mathbf{K}_h$  that can satisfied the following equation.

$$\|\mathbf{N}_h\|_\infty < \gamma, \quad \gamma > \gamma_{\min}, \quad (3.67)$$

where  $\gamma$  is a given value which is bigger than  $\gamma_{\min}$  that is the minimum value of  $\|\mathbf{N}_h\|_\infty$  over all stabilizing controllers  $\mathbf{K}_h$  that can be called suboptimal controllers.

Due to  $H_\infty$  being utilized on a linear system, the generalized plant  $\mathbf{P}_h$  can be described in state-space formation.

$$\mathbf{P}_h = \left( \begin{array}{c|cc} \mathbf{A}_h & \mathbf{B}_{h1} & \mathbf{B}_{h2} \\ \hline \mathbf{C}_{h1} & \mathbf{D}_{h11} & \mathbf{D}_{h12} \\ \mathbf{C}_{h2} & \mathbf{D}_{h21} & \mathbf{D}_{h22} \end{array} \right), \quad (3.68)$$

where  $\mathbf{A}_h$ ,  $\mathbf{B}_{h1}$ ,  $\mathbf{B}_{h2}$ ,  $\mathbf{C}_{h1}$ ,  $\mathbf{C}_{h2}$ ,  $\mathbf{D}_{h11}$ ,  $\mathbf{D}_{h12}$ ,  $\mathbf{D}_{h21}$  and  $\mathbf{D}_{h22}$  are system matrices.<sup>2</sup> The linear generalized system without the controller can be expressed in state-space formation as

$$\begin{aligned} \dot{\mathbf{x}}_h &= \mathbf{A}_h \mathbf{x}_h + \mathbf{B}_{h1} \mathbf{V}_n + \mathbf{B}_{h2} \mathbf{u} \\ \mathbf{z} &= \mathbf{C}_{h1} \mathbf{x}_h + \mathbf{D}_{h11} \mathbf{V}_n + \mathbf{D}_{h12} \mathbf{u} \quad , \\ \mathbf{y}_m &= \mathbf{C}_{h2} \mathbf{x}_h + \mathbf{D}_{h21} \mathbf{V}_n + \mathbf{D}_{h22} \mathbf{u} \end{aligned} \quad (3.69)$$

where  $\mathbf{x}_h$  is the internal state of the  $H_\infty$  closed system.

Three conditions [30] must be satisfied to obtain the optimal controllers  $\mathbf{K}_h$  :

- 1) The following algebraic Riccati equation has a nonnegative solution  $\mathbf{X}_\infty$

$$\mathbf{A}_h^H \mathbf{X}_\infty + \mathbf{X}_\infty \mathbf{A}_h + \mathbf{C}_{h1}^H \mathbf{C}_{h1} + \mathbf{X}_\infty \left( \gamma^{-2} \mathbf{B}_{h1} \mathbf{B}_{h1}^H - \mathbf{B}_{h2} \mathbf{B}_{h2}^H \right) \mathbf{X}_\infty = 0, \quad (3.70)$$

such that

$$\mathbf{R}_e \left\{ \lambda_i \left[ \mathbf{A}_h + \left( \gamma^{-2} \mathbf{B}_{h1} \mathbf{B}_{h1}^H - \mathbf{B}_{h2} \mathbf{B}_{h2}^H \right) \mathbf{X}_\infty \right] \right\} < 0, \forall i. \quad (3.71)$$

- 2) The following algebraic Riccati equation has a nonnegative solution  $\mathbf{Y}_\infty$

$$\mathbf{A}_h \mathbf{Y}_\infty + \mathbf{Y}_\infty \mathbf{A}_h^H + \mathbf{B}_{h1} \mathbf{B}_{h1}^H + \mathbf{Y}_\infty \left( \gamma^{-2} \mathbf{C}_{h1}^H \mathbf{C}_{h1} - \mathbf{C}_{h2}^H \mathbf{C}_{h2} \right) \mathbf{Y}_\infty = 0, \quad (3.72)$$

such that

---

<sup>2</sup> There are some important assumptions and discussions about them manifested in books [34] and [33] that are not presented in this dissertation. Readers who are interested in the assumptions can obtain details in the above books.



$$\mathbf{R}_e \left\{ \lambda_i \left[ \mathbf{A}_h + \mathbf{Y}_\infty \left( \gamma^{-2} \mathbf{C}_{h1}^H \mathbf{C}_{h1} - \mathbf{C}_{h2}^H \mathbf{C}_{h2} \right) \right] \right\} < 0, \forall i. \quad (3.73)$$

3) The following condition is also needed to be held

$$\rho(\mathbf{X}_\infty \mathbf{Y}_\infty) < \gamma^2, \quad (3.74)$$

where  $\rho(\bullet)$  is the spectral radius that can be given by

$$\rho(\mathbf{X}_\infty \mathbf{Y}_\infty) = \max_i \left| \lambda_i \left[ \mathbf{X}_\infty \mathbf{Y}_\infty (j\omega) \right] \right|, \forall \omega. \quad (3.75)$$

When the above three conditions are met, the form of all stabilizing controllers  $\mathbf{K}_h$  can be given by

$$\mathbf{K}_h(s) = F_{Nl}(\mathbf{K}_{hc}(s), \mathbf{Q}_h(s)), \quad (3.76)$$

where  $F_{Nl}(\mathbf{K}_{hc}, \mathbf{Q}_h)$  is the lower linear fractional transformation (LFT) of  $\mathbf{Q}_h$  and  $\mathbf{K}_{hc}$ ,

$\mathbf{K}_{hc}$  can be expressed as follows

$$\mathbf{K}_{hc}(s) = \left( \begin{array}{c|cc} \mathbf{A}_\infty & -\mathbf{Z}_\infty \mathbf{L}_\infty & \mathbf{Z}_\infty \mathbf{B}_{h2} \\ \hline \mathbf{F}_\infty & \mathbf{0} & \mathbf{I} \\ -\mathbf{C}_{h2} & \mathbf{I} & \mathbf{0} \end{array} \right), \quad (3.77)$$

and matrices  $\mathbf{A}_\infty, \mathbf{Z}_\infty, \mathbf{L}_\infty, \mathbf{F}_\infty$  can be respectively represented by the following equations

$$\mathbf{A}_\infty = \mathbf{A}_h + \gamma^{-2} \mathbf{B}_{h1} \mathbf{B}_{h1}^H \mathbf{X}_\infty + \mathbf{B}_{h2} \mathbf{F}_\infty + \mathbf{Z}_\infty \mathbf{L}_\infty \mathbf{C}_{h2}, \quad (3.78)$$

$$\mathbf{Z}_\infty = \left( \mathbf{I} - \gamma^{-2} \mathbf{Y}_\infty \mathbf{X}_\infty \right)^{-1}, \quad (3.79)$$

$$\mathbf{L}_\infty = -\mathbf{Y}_\infty \mathbf{C}_{h2}^H, \quad (3.80)$$

$$\mathbf{F}_\infty = -\mathbf{B}_{h2}^H \mathbf{X}_\infty, \quad (3.81)$$

and  $\mathbf{Q}_h(s)$  is any stable proper transfer function such that  $\|\mathbf{Q}_h(s)\|_\infty < \gamma$ . The  $\mathbf{Q}_h(s)$  can be defined to be proper that its degree of the numerator does not exceed the degree of the denominator. More information in detail about derivation process of  $H_\infty$  control is fully discussed in books [33] and [34].

### 3.4.2.3 Mixed Sensitivity $H_\infty$ Control Design

Figure 3-8 displays the detail construction of mixed sensitivity  $H_\infty$  control design for this poppet system which is selected as a SISO system having the poppet position error  $y - y_d$  as the output and the spool position error  $x_v - x_{vd}$  as the input. Because the system matrix of this poppet system is close to being singular, multiple outputs can not be applied to obtain the optimal solution in  $H_\infty$  design.  $\mathbf{W}_p$  is the selected weight function for shaping the sensitivity function  $\mathbf{S}$  to reject a disturbance  $\mathbf{V}_n$ , while  $\mathbf{W}_u$  is the selected weight function to avoid unacceptable control efforts that might be obtained from the controller.  $\mathbf{S}$  is the closed-loop transfer function from disturbance  $v_1$  to output  $y - y_d$  as follows

$$\mathbf{S} = (\mathbf{I} + \mathbf{G}_{\text{norm}} \mathbf{K}_h)^{-1}. \quad (3.82)$$

Generally,  $\mathbf{W}_p$  and  $\mathbf{W}_u$  are performance bounds of the closed-loop system. The following matrix can be applied to express the open-loop plant for the poppet system with performance specifications that is used for the controller design

$$\mathbf{P}_h = \begin{bmatrix} \mathbf{W}_p & \mathbf{W}_p \mathbf{G}_{\text{norm}} \\ \mathbf{0} & -\mathbf{W}_u \\ -\mathbf{I} & -\mathbf{G}_{\text{norm}} \end{bmatrix}. \quad (3.83)$$

This system can be expressed as Equation (3.59), and the states can be depicted as follows

$$\mathbf{z} = \begin{bmatrix} z_1 \\ z_2 \end{bmatrix} = \begin{bmatrix} \mathbf{W}_p ((y - y_d) + v_1) \\ -\mathbf{W}_u (x_v - x_{vd}) \end{bmatrix}, \quad (3.84)$$

$$\mathbf{y}_m = [ -((y - y_d) + v_1) ], \quad (3.85)$$

$$\mathbf{V}_n = [v_1], \quad (3.86)$$

$$\mathbf{u} = [x_v - x_{vd}]. \quad (3.87)$$

The purpose of mixed sensitivity  $H_\infty$  control design is to find all stabilizing controllers

$\mathbf{K}_h$  to minimize the  $H_\infty$  norm of  $\mathbf{N}_h = \begin{bmatrix} \mathbf{W}_p \mathbf{S} \\ \mathbf{W}_u \mathbf{K}_h \mathbf{S} \end{bmatrix}$ .  $\mathbf{N}_h$  can be defined as the

combination system of the weighted sensitivity functions  $\mathbf{W}_p \mathbf{S}$  and  $\mathbf{W}_u \mathbf{K}_h \mathbf{S}$ .  $\mathbf{S}$  and

$\mathbf{K}_h \mathbf{S}$  are sensitivity functions that represent system performances.

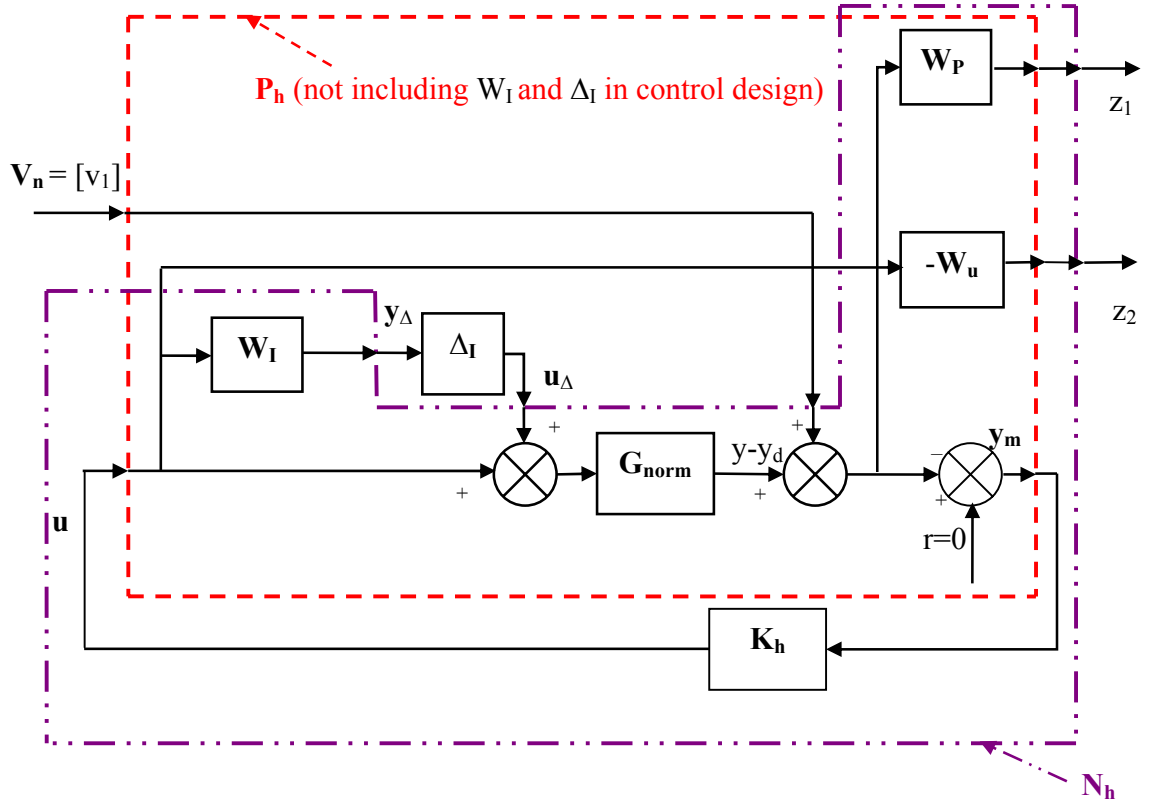


Figure 3-8. System structure for mixed sensitivity  $H_\infty$  control design

The common formation of  $\mathbf{W}_p$  can be given by

$$\mathbf{W}_p = \begin{bmatrix} W_{p1} & & & \\ & W_{p2} & & \\ & & \dots & \\ & & & W_{pn_v} \end{bmatrix}, \quad (3.88)$$

where  $\mathbf{W}_p$  is a diagonal matrix in which all elements are zero except the diagonal elements,  $W_{p_{i_v}}$  ( $i_v = 1 \dots n_v$ ) is the  $i_v$ th diagonal element,  $n_v$  means the number of the output disturbances. The following two choices may be used for specifying output performance.

$$W_{P_{i_v}} = \frac{s / M_{i_v} + \omega_{B_{i_v}}}{s + \omega_{B_{i_v}} A_{i_v}}, A_{i_v} \ll 1, \quad (3.89)$$

$$W_{P_{i_v}} = \frac{\left( s / \sqrt{M_{i_v}} + \omega_{B_{i_v}} \right)^2}{\left( s + \omega_{B_{i_v}} \sqrt{A_{i_v}} \right)^2}, A_{i_v} \ll 1, \quad (3.90)$$

where  $M_{i_v}$  is a constant (percentage) which is greater than the maximum peak value of  $|S_{i_v}|$ ,  $\omega_{B_{i_v}}$  is the minimum bandwidth, and  $A_{i_v}$  is steady-state error percentage that is much less than 1. The control cost weigh function  $\mathbf{W}_u$  can be chosen as constant diagonal matrix.

Associated with robust control, some important definitions are introduced here. Nominal stability (NS) is to check whether the closed-loop system without uncertainty is stable. Nominal performance (NP) is to check whether the performance of the nominal closed-loop system is consistent with requirements. Robust stability (RS) is to check whether the closed-loop system can remain stable for all possible perturbations. Robust performance (RP) is to check whether the performance of the closed-loop system can be satisfied according to design requirements for all possible perturbations. The stability criterion for a SISO system can be expressed as

$$\begin{aligned} NS &\Leftrightarrow \mathbf{N}_h \text{ is internally stable} \\ NP &\Leftrightarrow |\mathbf{W}_p \mathbf{S}| < 1, \forall \omega \\ RS &\Leftrightarrow |\mathbf{W}_I \mathbf{T}_I| < 1, \forall \omega \\ RP &\Leftrightarrow |\mathbf{W}_p \mathbf{S}| + |\mathbf{W}_I \mathbf{T}_I| < 1, \forall \omega \end{aligned} \quad (3.91)$$

where  $\mathbf{T}_1$  is the closed-loop transfer function from reference signal  $r$  to output  $y - y_d$  as follows

$$\mathbf{T}_1 = \mathbf{I} - \mathbf{S} = \frac{\mathbf{G}_{\text{norm}} \mathbf{K}_h}{(\mathbf{I} + \mathbf{G}_{\text{norm}} \mathbf{K}_h)}. \quad (3.92)$$

Because the output  $y - y_d$  is a poppet displacement error between the actual value and the desired value, this reference signal is treated as zero.

### 3.5 Nonlinear Controller Design for the Nonlinear System

#### 3.5.1 System Nonlinearities

The nonlinearities in this system can be mainly summarized in three main areas:

- 1) There are inherent nonlinear features of the flow in the poppet system, for examples, the square root relationship in the classical orifice equation for flows across the poppet opening, the spool opening and the fixed-area orifice on the piping channel.
- 2) The bidirectional spool opening side is a very important element with the high nonlinear property. When the spool which is moving along  $+x_v$  direction goes across the poppet symmetrical center line, the right-side opening will connect the nose-side pressure  $P_1$  with the control chamber. When the spool which is moving along  $-x_v$  direction goes across the symmetrical center line, the left-side opening will connect the back-side pressure  $P_2$  with the control chamber. Therefore, every time when the spool crosses the central point, the

flow will instantly change its fluid characteristics. This pressure nonlinearity plays a significant role in the control law.

3) Bidirectional movements of flows across the poppet opening, the spool opening and the fixed-area orifice in the pipeline due to pressure drop changes, for example  $P_1 - P_2$ ,  $P_1 - P_c$ ,  $P_c - P_2$  and  $P_2 - P_k$ . Actually, this nonlinear item is not considered in this study, because it is not allowed that the pressure drops change from positive values to negative values in the operating process. The pressure drops are either positive or negative under sample working conditions.

### 3.5.2 Control Law

Lyapunov's direct method gives the following theorem to prove global stability for the overall system.

Theorem [15]: *Assume that there exists a scalar function  $V$  of the state  $\mathbf{x}$ , with continuous first order derivative such that*

- 1)  $V(\mathbf{x})$  is positive definite
- 2)  $\dot{V}(\mathbf{x})$  is negative definite
- 3)  $V(\mathbf{x}) \rightarrow \infty$  as  $\|\mathbf{x}\| \rightarrow \infty$

*then the equilibrium at the origin is globally asymptotically stable.*

If a scalar function  $V(\mathbf{x})$  which satisfies the above requirements can be found, the globally asymptotical stability of the system can be guaranteed. The tracking performance problem in this research can be achieved by making system variable errors approach zero. Therefore the above stability theorem can be used to prove system stability here.

From Chapter 2, the nonlinear governing equations for open-loop poppet-valve system can be summarized as follows

$$m\ddot{y} + C_{eff}\dot{y} + K_{eff}y - K_{jq}y_d = (A - K_{fct})P_1 + A_{eff}P_2 - A_cP_c + \rho LK_c\dot{P}_2, \quad (3.93)$$

$$\frac{V_L}{\beta}\dot{P}_2 = Q + K_2(P_c - P_2) - Q_L - KP_2 - Q_c\delta P_c, \quad (3.94)$$

$$\delta P_c = \begin{cases} 0 & x_v \geq 0 \\ 1 & x_v < 0 \end{cases}, \quad (3.95)$$

$$Q = \pi D y \sin(\theta) C_d \sqrt{\frac{2}{\rho}} |P_1 - P_2| \text{sign}(P_1 - P_2), \quad (3.96)$$

$$Q_L = A_k C_d \sqrt{\frac{2}{\rho}} |P_2 - P_k| \text{sign}(P_2 - P_k), \quad (3.97)$$

$$Q_c = h x_v C_d \sqrt{\frac{2}{\rho}} |\delta P| \text{sign}(\delta P), \quad (3.98)$$

$$\delta P = \begin{cases} P_1 - P_c & x_v \geq 0 \\ P_c - P_2 & x_v < 0 \end{cases}, \quad (3.99)$$

$$Q_c - K_2(P_c - P_2) + A_c\dot{y} = 0, \quad (3.100)$$

By substituting the desired values into Equations (3.93), (3.94), (3.96), (3.97) and (3.100), and selecting the control law, the following equations can be given by

$$m\ddot{y}_d + C_{eff}\dot{y}_d + K_{eff}y_d - K_{jq}y_d = (A - K_{fct})P_1 + A_{eff}P_{2d} - A_cP_{cd} + \rho LK_c\dot{P}_{2d}, \quad (3.101)$$

$$\frac{V_L}{\beta}\dot{P}_{2d} = Q_d + K_2(P_{cd} - P_{2d}) - Q_{Ld} - KP_{2d} - Q_c\delta P_c, \quad (3.102)$$



$$\delta P_c = \begin{cases} 0 & x_v \geq 0 \\ 1 & x_v < 0 \end{cases}, \quad (3.103)$$

$$Q_d = \pi D y_d \sin(\theta) C_d \sqrt{\frac{2}{\rho} |P_1 - P_{2d}|} \text{sign}(P_1 - P_{2d}), \quad (3.104)$$

$$Q_{Ld} = A_k C_d \sqrt{\frac{2}{\rho} |P_{2d} - P_k|} \text{sign}(P_{2d} - P_k), \quad (3.105)$$

$$Q_c - K_2 (P_{cd} - P_{2d}) + A_c \dot{y}_d = 0, \quad (3.106)$$

and the control law is given by

$$x_v = \frac{K_2 (P_c - P_2) - A_c \dot{y}_d - K_p (y_d - y) - K_I \int (y_d - y) dt}{h C_d \sqrt{\frac{2}{\rho} |\delta P|} \text{sign}(\delta P)}, \quad (3.107)$$

$$\delta P = \begin{cases} P_1 - P_c & x_v \geq 0 \\ P_c - P_2 & x_v < 0 \end{cases}. \quad (3.108)$$

The similar control law was introduced in [1]. However, the integral item of the poppet displacement error is included to cancel the steady-state error. The method by which it is derived and why it is proven to be useful to the poppet system with the simple back-side operating condition are presented in this study. This control law is mainly a combination of a PI controller and nonlinear pressure compensation. Therefore, the proportional gain  $K_p$  and the integral gain  $K_I$  are positive numbers, i.e.

$$K_p > 0, \text{ and } K_I > 0 \quad (1.109)$$

Substituting Equations (3.98) and (3.107) into Equation (3.100) and differentiating the results produce

$$A_c \Delta \ddot{y} + K_p \Delta \dot{y} + K_I \Delta y = 0, \quad (3.110)$$

where  $\Delta \ddot{y} = \ddot{y}_d - \ddot{y}$ ,  $\Delta \dot{y} = \dot{y}_d - \dot{y}$ ,  $\Delta y = y_d - y$ . It is obvious that  $K_p > 0, K_I > 0$  can guarantee its stability.

Subtracting Equations (3.93), (3.94), (3.95), (3.96), (3.97) and (3.100) from Equations (3.101), (3.102), (3.103), (3.104), (3.105) and (3.106) correspondingly produces

$$m \Delta \ddot{y} + C_{eff} \Delta \dot{y} + K_{eff} \Delta y = \rho L K_c \Delta \dot{P}_2 + A_{eff} \Delta P_2, \quad (3.111)$$

$$\frac{V_L}{\beta} \Delta \dot{P}_2 = \Delta Q - (K_2 + K) \Delta P_2 - \Delta Q_L, \quad (3.112)$$

$$\Delta Q = \pi D \sin(\theta) C_d \sqrt{\frac{2}{\rho}} \left( y_d \sqrt{|P_1 - P_{2d}|} \text{sign}(P_1 - P_{2d}) - y \sqrt{|P_1 - P_2|} \text{sign}(P_1 - P_2) \right), \quad (3.113)$$

$$\Delta Q_L = A_k C_d \sqrt{\frac{2}{\rho}} \left( \sqrt{|P_{2d} - P_k|} \text{sign}(P_{2d} - P_k) - \sqrt{|P_2 - P_k|} \text{sign}(P_2 - P_k) \right), \quad (3.114)$$

$$\Delta P_2 = -\frac{A_c}{K_2} \Delta \dot{y}, \quad (3.115)$$

where  $\Delta \dot{P}_2 = \dot{P}_{2d} - \dot{P}_2$ ,  $\Delta P_2 = P_{2d} - P_2$ ,  $\Delta Q = Q_d - Q$ ,  $\Delta Q_L = Q_{Ld} - Q_L$ .

It is assumed that  $\text{sign}(P_1 - P_2) = \text{sign}(P_1 - P_{2d})$  and  $\text{sign}(P_2 - P_k) \text{sign}(P_{2d} - P_k)$ .

Then, the following equations can be derived as

$$\begin{aligned}\Delta Q &= \pi D \sin(\theta) C_d \sqrt{\frac{2}{\rho}} \left( \frac{-y_d \Delta P_2}{\sqrt{|P_1 - P_{2d}|} + \sqrt{|P_1 - P_2|}} + \Delta y \sqrt{|P_1 - P_2|} \operatorname{sign}(P_1 - P_2) \right) \\ &= K_Q \left( \frac{-y_d \Delta P_2}{\sqrt{|P_1 - P_{2d}|} + \sqrt{|P_1 - P_2|}} + \Delta y \sqrt{|P_1 - P_2|} \operatorname{sign}(P_1 - P_2) \right)\end{aligned}\quad (3.116)$$

where the constant  $K_Q$  can be given by

$$K_Q = \pi D \sin(\theta) C_d \sqrt{\frac{2}{\rho}}, \quad (3.117)$$

$$\Delta Q_L = A_k C_d \sqrt{\frac{2}{\rho}} \frac{\Delta P_2}{\sqrt{|P_{2d} - P_k|} + \sqrt{|P_2 - P_k|}} = K_{QK} \Delta P_2, \quad (3.118)$$

where the constant  $K_{QK}$  can be given by

$$K_{QK} = \frac{A_k C_d}{\sqrt{|P_{2d} - P_k|} + \sqrt{|P_2 - P_k|}} \sqrt{\frac{2}{\rho}}. \quad (3.119)$$

Differentiating Equation (3.115) with time produces

$$\Delta \dot{P}_2 = -\frac{A_c}{K_2} \Delta \dot{y}. \quad (3.120)$$

### 3.5.3 Lyapunov Function and Globally Asymptotical Stability

The equilibrium positions for the above error dynamics system are zeros, that is, all errors finally need to approach zeros. The following Lyapunov function is chosen to verify the system stability

$$V = \frac{1}{2} \left( \frac{V_L}{\beta} \Delta P_2^2 + K_y K_I \Delta y^2 + K_y A_c \Delta \dot{y}^2 \right), \quad (3.121)$$

where  $K_y$  is a pending positive constant which will be decided in the following analysis.

It is obvious that  $V(\mathbf{x}) > 0$ , for  $\mathbf{x} \neq 0$ ,  $V(\mathbf{x}) = 0$ , for  $\mathbf{x} = 0$  and  $V(\mathbf{x}) \rightarrow \infty$ , when  $\|\mathbf{x}\| \rightarrow \infty$ ,

where  $\mathbf{x} = [\Delta y, \Delta \dot{y}, \Delta P_2]^T$ . Substituting Equations (3.110) and (3.120) into Equation (3.111) and rearranging the similar items produce

$$\Delta y = \frac{C_{eff} + \frac{A_{eff} A_c}{K_2} - \frac{K_p}{A_c} \left( m + \rho L K_c \frac{A_c}{K_2} \right)}{-K_{eff} + \frac{K_l}{A_c} \left( m + \rho L K_c \frac{A_c}{K_2} \right)} \Delta \dot{y}. \quad (3.122)$$

Differentiating Equation (3.121) produces

$$\dot{V} = \frac{V_L}{\beta} \Delta P_2 \Delta \dot{P}_2 + K_{y1} K_l \Delta y \Delta \dot{y} + K_{y1} A_c \Delta \dot{y} \Delta \ddot{y}. \quad (3.123)$$

Substituting Equations (3.112), (3.116), (3.118) and (3.110) into Equation (3.123) and rearranging items produce

$$\begin{aligned} \dot{V} = & K_Q \sqrt{|P_1 - P_2|} \text{sign}(P_1 - P_2) \Delta y \Delta P_2 \\ & - \left( \frac{K_Q y_d}{\sqrt{|P_1 - P_{2d}|} + \sqrt{|P_1 - P_2|}} + K + K_2 + K_{QK} \right) \Delta P_2^2 - K_y K_\rho \Delta \dot{y}^2. \end{aligned} \quad (3.124)$$

By substituting Equations (3.115) and (3.122), the first item in the right side of the above equation can be altered as follows

$$\begin{aligned} K_Q \sqrt{|P_1 - P_2|} \text{sign}(P_1 - P_2) \Delta y \Delta P_2 &= -\frac{A_c}{K_2} K_Q \sqrt{|P_1 - P_2|} \text{sign}(P_1 - P_2) \Delta y \Delta \dot{y} \\ &= \frac{A_c K_Q \left[ C_{eff} + \frac{A_{eff} A_c}{K_2} - \frac{K_p}{A_c} \left( m + \rho L K_c \frac{A_c}{K_2} \right) \right]}{K_2 \left[ K_{eff} - \frac{K_l}{A_c} \left( m + \rho L K_c \frac{A_c}{K_2} \right) \right]} \sqrt{|P_1 - P_2|} \text{sign}(P_1 - P_2) \Delta \dot{y}^2 \end{aligned} \quad (3.125)$$

Substituting Equation (3.125) into Equation (3.124) and choosing the positive constant  $K_y$  which satisfies the following equation can maintain that  $\dot{V} < 0$  always exists

$$K_y > \frac{A_c K_Q \left[ C_{eff} + \frac{A_{eff} A_c}{K_2} - \frac{K_P}{A_c} \left( m + \rho L K_c \frac{A_c}{K_2} \right) \right]}{K_2 K_P \left[ K_{eff} - \frac{K_I}{A_c} \left( m + \rho L K_c \frac{A_c}{K_2} \right) \right]} \sqrt{|P_1 - P_2|} \text{sign}(P_1 - P_2). \quad (3.126)$$

It is obvious that the following equation needs to be met to support the above requirement.

$$K_I \neq \frac{K_{eff} A_c}{m + \rho L K_c \frac{A_c}{K_2}}. \quad (1.127)$$

Otherwise the right side of the inequality equation will be infinite. And it is impossible to get the positive constant  $K_y$ . Therefore, according to Lyapunov theorem and considering Equations (1.109), (3.126) and (1.127), it can be summarized that choosing the following positive  $K_y$  can guarantee the globally asymptotical stability of the closed-loop poppet-valve system with the nonlinear controller

$$K_y > \max \left( 0, \frac{A_c K_Q \left[ C_{eff} + \frac{A_{eff} A_c}{K_2} - \frac{K_P}{A_c} \left( m + \rho L K_c \frac{A_c}{K_2} \right) \right]}{K_2 K_P \left[ K_{eff} - \frac{K_I}{A_c} \left( m + \rho L K_c \frac{A_c}{K_2} \right) \right]} \sqrt{|P_1 - P_2|} \text{sign}(P_1 - P_2) \right) \quad (3.128)$$

$$K_P > 0$$

$$K_I > 0, \text{ and } \neq \frac{K_{eff} A_c}{m + \rho L K_c \frac{A_c}{K_2}}$$

### 3.6 Summary

In this chapter, the control designs that are based on either the linear system or the nonlinear system are presented. Four control methods are introduced to construct the closed-loop systems: modified PI control, LQG control,  $H_\infty$  control and nonlinear feedback control. The basic requirements of proportional and integral gains in PI control are derived. The elementary procedures of control designs are expounded. With the help of Matlab and Simulink, the simulation results of the closed-loop systems will be obtained in the next chapter. The regulation and tracking behavior of the nonlinear systems armed with the three linear controllers will also be computationally tested in the next chapter.

## CHAPTER 4. SIMULATION RESULTS

### 4.1 Introduction

This chapter can be roughly divided into two important parts. The first part is to examine the effects of key parameters on the open-loop system stability criteria with the help of Mathematica. The second part shows the simulation results to illustrate the dynamic characteristics of systems utilizing Matlab and Simulink. The closed-loop systems are separated into two groups. The first group contains five closed-loop systems that are the full-model linear system with the modified PI controller, the reduced-order linear system with the modified PI controller, the full-model linear system with the LQG controller, the full-model linear system with the  $H_\infty$  controller and the nonlinear system with the nonlinear controller. Another group consists of four nonlinear closed-loop systems that are the nonlinear system with the modified PI controller, the nonlinear system with the LQG controller, the nonlinear system with the  $H_\infty$  controller and the nonlinear system with the nonlinear controller. For the sake of comparison, the results of these two groups of systems are classified into two sets of figures. Both typical regulation and tracking problems are demonstrated and discussed to give a basic view of system performances. All parameter values used in models and calculations are shown in the following two tables: Tables 4-1 and 4-2.

Table 4- 1. Parameters of system operation conditions

Symbol	Description	Value	Units
$P_1$	Nominal Nose-Side Pressure	1) $22(10^6)$ 2) $22(10^6)+5(10^6)*\sin(62.8*t)$	Pa
$P_{2d}$	Nominal Back-Side Pressure	1) $20(10^6)$ 2) $22(10^6)+5(10^6)*\sin(62.8*t)$	Pa
$P_k$	Nominal Load Pressure	$5(10^6)$	Pa
$K$	Pipeline Leakage Coefficient	$10^{-11}$	$m^3/(Pa \cdot s)$
$V_L$	Back-side Chamber Volume	0.00304	$m^3$
$V_{co}$	Control Chamber Volume	9.2e-6	$m^3$
$\beta$	Fluid Bulk Modulus of Elasticity	$1.33365(10^9)$	Pa
$\mu$	Fluid Viscosity	0.01	Pa·s
$C_d$	Orifice Discharge Coefficient	0.62	no unit
$\rho$	Fluid Density	833	$Kg/m^3$
$D_k$	Fixed Orifice Diameter	0.0025	m

Table 4- 2. Poppet parameters

Symbol	Description	Value	Units
$D$	Poppet Port Diameter	0.025	m
$L$	Length of Nose-side Chamber	0.0181	m
$D_c$	Poppet Land Diameter	0.031245	m
$A_c$	Poppet Land Area	$7.667(10^{-4})$	$m^2$
$D_{cbore}$	Poppet-Land Hole Diameter	0.03127	m
$d_c$	Clearance between the Poppet Land and Its Hole	$2.5(10^{-5})$	m
$l_c$	Poppet Metering Length	0.028	m
$m$	Poppet Valve Mass	0.136	Kg
$c$	Poppet Valve Drag Coefficient	18	N·s/m
$k$	Poppet Spring Rate	0	N/m
$\theta$	Poppet Angle	0.785	rad
$K_2$	Leakage Coefficient of Leakage between the Poppet Land and Its Hole	$1.42761(10^{-13})$	$m^3/(Pa \cdot s)$



## 4.2 System Requirements

Two main goals of the controller design are to make the system stable under the bi-direction flowing fluid across the poppet and to improve system performances. It will be shown in the next section that the open-loop system will experience instability when the nominal back-side pressure  $P_{2d}$  is higher than the nominal nose-side pressure  $P_1$ . Even though it can be stable when  $P_{2d}$  is less than  $P_1$ , the open-loop system still has a very slow response. The poppet displacement is the first primary object that is interested in this design, though the control of the back-side pressure is also valuable. The poppet is anticipated to quickly track the desired sine-wave movement with 10 HZ frequency. The phase lag of the actual poppet displacement can not be bigger than 90 degree. The theoretical state-state error of the poppet position is less than 10%. The moving range of the poppet is from 0 mm to 15 mm, while the spool can only move 1 mm away from its central position in bi-directions. For regulation ability, the expecting settling time is less than 30ms.

## 4.3 Influences of Key Parameters on the Open-loop System Stability

This section will display how variations of key parameters take effect on the full-model linear open-loop system stability. Some of them are the sources of system uncertainty that are taken into consideration in the  $H_\infty$  robust analysis, for example fluid bulk modulus  $\beta$ , orifice discharge coefficient  $C_d$  and spring rate  $k$ . Some of them are working condition varieties, e.g. system pressures. Some of them are system geometry

structures, for instance the back-side chamber volume  $V_L$  and the ratio of section

areas  $rA_c = \frac{A_c}{A}$ . Mathematica results will be presented in the following subsections.

#### 4.3.1 Characteristic Equation of the Full-model Linear Open-loop System

Considering to the linear governing equations for the full-model linear open-loop poppet system in Equations (2.93), (2.94) and (2.95), the 3<sup>rd</sup>-order characteristic equation of the full-model linear open-loop system can be given by

$$a_0s^3 + a_1s^2 + a_2s + a_3 = 0 \quad (4.1)$$

where  $a_0, a_1, a_2$  and  $a_3$  are constants responding to the nominal working conditions as follows

$$a_0 = \frac{mV_L}{\beta} \quad (4.2)$$

$$a_1 = -\frac{mK_2^2}{K_s} + mK_v + \frac{V_L}{\beta} \left( C_{eff} + \frac{A_c^2}{K_s} \right) - \frac{A_cK_2\rho LK_c}{K_s} \quad (4.3)$$

$$a_2 = \left( C_{eff} + \frac{A_c^2}{K_s} \right) K_v + K_{eff} \frac{V_L}{\beta} - \frac{K_2}{K_s} \left( C_{eff}K_2 + A_cA_{eff} \right) - \rho LK_cK_{qt} \quad (4.4)$$

$$a_3 = K_{qt} \left( -A_{eff} + \frac{A_cK_2}{K_s} \right) - \frac{K_2^2K_{eff}}{K_s} + K_{eff}K_v \quad (4.5)$$

#### 4.3.2 Non-Dimension Stability Criteria of the Full-model Linear Open-loop System

According to Routh-Hurwitz stability criterion, four stability criteria of this third-order system are given as

$$a_0, a_1, a_2, a_3 > 0 \text{ and } a_1 a_2 > a_0 a_3. \quad (4.6)$$

The scaled stability criteria can help us investigate how system dynamic behavior can be brought out under variations. The following non-dimension stability criteria of the full-model linear open-loop system can be given by

$$StN_1 = \frac{a_1}{|mK_v|}, \quad (4.7)$$

$$StN_2 = \frac{a_2}{|C_{eff}K_v|}, \quad (4.8)$$

$$StN_3 = \frac{a_3}{|K_{eff}K_v|}, \quad (4.9)$$

$$StN_4 = StN_1 StN_2 - \left| \frac{K_{eff}V_L}{C_{eff}K_v\beta} \right| StN_3. \quad (4.10)$$

The stability criteria mentioned in the following sections are all pointed to dimensionless stability criteria.

#### 4.3.3 System Pressures $P_1, P_{2d}$

Two sets of the nominal nose-side pressure  $P_1$  and the nominal back-side pressure  $P_{2d}$  are picked out to dig out their influences on system stability. The first set of the ranges of  $P_1$  and  $P_{2d}$  can be respectively given from  $22(10^6)$  Pa to  $35(10^6)$  Pa and from  $7(10^6)$  Pa to  $21(10^6)$  Pa. The nominal piping pressure  $P_k$  is  $5(10^6)$  Pa. Other parameters and working conditions can be kept as shown in Table 4-1 and 4-2. The

results are shown in Figure 4-1. F-M O-L means full-model open-loop. The second set of the ranges of  $P_1$  and  $P_{2d}$  can be respectively given from  $10^6$  Pa to  $14(10^6)$  Pa and from  $15(10^6)$  Pa to  $26(10^6)$  Pa. And the pressure  $P_k$  is changed to be  $27(10^6)$  Pa. The results are shown in Figure 4-2.

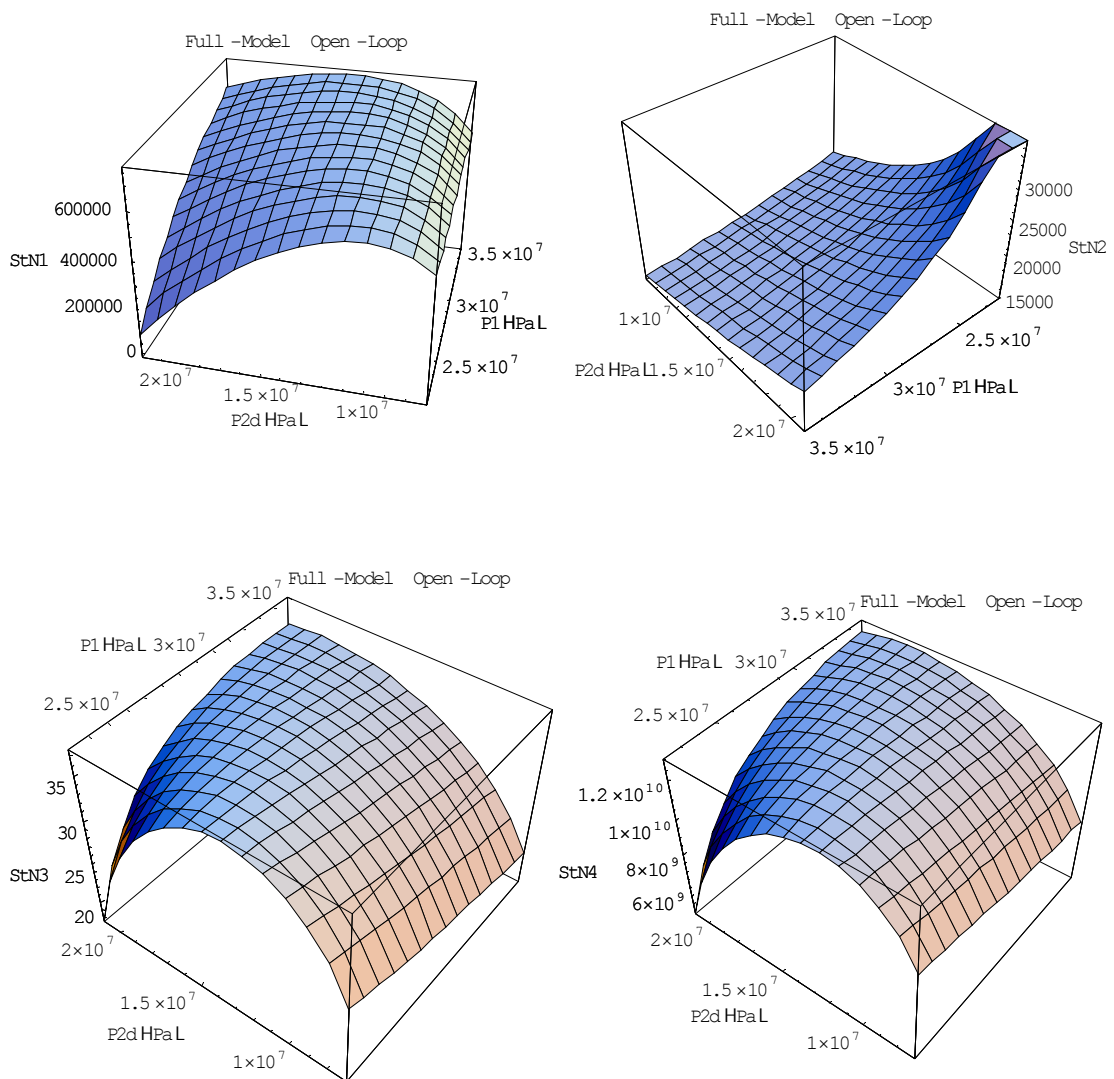


Figure 4-1. F-M O-L system stability criteria for the 1<sup>st</sup> set of working pressures

The most important information that can be got from the above plots is that the system will become unstable when the flow moves from the back-side chamber to the nose-side chamber due to the 3<sup>rd</sup> stability criterion showing to be negative in this case. It can be found out that in  $a_3$ , the power of the first item is at least one greater than those of the other items. This item is related to the transient fluid force due to the poppet velocity.

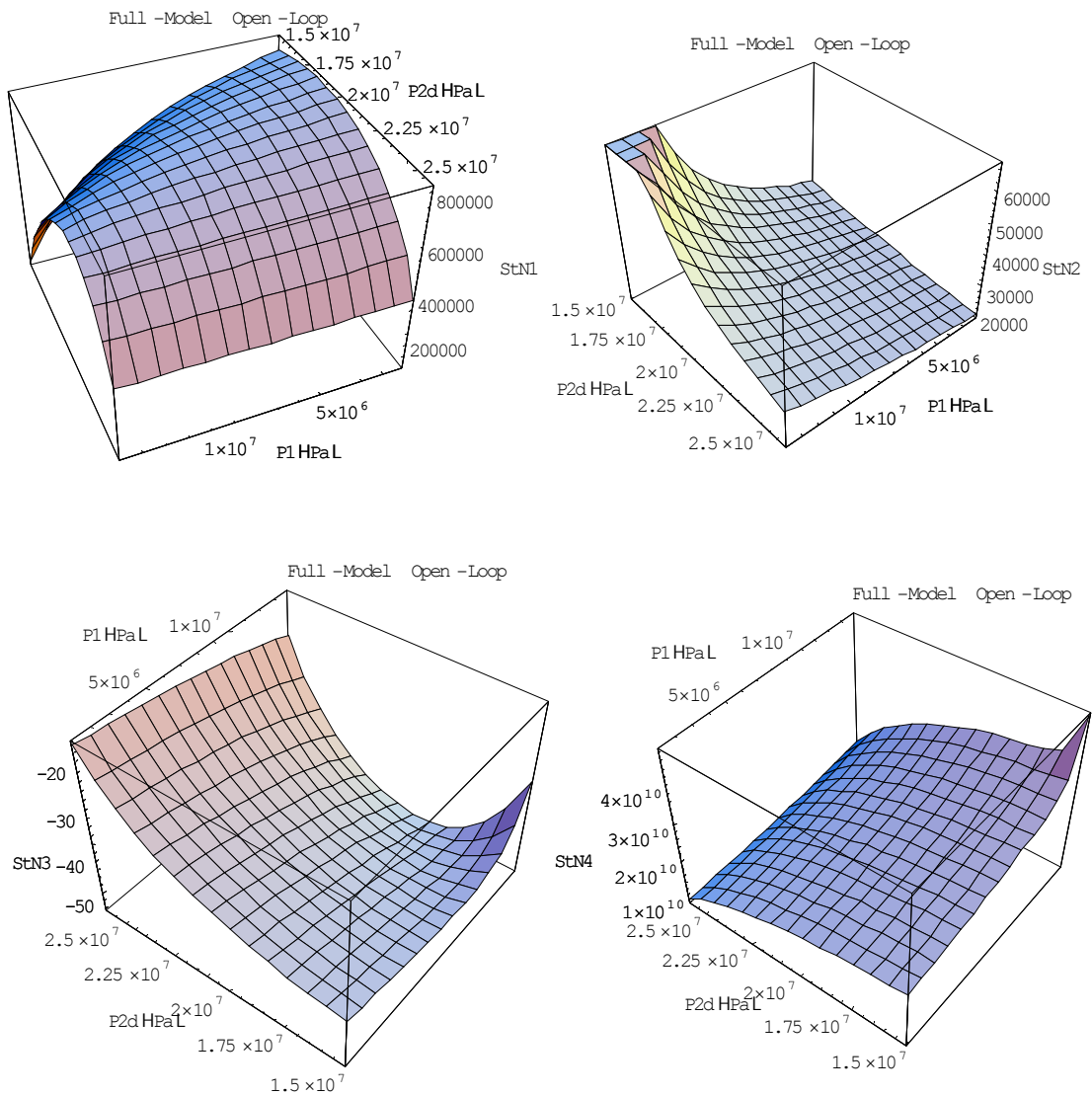


Figure 4-2. F-M O-L system stability criteria for the 2<sup>nd</sup> set of working pressures

Except this, there are no clear trends of the relationships between the pressures and the stability. For instance, when only the change of  $P_{2d}$  is taken into consideration, it shows that in the first case it roughly makes a positive contribution to the system stability while in the second case it, in general, makes the system goes to the unstable side. However, as to  $P_1$ , the effect will be so complicate that it is hard to draw a conclusion that it gives either positive or negative influences on the system stability.

#### 4.3.4 Leakage Coefficients $K_2, K$

The system leakage always plays an important role to affect system dynamics. The two main leakages (the leakage across the poppet land and the hole that contains it, and the leakage occurring in the back-side delivery line) that have close relations to load conditions are primarily considered. Two sets of the nominal nose-side pressure  $P_1$  and the nominal back-side pressure  $P_{2d}$  are picked out to dig out leakage influence on stability. There are named as Case 1 and Case 2. In Case 1, the set of the system pressures is  $P_1 = 22(10^6) P_a$ ,  $P_{2d} = 20(10^6) P_a$  and  $P_k = 5(10^6) P_a$ . Another pressure set of  $P_1 = 5(10^6) P_a$ ,  $P_{2d} = 20(10^6) P_a$  and  $P_k = 22(10^6) P_a$  is for Case 2, in which the fluid flows in the reverse direction as that in Case 1. The ranges of leakage coefficient  $K_2$  and  $K$  can be respectively given from  $1.42761(10^{-15}) \text{ m}^3/(P_a \cdot \text{s})$  to  $1.42761(10^{-11}) \text{ m}^3/(P_a \cdot \text{s})$  and from  $10^{-13} \text{ m}^3/(P_a \cdot \text{s})$  to  $10^{-9} \text{ m}^3/(P_a \cdot \text{s})$ . The upper limit is 100 times of the original value, while the lower limit is one hundredth of the original value. The results are shown respectively in Figure 4-3 and Figure 4-4.

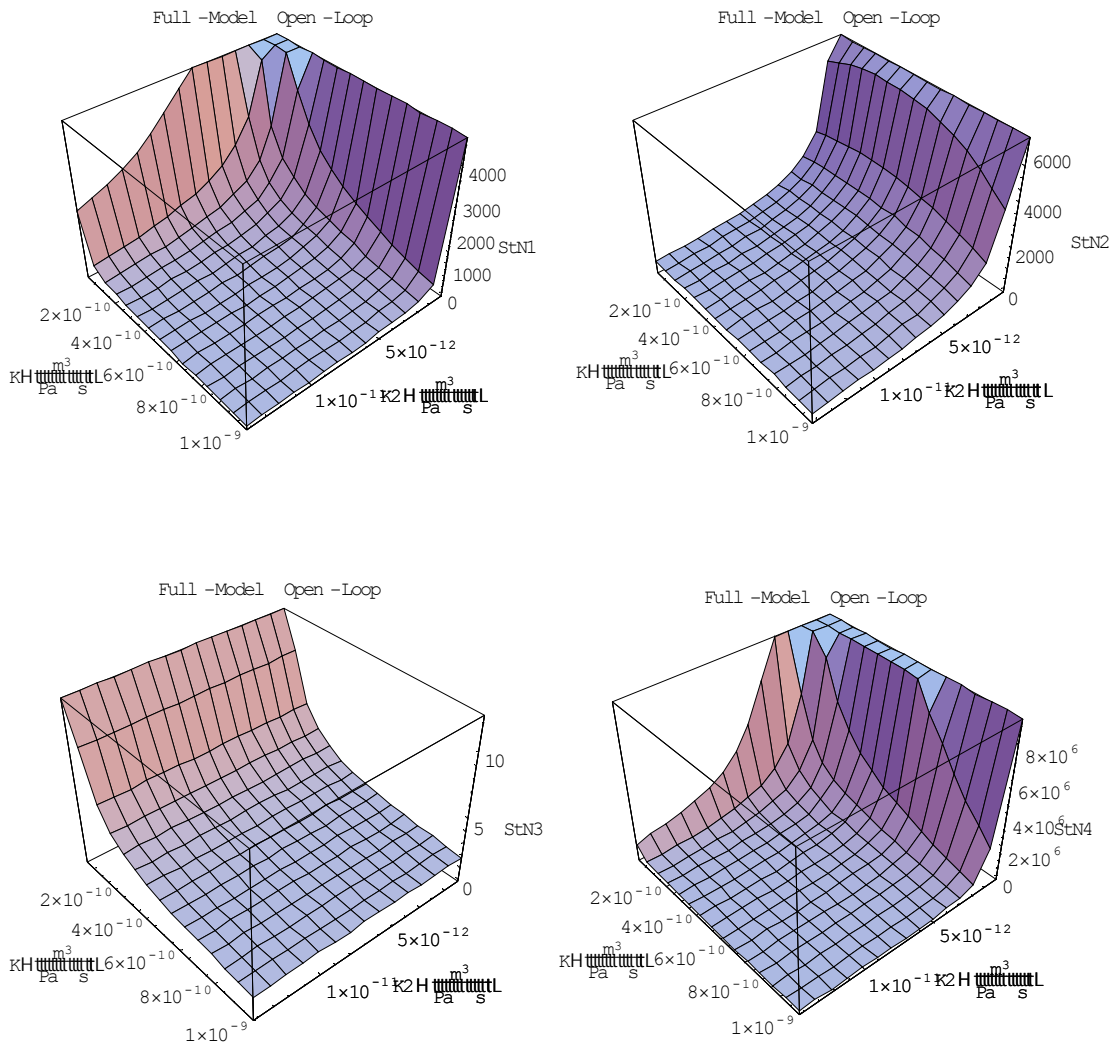


Figure 4-3. F-M O-L system stability criteria for Case 1 of leakage coefficients

It is always demonstrated that the 3<sup>rd</sup> criterion goes to be negative in Case 2 from Figure 4-4. In the Case 1, the system stability will go to the negative direction when  $K_2$  increases. In Case 2, the increase of  $K_2$  will make the 1<sup>st</sup>, 2<sup>nd</sup> and 4<sup>th</sup> criteria decrease and slowly increase the 3<sup>rd</sup> criterion though it is still negative. The change of  $K$  always have little effects on the 1<sup>st</sup>, 2<sup>nd</sup> and 4<sup>th</sup> criteria, except make the 3<sup>rd</sup> one decreases in Case 1

and increases in Case 2. It can be summarized that the increase of  $K_2$  and  $K$  will make the decrease of the absolute value of the 3<sup>rd</sup> criterion. Considering the minus sign is introduced by the flow gain  $K_{qt}$ , a surprising conclusion may be drawn that the increase of  $K_2$  and  $K$  will slow down the system stability, though in the common sense, it helps stability.

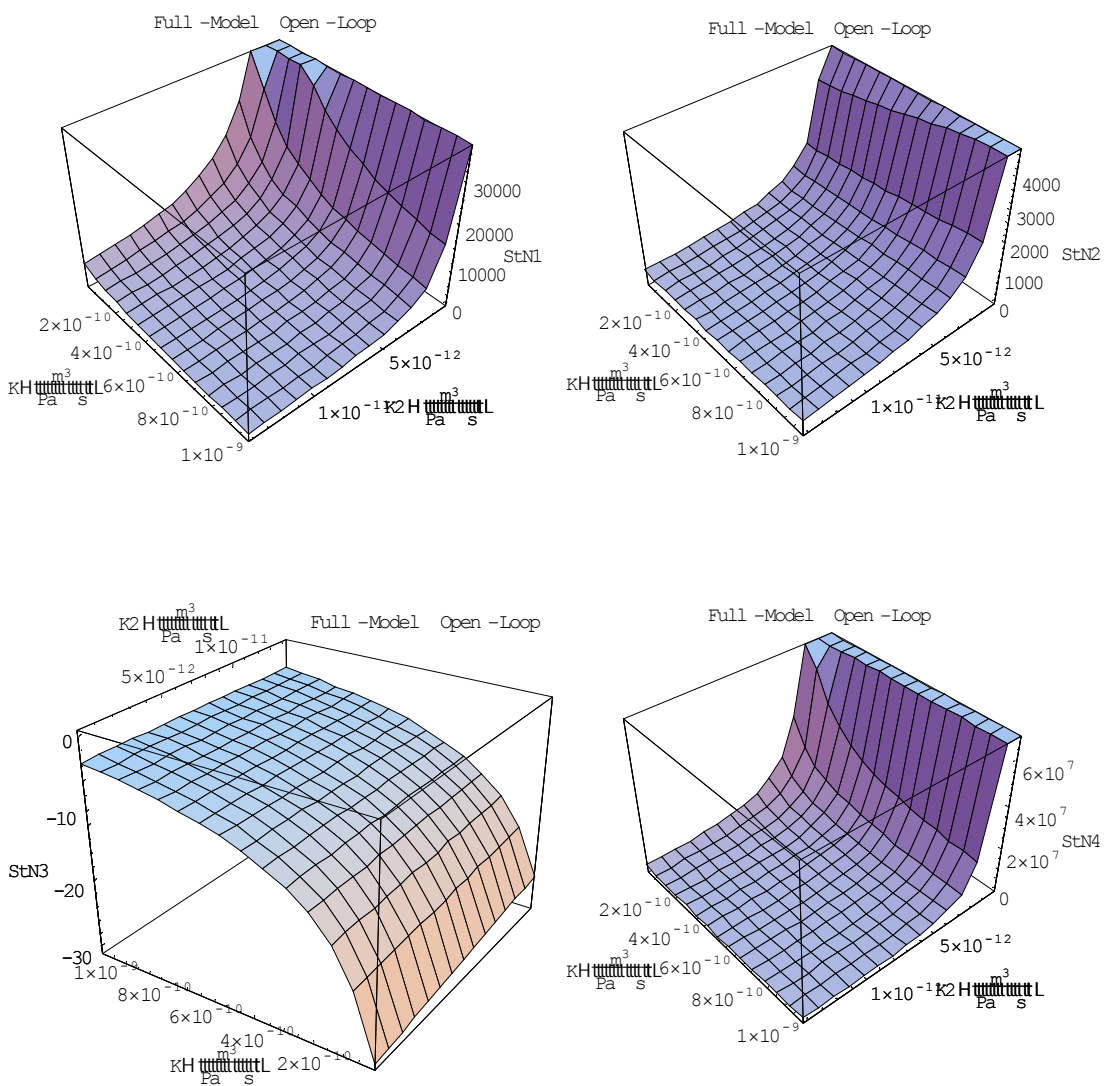


Figure 4-4. F-M O-L system stability criteria for Case 2 of leakage coefficients



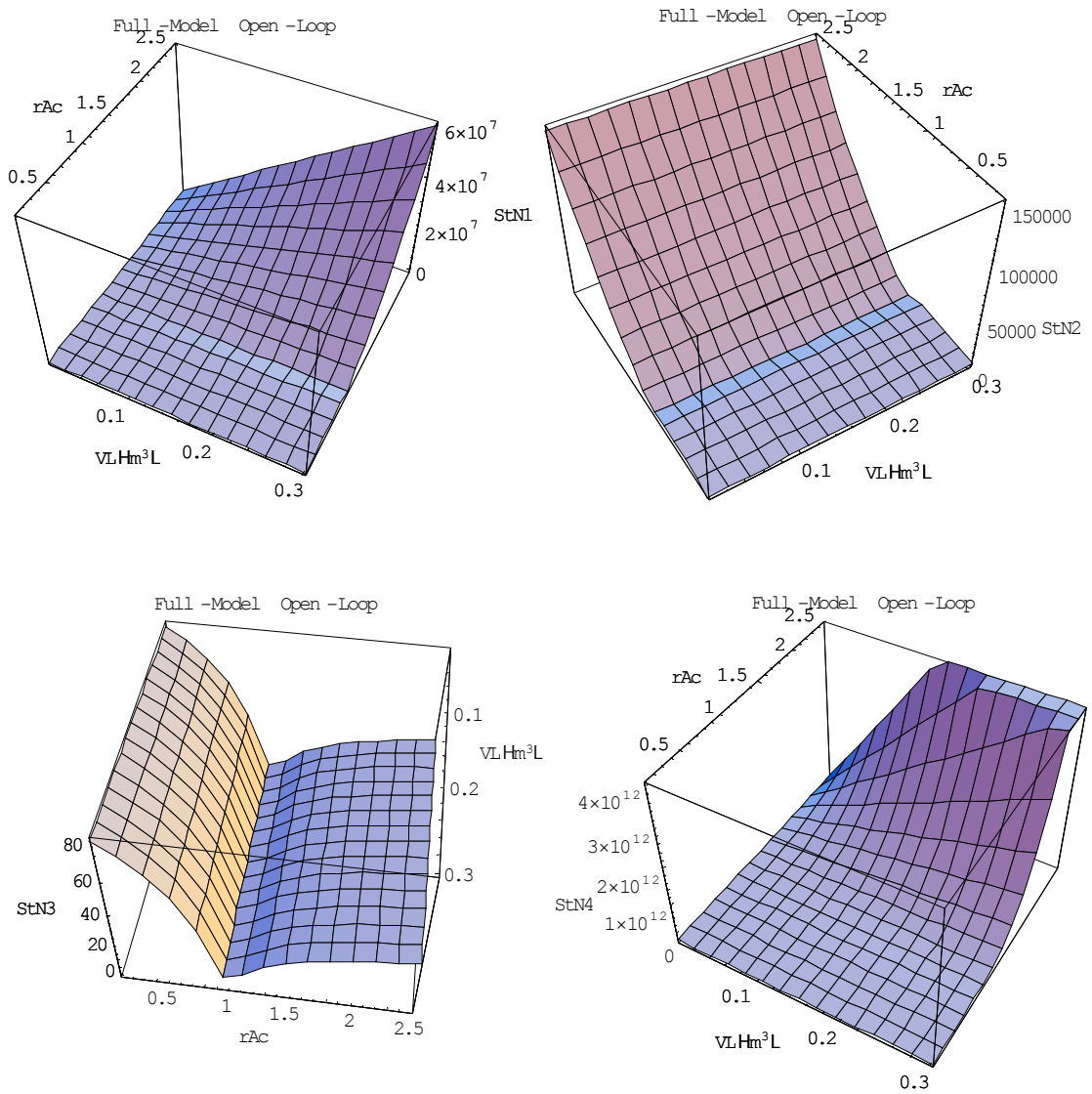


Figure 4-5. F-M O-L system stability criteria for Case 1 of system geometries

#### 4.3.5 System Geometries $V_L, rA_c$

Two important structure geometries are studied as stability factors: the back-side volume  $V_L$  and the ratio of the poppet land cross-section area and the cross-section area

of the poppet port  $rA_c = \frac{A_c}{A}$ . Two sets of the nominal nose-side pressure  $P_1$  and the nominal back-side pressure  $P_{2d}$  that are picked out to fulfill this analysis are same as those in the previous subsection. The ranges of the back-side volume  $V_L$  and the ratio  $rA_c$  can be respectively given from  $3.04(10^{-5}) \text{ m}^3$  to  $3.04(10^{-1}) \text{ m}^3$  and from 0.1 to 2.5. The ratio changes based on that the poppet port area is kept as constant. The results are shown respectively in Figure 4-5 and Figure 4-6.

The static change of back-side volume has almost no effect on the system stability when the area ratio is small. When the area ratio becomes big, the volume growth will make the system more stable. That is because when the fluid system has a constant compressible capability, the total pressure change required by a same volume change in a bigger fluid chamber falls off. Therefore, generally speaking, a larger back-side chamber can make the system more stable. Figures 4-5 and 4-6 shows that the increase of area ratio will has the unfavorable influence on the 3<sup>rd</sup> stability criterion in both Case 1 and Case 2, though it generally make the values of the 1<sup>st</sup>, 2<sup>nd</sup> and 4<sup>th</sup> stability criteria go up. In Case 1, when the value of the area ratio is rising, the 3<sup>rd</sup> criterion decreases first; after the poppet land has the same cross-section area as that of the poppet port, it increases. It has the same trend for the absolute value of the 3<sup>rd</sup> criterion and is negative in Case 2.

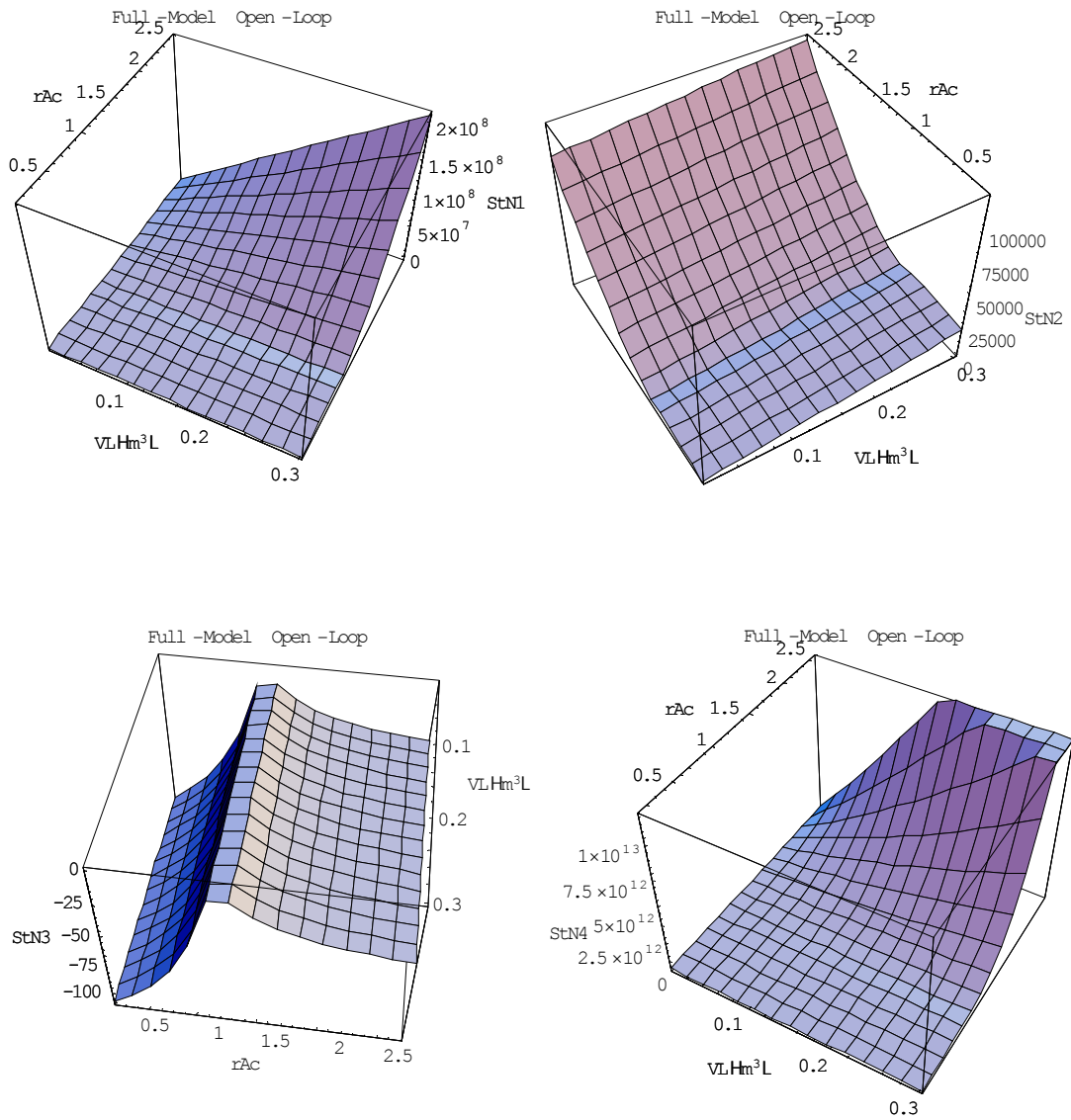


Figure 4-6. F-M O-L system stability criteria for Case 2 of system geometries

#### 4.3.6 Fluid Properties $\beta, C_d$

Fluid bulk modulus of elasticity  $\beta$  and orifice coefficient  $C_d$  are investigated as the potential changing sources of fluid properties. The basic working pressures are same as the previous two subsections. The ranges of fluid bulk modulus  $\beta$  and the orifice

coefficient  $C_d$  can be respectively given from  $1333.65(10^4)$  Pa to  $1333.65(10^8)$  Pa and from 0.2 to 1. The results are shown respectively in Figure 4-7 and Figure 4-8. “beta” means  $\beta$ .

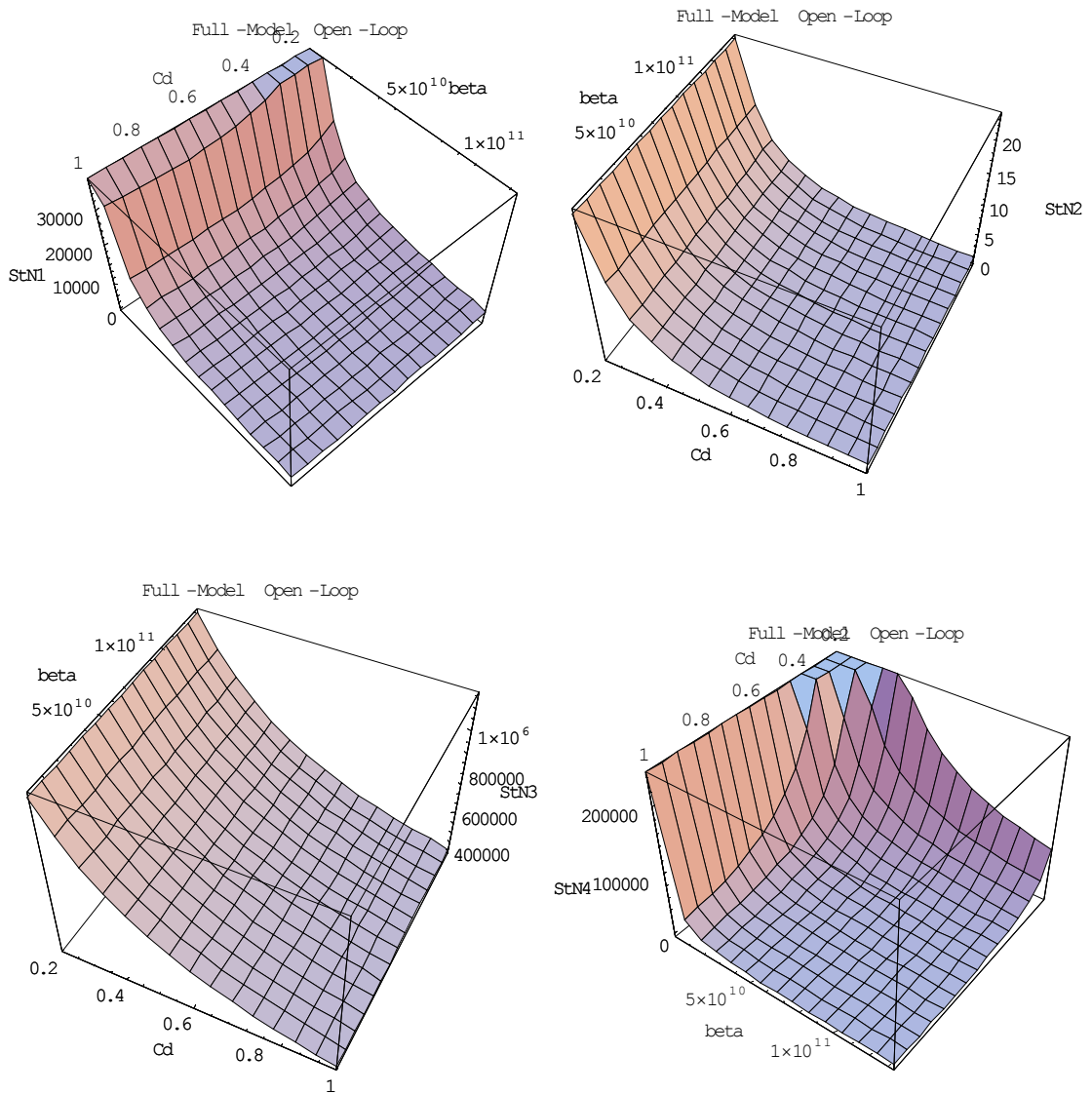


Figure 4-7. F-M O-L system stability criteria for Case 1 of fluid properties

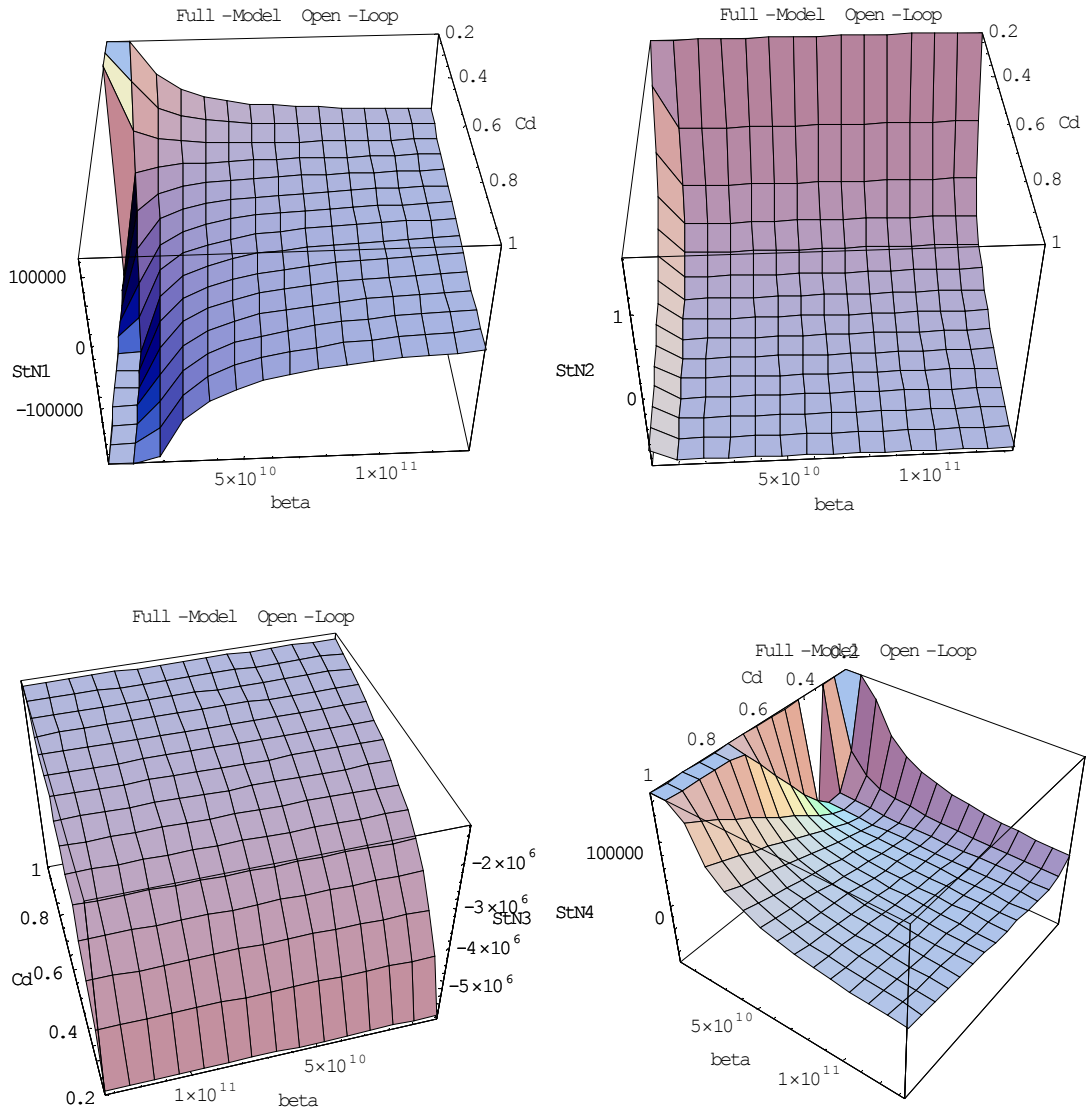


Figure 4-8. F-M O-L system stability criteria for Case 2 of fluid properties

Bulk modulus  $\beta$ , namely isothermal fluid bulk modulus, is the measure of a system's resistant ability to a given amount of uniform external pressure. Orifice coefficient  $C_d$  basically accounts for the effect of the orifice geometry on the relationship between the pressure and the fluid velocity. It is illustrated from Figures 4-7 and 4-8 that the increase of  $C_d$  will cause the decrease of the absolute value of the 3<sup>rd</sup> criterion. On

the whole, both  $\beta$  and  $C_d$  can be treated as negative causes of the system stability, although the increase of  $\beta$  at big  $C_d$  makes the value of the 1<sup>st</sup> stability criterion goes up while the increase of  $\beta$  at small  $C_d$  makes it goes down in Case 2. Generally, when  $\beta$  and  $C_d$  increase, the system has the trend to go to the unstable way. There is no surprise to see negative values of the 3<sup>rd</sup> stability criterion in Case 2. However, till now, it is the first time to have negative 1<sup>st</sup> and 2<sup>nd</sup> stability criteria that appears as  $C_d$  is big (shown in Figure 4-8). A big  $\beta$  means that the system has a “softer” elasticity in pressure to the change of fractional volume. A slight relative volume change can cause a bigger pressure recovery capability. It will also be illustrated later in this chapter that  $C_d$  can introduce 30% error of the nominal plant. And probably, it is also related to the increment of the transient flow force.

#### 4.3.7 Spring Rate $k$

The examination of the spring rate  $k$  accompanies with the change of the nominal nose-side pressure  $P_1$ . Though in this dissertation, the spring is not taken into consideration in both system modeling and control design, its effect on the linear open-loop stability criteria is also discussed here. The first set of pressures can be given as  $P_{2d} = 20(10^6)$  Pa,  $P_k = 5(10^6)$  Pa and the range of  $P_1$  can be set from  $22(10^6)$  Pa to  $35(10^6)$  Pa. The second set of pressures can be given as  $P_{2d} = 20(10^6)$  Pa,  $P_k = 22(10^6)$  Pa and the range of  $P_1$  can be selected from  $10^6$  Pa to  $19(10^6)$  Pa. The range of  $k$  can

be respectively given from 0 N/m to  $10^6$  N/m. The results are shown separately in Figure 4-9 and Figure 4-10.

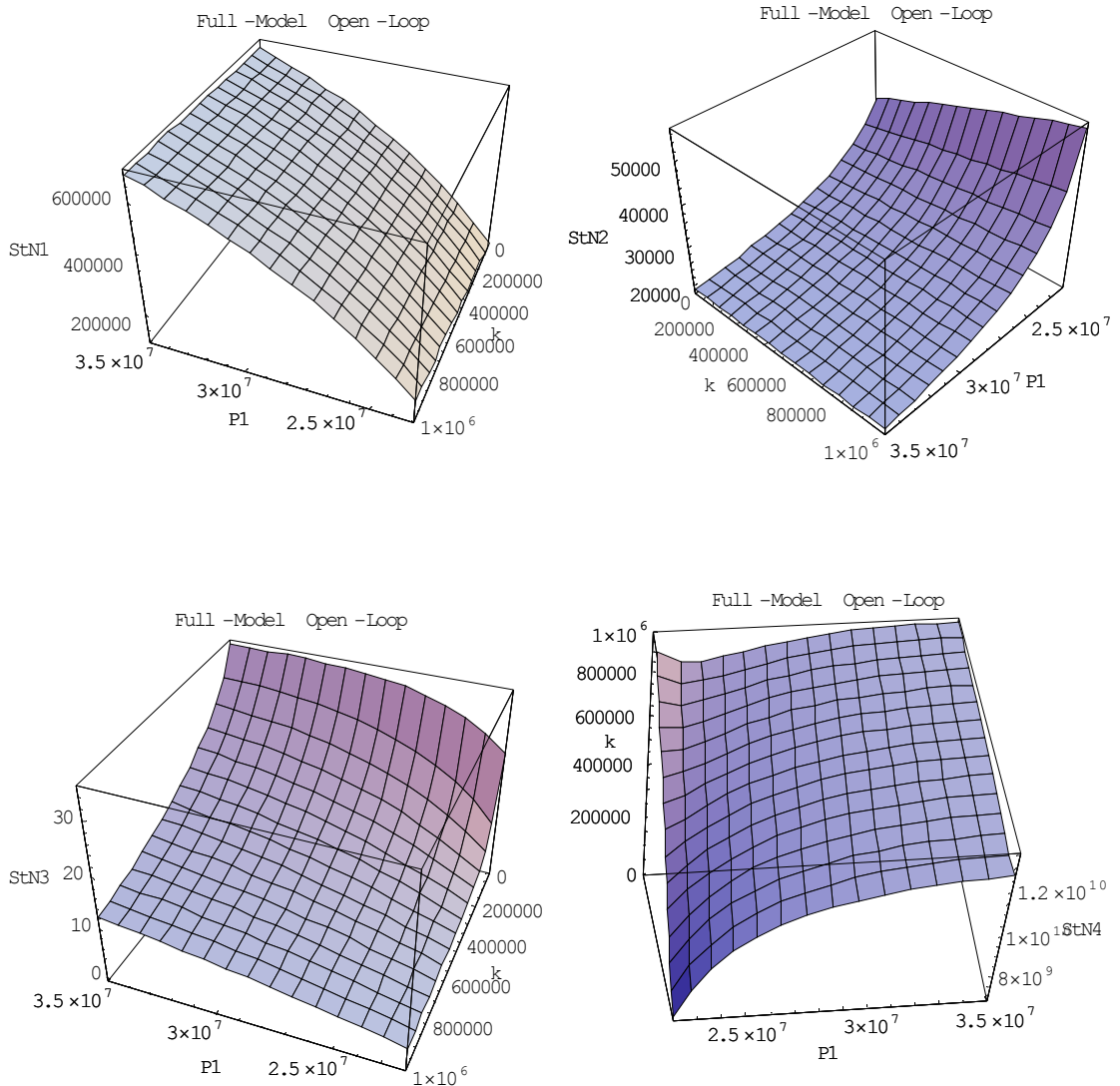


Figure 4-9. F-M O-L system stability criteria for Case 1 of spring rate

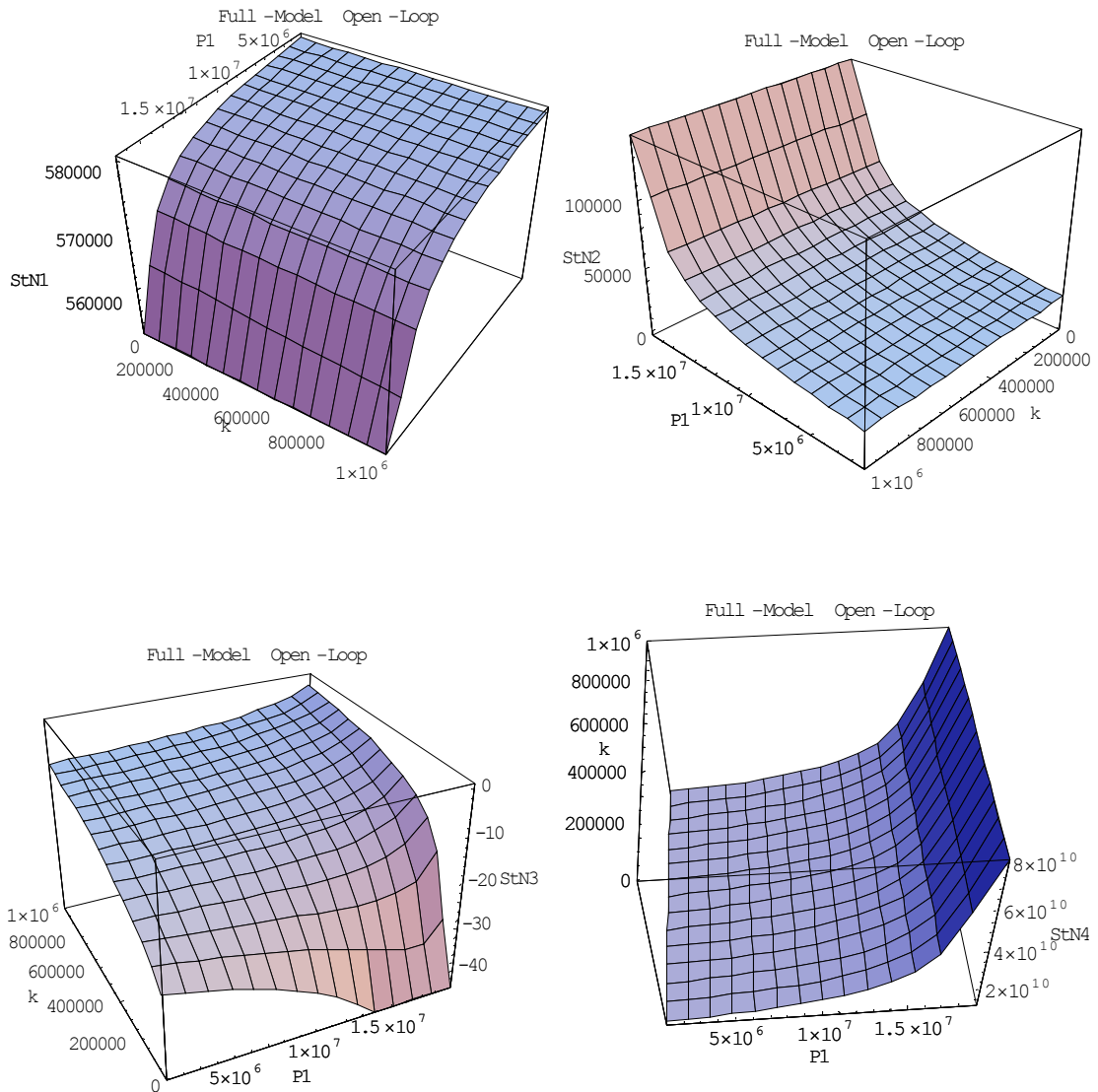


Figure 4-10. F-M O-L system stability criteria for Case 2 of spring rate

According to the results, the effect of the change of the spring rate on the 1<sup>st</sup>, 2<sup>nd</sup> and 4<sup>th</sup> stability criteria is so small to be negligible, except its increase corresponds to the increase of 4<sup>th</sup> stability criterion in Case 1. It roughly can only introduce influence on the 3<sup>rd</sup> stability criterion. A harder spring with a big spring rate  $k$  will provide less stability guarantee under the first set of working pressures. However, it will make the system



tends to be stable under the second pressure case, though the system is still unstable. It is obvious that the spring rate is not the dominant factor of the 3<sup>rd</sup> criterion, because the criterion's sign is mainly decided by THE poppet flow gain  $K_{qt}$ . Therefore, in general, a conclusion can be drawn that the spring rate is a negative factor of the system stability.

#### 4.4 Regulation Problem of Open-loop Systems

Figure 4-11 demonstrates the simulation results for the regulating problem of the full-model linear open-loop system, the reduced-order linear open-loop system and the nonlinear open-loop system. The step response signal is given to investigate the system regulation ability. The set of system pressures are chosen as  $P_1 = 22(10^6)$  Pa,  $P_{2d} = 20(10^6)$  Pa and  $P_k = 5(10^6)$  Pa. The initial conditions for both the full-model linear and reduced-order linear open-loop systems are  $[y - y_d, \dot{y}, P_2 - P_{2d}] = [1.35(10^{-4}), 0, 0]$ . The initial condition for the nonlinear open-loop system is  $[y, \dot{y}, P_2] = [4.6105(10^{-4}), 0, 20(10^6)]$ . The steady-state positions for the poppet and spool are respectively  $1.5795(10^{-6})$  m and  $6.6699(10^{-6})$  m. Only is the small poppet opening investigated, because the instability usually appears when the poppet is crackly opened. The steady-state poppet velocity is assumed as zero.

In Figure 4-11, Nonlinear-\* with the red solid thick line represents variables for the nonlinear system. Fu-\* with the blue dash-dot thick line symbolizes variables for the full-model linear system. Re-\* with the green dash thick line depicts variables for the

reduced-order linear system. The magenta dot line stands for the desired values.  $\dot{y}$

means  $\dot{y} = \frac{dy}{dt}$ . The spool position is considered as a constant input.

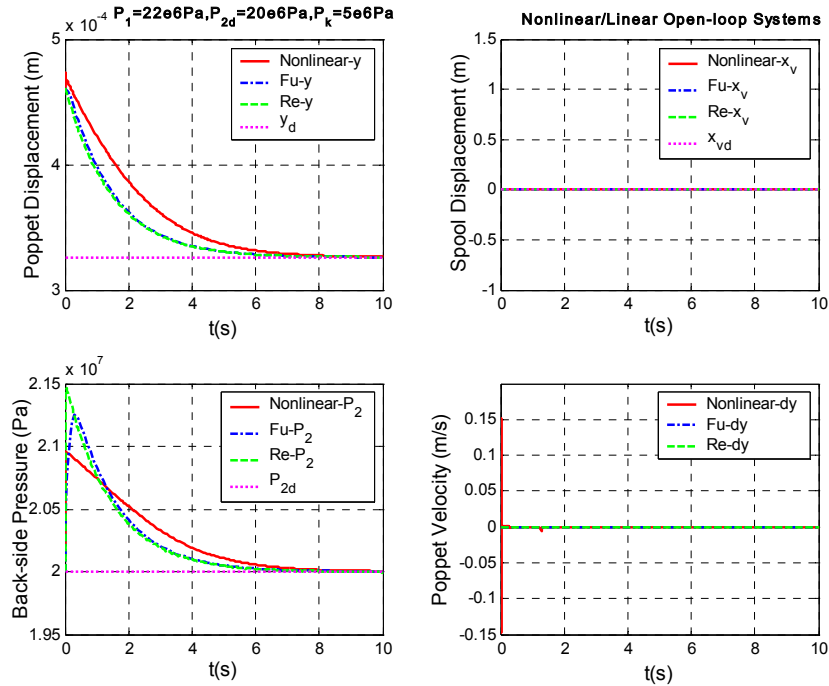


Figure 4-11. Regulation of open-loop systems

It is obvious that the systems can not response promptly. The settling time for the poppet displacement  $y$  and the back-side pressure  $P_2$  is about 6s, which is much larger than the speed requirement. The nonlinear system, in which the time-rate-of-change of control pressure,  $\dot{P}_c$  is considered, is a little bit slower than the linear systems. The flow force on the poppet is linearly simulated in the nonlinear system. It also shows that the performance of the reduced-order linear system matches closely with that of the full-model linear one, which provides another confirmation of evaluating control gains of the modified PI controller according to the reduced-order linear system. The poppet velocity

suffers a serious oscillation in the nonlinear system. Note that although it is not illustrated in the plot, for the case of  $P_1 < P_{2d} < P_k$ , the open-loop systems will become unstable, which is consistent with the negative values of the stability criterion in the parameter analysis section.

#### 4.5 Regulation Problem of the First Group of Closed-loop Systems

The step responses of five closed-loop systems are illustrated in this section: the full-model linear system with the modified PI controller, the reduced-order linear system with the modified PI controller, the full-model linear system with the LQG controller, the full-model linear system with the  $H_\infty$  controller and the nonlinear system with the nonlinear controller. Working pressures, initial condition and steady-state values are same as those in the previous section. Two saturation components are used in all the models to limit the spool displacement ranged from -1 mm to 1 mm and the poppet displacement ranged from 0 mm to 15 mm.

In the PI controller, the proportional gain  $K_p$  is chosen as 0.1 and the integral gain  $K_I$  is chosen as 0.005. The proportional gain  $K_{p2}$ , the integral  $K_{I2}$  and the gain Pressure gain  $K_{pp}$  are constants according to the equilibrium conditions.

In the nonlinear system, a 50 HZ filter is put into the controller to prevent the infinite velocity due to possible sudden step inputs. And a memory component in Simulink is used to recorder the last spool position to judge the opening direction of the control orifice. An integral limitation is activated to restrict the integral accumulation. A saturation component is added to avoid zero pressure drops in the nonlinear controller.

In LQG control design, the flat constant power spectral density matrices  $Q_n, R_n$  are respectively given by

$$\begin{aligned} Q_n &= [\sigma_w^2] = [0.001^2] \\ R_n &= \begin{bmatrix} \sigma_{v_1}^2 & 0 \\ 0 & \sigma_{v_2}^2 \end{bmatrix} = \begin{bmatrix} 0.001^2 & 0 \\ 0 & 100^2 \end{bmatrix}. \end{aligned} \quad (4.11)$$

The weight matrices  $Q, R$  for getting reasonable LQ regulator are selected as

$$\begin{aligned} Q &= \begin{bmatrix} 1/q_1^2 & 0 & 0 \\ 0 & 1/q_2^2 & 0 \\ 0 & 0 & 1/q_3^2 \end{bmatrix} = \begin{bmatrix} 1/0.1^2 & 0 & 0 \\ 0 & 1/100^2 & 0 \\ 0 & 0 & 1/(6(10^7))^2 \end{bmatrix}, \\ R &= [8] \end{aligned} \quad (4.12)$$

In  $H_\infty$  control design, the system uncertainties come from three parameters: fluid bulk modulus  $\beta$ , orifice coefficient  $C_d$  and the spring rate  $k$ . Their ranges are given respectively from  $0.67 \times 1333.65(10^6)$  Pa to  $1.37 \times 1333.65(10^6)$  Pa, from 0.52 to 0.72, and from 0 to 6500 N/m. The plots according to the uncertainty form of Equation (3.56) are shown in Figure 4-12. The orifice coefficient  $C_d$  carries the biggest uncertainty, followed by the spring rate  $k$  and fluid bulk modulus  $\beta$ . The uncertainty weight function  $W_I$  (red line shown in Figure 4-12) can be given according to Equation (3.57) as follows

$$W_I(s) = \frac{0.168s^3 + 12.887s^2 + 18.334s + 5.653}{s^3 + 75.398s^2 + 75.736s + 19.106}. \quad (4.13)$$

The weight functions  $W_p$  and  $W_u$  are chosen as follows

$$W_P = \left[ \frac{(s/\sqrt{2.5} + 20\pi)^2}{(s + 20\pi\sqrt{0.1})^2} \right]. \quad (4.14)$$

$$W_u = [0.01]$$

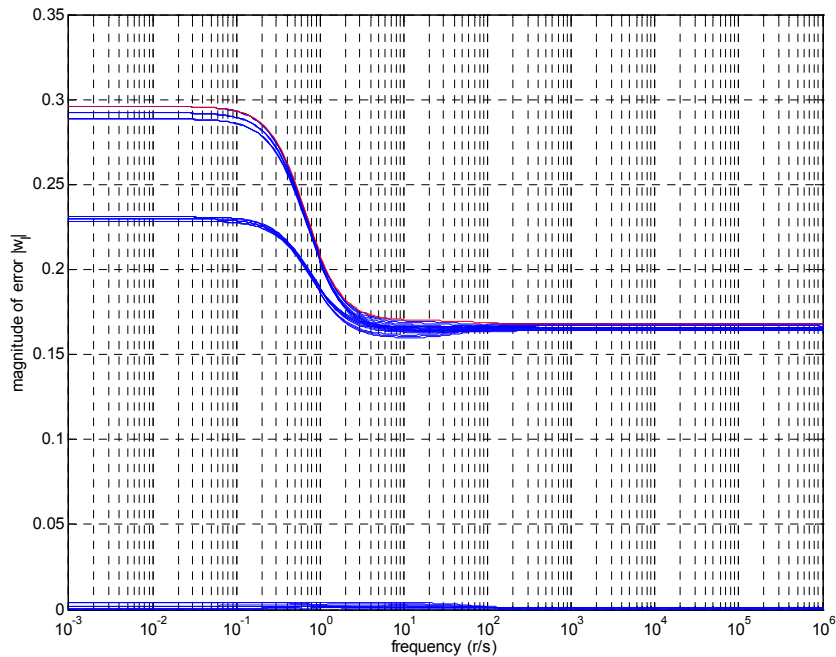


Figure 4-12. Input uncertainty and weight function  $W_f$  (red line) for regulation problem

The sensitivity weight  $W_p$  has a 40 dB/decade slope at the frequencies lower than the bandwidth of 10 Hz. The control weight  $W_u$  restrains the control effort of the spool.

In Figure 4-13 and 4-14, Nonlinear-\* with the red solid thick line represents variables for the nonlinear system with the nonlinear controller. Fu-\* with the blue dash-dot thick line symbolizes variables for the full-model linear system with the modified PI controller. Re-\* with the green dash thick line depicts variables for the reduced-order

linear system with the modified PI controller. The magenta dot line stands for the desired values.  $hinf^*$  with the cyan dash thin line means variables for the full-model linear system with the  $H_\infty$  controller.  $lqg^*$  with the black solid thin line denotes variables for the full-model linear system with the LQG controller. This keeps same in the tracking problem for the first group of closed-loop systems.

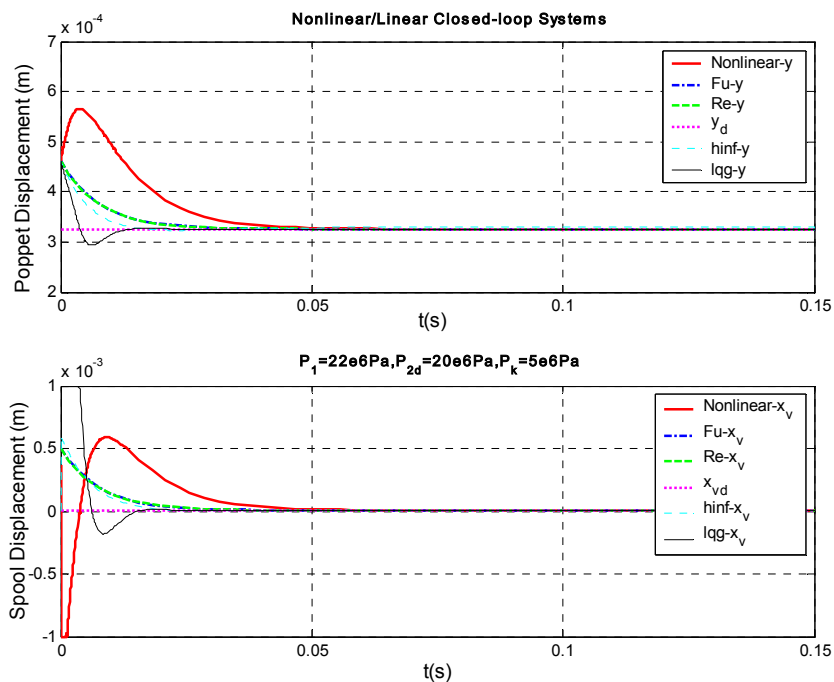


Figure 4-13. Regulation of nonlinear/linear closed-loop systems-  $y$  and  $x_v$

Figure 4-13 and 4-14 show the step responses of poppet displacement  $y$ , spool displacement  $x_v$ , back-side pressure  $P_2$  and poppet velocity  $\dot{y}$ . It can be illustrated that all system variables except the back-side pressure  $P_2$  can reach their equilibrium points from the initial deviations in about 30ms that is 20 times faster than the stable open-loop systems. The nonlinear system is a little bit slower than the linear systems whose settling

times for  $y$ ,  $\dot{y}$  and  $x_v$  are less than 20 ms. It also has obvious highest peak values for variables  $y$ ,  $P_2$  and  $\dot{y}$ . It takes the nonlinear system the lowest time period of more than 50 ms to reach its equilibrium pressure  $P_2$ , which will lead to the clear delay of its pressure behavior, followed by the reduced-order line closed-loop system, the  $H_\infty$  linear closed-loop system and the LQG linear closed-loop system. Back-side pressure  $P_2$  of the full-model linear closed-loop system in Figure 4-13 does not change much (less than 2 percent of its nominal value) because the initial deviation is none and this system has a very quick response. The performance of the linear system with  $H_\infty$  is closely in line with those of the linear systems with the modified PI controller.

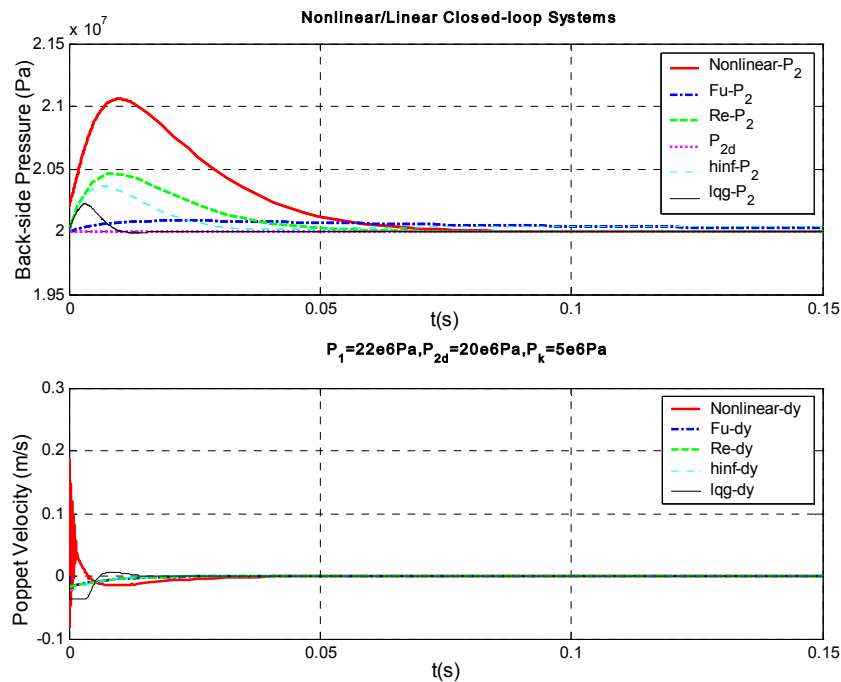


Figure 4-14. Regulation of nonlinear/linear closed-loop systems-  $P_2$  and  $\dot{y}$

The second plot in Figure 4-13 illustrates that the LQG control asks for a very big control effort that might bring the failure of this method, though it can reach the equilibrium status in the shortest time period. The initial condition brings big influence on the nonlinear system, which is represented by the spool going beyond its lower limitation and the poppet having a vibratory velocity at the very first beginning of movement (shown in Figure -14). The linear system with the  $H_\infty$  controller has distinct steady-state errors of  $y$  and  $P_2$ , though they are small enough to be negligible.

#### 4.6 Regulation Problem for the Second Group of Closed-loop Systems

The results in this section aim at comparing the regulating performances of the four nonlinear closed-loop systems. The only difference among these nonlinear systems is that the loops of the system are closed by diverse controllers: the modified PI controller, the LQG controller, the  $H_\infty$  controller and the nonlinear controller. Working pressures, initial condition and the steady-state values are same as those in the previous section. Performance matrices in LQG control, weight functions and uncertainty function in  $H_\infty$  control are same as those in section 4.5 too.

In Figures 4-15 and 4-16, Nonlinear-\* with the red solid thick line represents variables for the nonlinear system with the nonlinear controller. Non-PI-\* with the blue dash-dot thick line symbolizes variables for the nonlinear system with the modified PI controller. The magenta dot line stands for the desired values. Non-hinf-\* with the cyan dash thin line means variables for the nonlinear system with the  $H_\infty$  controller. Non-lqg-\* with the black solid thin line denotes variables for the nonlinear system with the LQG controller. Section 4.8 uses the same denotation.



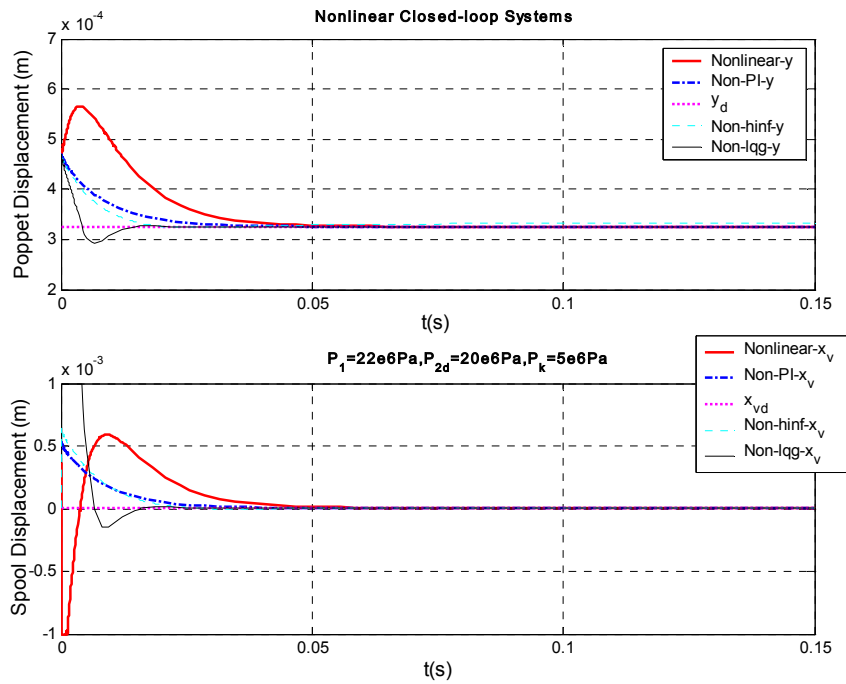


Figure 4-15. Regulation of nonlinear closed-loop systems-  $y$  and  $x_v$

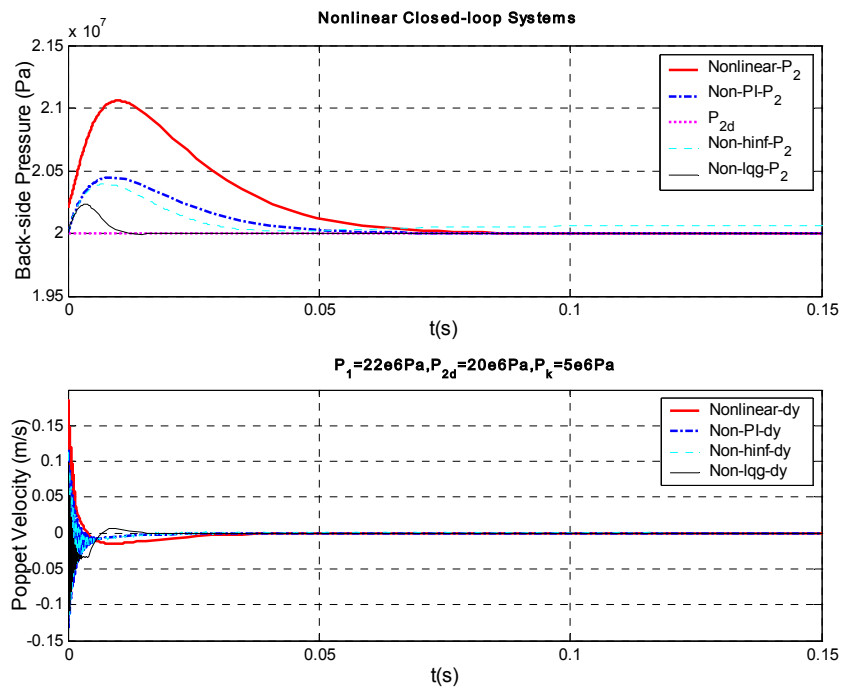


Figure 4-16. Regulation of nonlinear closed-loop systems-  $P_2$  and  $\dot{y}$

Figures 4-15 and 4-16 demonstrate that the nonlinear systems with the LQG controller and the  $H_\infty$  controller have quite similar behaviors as those of the corresponding linear closed-loop systems except that the poppet velocities exhibit the serious high frequency oscillation at the starting time. The nonlinear system with the modified PI controller performs like the reduced-order linear system in the previous section. Its poppet velocity also can not avoid heavily vibrating at the very first beginning from the initial condition.

#### 4.7 Tracking Problem of the First Group of Closed-loop Systems

The systems in this section are exactly same as those in section 4.5. System pressures can be chosen as  $P_k = 5(10^6) \text{ Pa}$ ,  $P_1 = 22(10^6) + 5(10^6)\sin(62.8t) \text{ Pa}$ , and  $P_{2d} = 20(10^6) + 5(10^6)\sin(62.8t) \text{ Pa}$  (shown in Figure 2-10). The identical initial conditions are used. The pressure drop across the poppet opening is held as  $2 \text{ MP}_a$ . Both the desired nose-side pressure (represented by the red solid line) and the desired back-side pressure (represented by the blue dash-dot line) are operated as sinusoidal waves with 10 HZ frequency. The desired piping pressure (represented by the magenta dot line) is kept as a constant of  $5 \text{ MP}_a$ . The initial nominal poppet velocity is assumed as 0. The rest ones can be given by

$$\dot{y}_{di_b} = \frac{y_{di_b} - y_{di_b-1}}{t_{sp}}, \quad i_b = 2, \dots, n_b \quad (4.15)$$

where  $\dot{y}_{di_b}$  is the  $i_b$ th poppet velocity on the poppet trajectory,  $y_{di}$  is the  $i_b$ th poppet location on the poppet trajectory,  $t_{sp}$  is the sample time that is chosen as 0.01 s and  $n_b$  is

the maximum number of how many sample times there are in the whole chosen simulation time of 0.4 s. Except the uncertainty weight function  $W_I$ , all other parameters are kept same as those in section 4.5. The weight function  $W_I$  can be given according to the uncertainty shown in Figure 4-17 by

$$W_I(s) = \frac{0.168s^4 + 41.011s^3 + 50.75s^2 + 20.181s + 12.269}{s^4 + 241.837s^3 + 191.189s^2 + 98.102s + 40.942}. \quad (4.16)$$

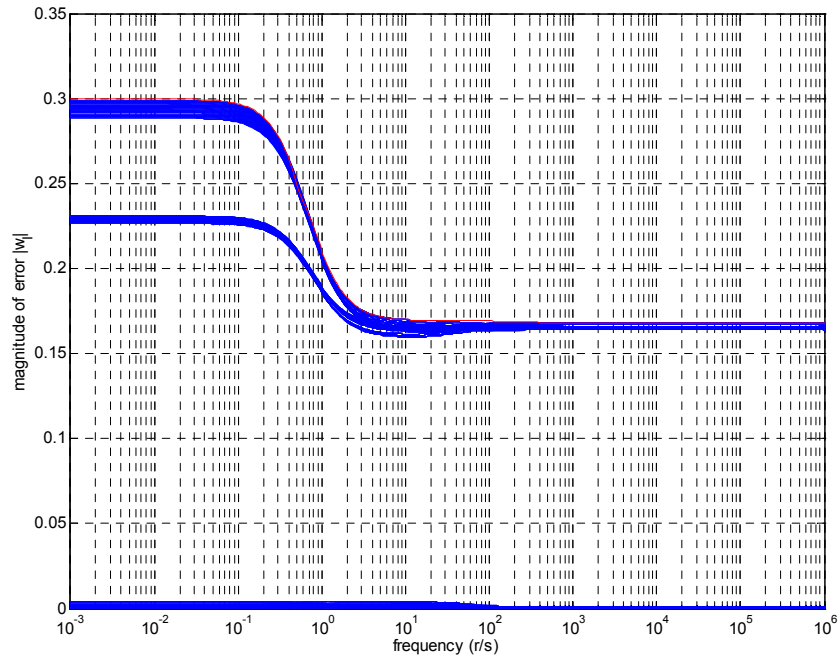


Figure 4-17. Input uncertainty and weight function  $W_I$  (red line) for tracking problem

For LQG and  $H_\infty$  control design, the sinusoidal trajectories are represented by  $n_b$  equilibrium points that individually execute their step responses. The calculating time of one regulating process for every equilibrium point is 10 ms, which is one tenth of the cycle time of a sine wave with 10 HZ frequency. It can be treated by the way that a

period of a sine wave consists of 10 points. The time period from one point to another point is 10 ms. If the acceptable step response of every equilibrium point can be accomplished in this short period, the whole sine wave can be followed through in one period time of 0.1 s. This is absolutely much faster than any hydraulic element in the fluid circuit. The final values of each step response are recorded as the positions, velocities and pressures that can be reached by the system in a consecutive period, for example 0.4 s in these simulations. This concept is used in the whole section of tracking problem.

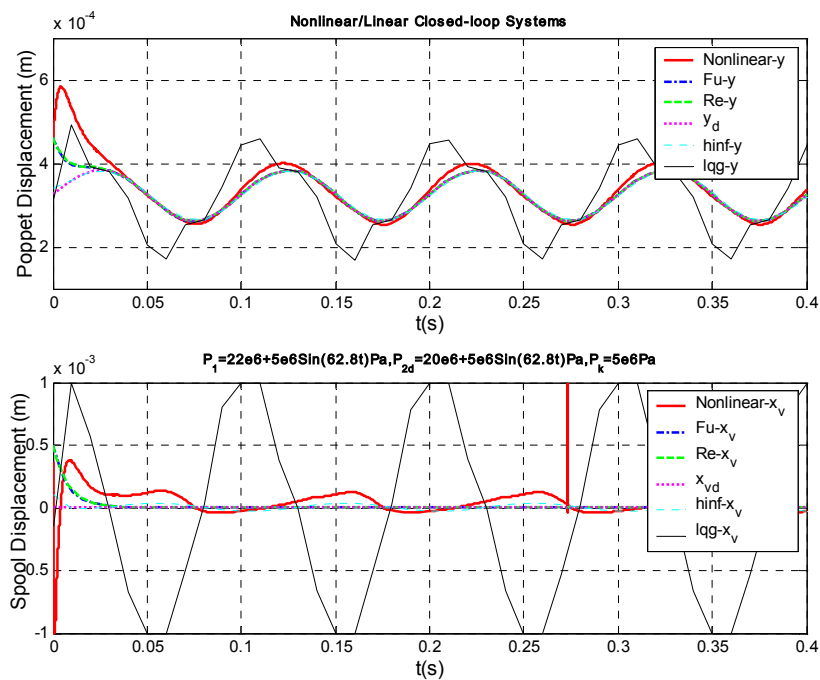


Figure 4-18. Tracking of nonlinear/linear closed-loop systems-  $y$  and  $x_v$

The upper plot in Figure 4-18 brings forth the tracking behaviors of the poppet position  $y$  in the five closed-loop systems. It indicates clearly that except the full-model

linear system with the LQG controller, all other four systems execute the acceptable capabilities to track the sine trajectory with 10 HZ frequency. The linear system with the LQG controller has a phase lead of about 45 degree and a steady-state error of more than 60% compared with the desired position. The lower plot in Figure 4-18 illuminates the control signals  $x_v$  in which the spool reaches its utmost in bi-directions in the linear system with the LQG controller. This can explain why this linear system can not fulfill the tracking function. For example, at 0.05 second, although the spool makes its biggest opening, more flow still needs to exit from the control chamber to make the poppet lifts more from its seat. Therefore, the control effort is too big to be realized by this system. Other systems, though some of them also require much more spool movement than the desired one, can fulfill their tracking function properly. The strange spike in the nonlinear closed-loop system appears when the second item of the poppet flow force pressure coefficient  $K_{fqt}$  is taken into account.

Back-side pressures  $P_2$  plots in Figure 4-19 point up that the full-model linear system with the  $H_\infty$  controller has a slight phase delay and a small steady-state error of the amplitude as well as the nonlinear system with the nonlinear controller. Although the poppet can not arrive at the desired position, the back-side pressure  $P_2$  of the full-model linear system with the LQG controller still can track well and there is no surprise to see the big sinusoidal poppet velocity wave (shown in the lower plot of Figure 4-19) in this system. Both the full-model linear system with the modified PI controller and the reduced-order linear system with the modified PI controller can make a good agreement with the desired system in  $y$ ,  $x_v$  and  $P_2$ . The linear poppet with the  $H_\infty$  controller has a

poppet velocity that is in a great conformity with the desired values. The nonlinear closed-loop system can not execute the smooth velocity change, which has high frequency vibration at the most part of the sine wave. The poppet velocity of the linear systems with the modified PI controller trends to be zeros, which is not feasible in practice.

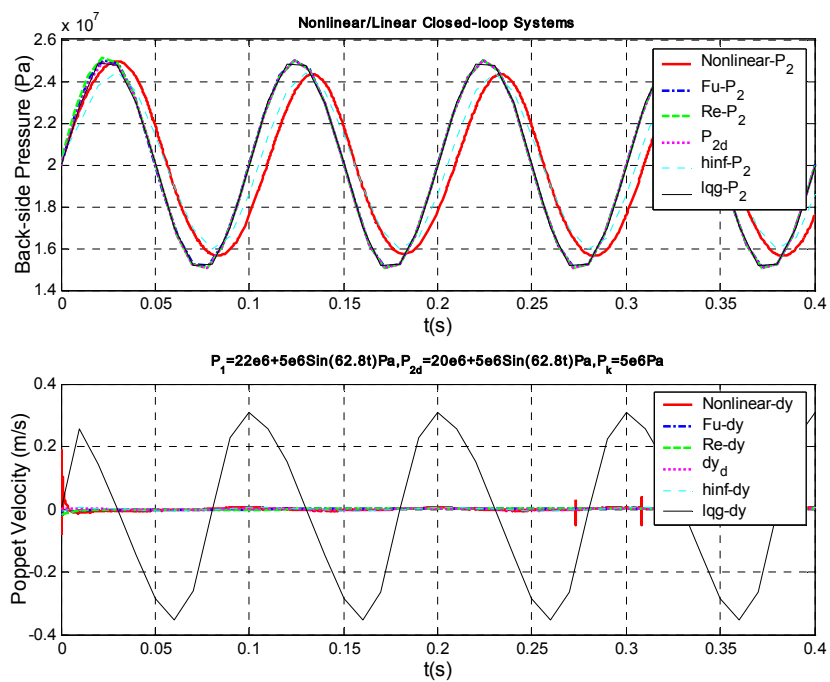


Figure 4-19. Tracking of nonlinear/linear closed-loop systems-  $P_2$  and  $\dot{y}$

Figure 4-20 shows the corresponding change of the control gains of the PI controller.

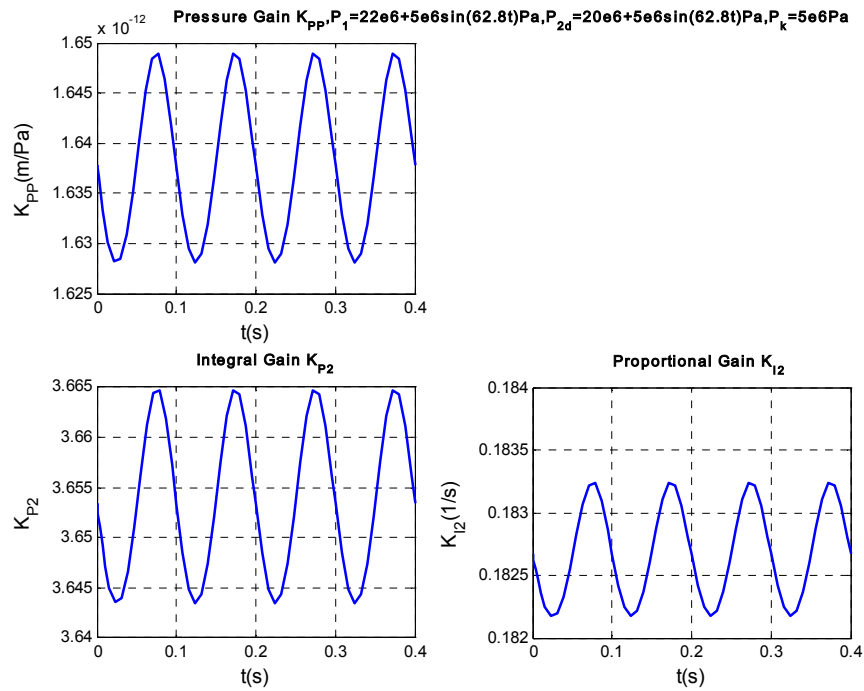


Figure 4-20. Gains of the modified PI controller for tracking problem

#### 4.8 Tracking Problem of the Second Group of Closed-loop Systems

The results displayed in this section present the tracking behavior for the nonlinear systems that are exactly same as those in section 4.6. Operating system pressures and initial conditions are equivalent as those in the previous section.

It can be said that both LQG and  $H_\infty$  control design produce the totally undesirable performance when they are combined with the nonlinear system. The amplitudes of the poppet positions  $y$  are much greater than the desired values (shown in Figure. 4-21). And the back-side pressures  $P_2$  are always much less than the required pressures (shown in Figure. 4-22). The poppet velocities  $\dot{y}$  are quite bigger than the required ones (shown in Figure. 4-22).

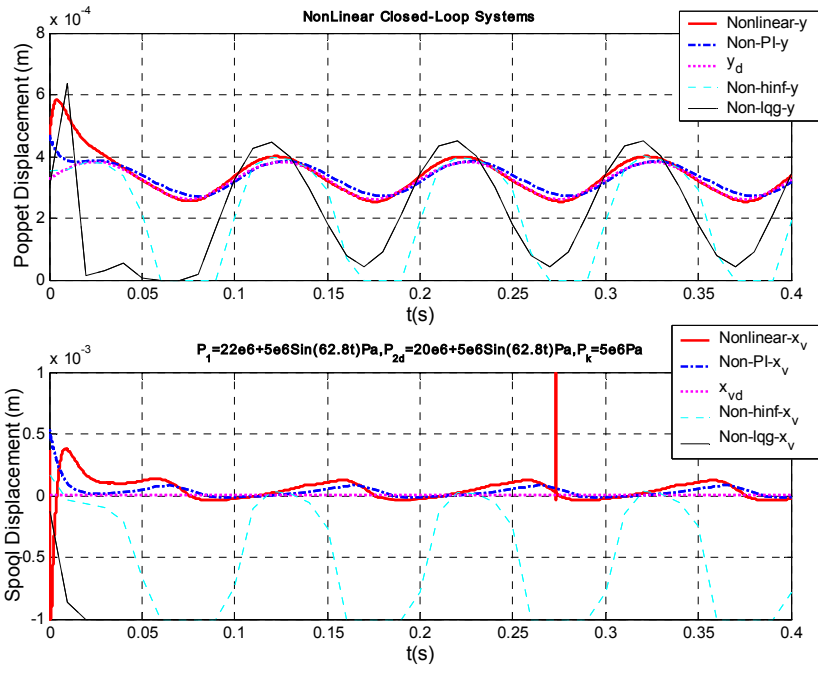


Figure 4-21. Tracking of nonlinear/linear closed-loop systems-  $y$  and  $x_v$

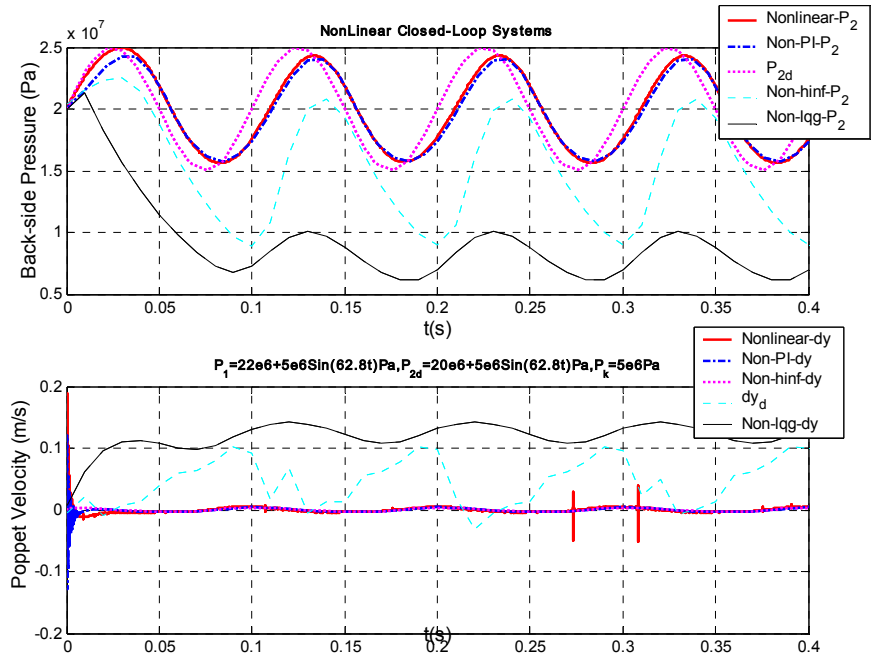


Figure 4-22. Tracking of nonlinear closed-loop systems-  $P_2$  and  $\dot{y}$



The spool in the nonlinear system with the LQG controller widely opens in its negative moving direction. The control chamber always connects with the back-side chamber. The poppet position  $y$  only can be adjusted by the pressure drop across the control orifice. The nonlinear system with the  $H_\infty$  controller demonstrated the unavailability of astonishing tracking problem when it shows the pleasant behavior in the linear system. Only can less than 25 percent of the sine wave of the poppet displacement  $y$  be followed. The poppet totally shuts off and the spool reaches its negative limitation in some period. This might be caused by the fact that the linear system does not include information about the left opening of the control orifice that connects the control chamber and the back-side chamber.

The nonlinear systems with either the nonlinear controller or the modified PI controller make obviously favorable behavior as they are expected. The previous nonlinear system has a slight phase lag which matches with the relatively slow pressure action in the step response. The spike of its spool displacement might be introduced by the steady-state flow force due to the change of the poppet position.

#### 4.9 Summary

What are presented in this chapter are all the simulation results. The influences of the important parameters on the open-loop stability criteria are depicted. The closed-loop systems are classified into two groups for making comparison of both regulation and tracking behavior. The linear controllers are also validated by being combined with the nonlinear system as well as the linear systems. The conclusion can be made roughly that both the modified PI controller and the nonlinear controller might be the good

choices to implement the closed loop for the real poppet valve system. The discussion will be fully carried out in the next chapter.

## CHAPTER 5. CONCLUSIONS AND CONTRIBUTIONS

### 5.1 Introduction

The goal of this two-stage poppet valve system aims at achieving its metering function with specific behavior requirements. This dissertation focuses on system dynamics modeling and control design for this system. Simulink models and Matlab programs were constructed for both the linear systems and the nonlinear systems that are combined with four control methods including modified PI control, LQG control,  $H_\infty$  control and a nonlinear control. The simulation results of regulation and tracking behavior for various closed-loop systems were graphically shown and briefly discussed in Chapter 4. The summary of conclusions is addressed in this chapter.

### 5.2 System Modeling

A two-stage poppet valve system with a simple back-side operating condition that includes an orifice with a fixed area and a constant pressure reservoir was investigated in this dissertation. There are two evident nonlinear characteristics of this system in addition to the nonlinearity of the flow itself. The first one is that the control orifice can connect the control chamber with either the back-side chamber or the nose-side chamber depending on the system pressure conditions. Another is that the fluid across the poppet opening can run in both directions. The later nonlinearity was ignored in this analysis, while the former one was seriously considered. The nonlinear mathematical model was proposed to describe the system dynamics. And, linear systems were created by using the Taylor series expansion and neglecting the high-order items according to local

equilibrium positions. A reduced-order system was also created by leaving out the poppet mass and the control pressure change in the back-side chamber. The spring mounted in the poppet cartridge is weak enough to be assumed to be none. There is a big difference between a relief poppet and a metering poppet, in which the spring is unavoidably a vital force component for the relief one to keep the poppet tightly seat on the port base. The size and the opening velocity of the control orifice are essential factors to determine the accomplishment of distributing an amount of flow required.

Navier-stokes equations that do not contain the body forces and viscosity effect were used in the axial direction for the poppet nose-side chamber to obtain the linear formation of the flow force acting on the poppet head. An analytical expression was presented to take the transient flow force into consideration. The transient flow force was proved to possibly bring into unstable features to the system in the parameter stability analysis in Chapter 4. The leakage occurring across the cylindrical geometry of the poppet land was modeled as an annular Poiseuille flow passage. The pipeline leakage was considered as a low Reynolds flow that is proportional to the back-side pressure  $P_2$ .

### 5.3 Control Design

All control analysis is carried out for a very small poppet opening that is usually the worst case of the poppet local stability according to particular operating situations. Mathematica plots in Chapter 4 graphically disclosed some important findings of how the selected system parameters work on the open-loop local stability criteria. It was greatly surprising to find out that the leakage across the poppet land  $Q_2$  provided a negative effect on the stability. In general, leakages will dissipate the system energy disturbance to

benefit the stability. Therefore more study on the form of the leakage  $Q_2$  and its unusual performance for the stability is needed to be conducted in the future. Fluid bulk modulus  $\beta$  is the inverse of the fluid compressibility, which is the change in pressure caused by the internal fluid strain change. The bigger the bulk modulus is; the bigger pressure response is needed to a constant fluid strain change. Therefore, the increase of the bulk modulus will no doubt lead to a more unstable system. A larger back-side chamber  $V_L$  can provide substantial assistance in the system stability. When it goes up, the system takes less effort to overcome the smaller pressure change caused by a same amount of volume change in a bigger chamber as the fluid elasticity is constant. The poppet containing a poppet land cross section area that is larger than the area of the poppet port is a desirable design. Orifice coefficient  $C_d$  has given evidence that it introduced the very serious uncertainty to the system and its increase does not help stability. The change of this parameter can introduce proximately 30% uncertainty of the nominal plant value to the system. A possible explanation for this is that the transient flow force likely can be a crucial factor to lead to instability. And the poppet flow gain  $K_{qt}$  that is nearly related with the transient flow force due to the poppet velocity  $\dot{y}$  is proportional to orifice coefficient  $C_d$  under certain system pressures. The influence of the spring rate on the system stability has the same trend as that of fluid bulk modulus. When the spring rate is bigger, it is harder for the system to be stable.

The goal of tracking the poppet position trajectories of sine signals with the high frequency of 10 HZ was accomplished theoretically. Linear controllers are validated by the model that is a combination of the controller with the nonlinear system as well as the

linear system. Nonlinear control and PI control with changing gains were proved to be better choices.

In PI control, the gain scheduling was fulfilled by dividing the constant proportional and integral gains by the spool flow gain  $K_{ql}$  that is associated with the fluid going through the control orifice. The essential of this strategy is to make allowance for the change of the nominal pressure drop, which is the similar clever idea in the nonlinear control design. The control gains in PI controller can be chosen according to the stability criteria derived from the Routh-Hurwitz method. The nonlinear system with the nonlinear control was verified by Lyapunov theorem to be globally asymptotically stable.

Both  $H_\infty$  and LQG control algorithm were achieved to design the local controllers. They performed suitable behavior to implement the regulation requirement under typical working condition marked out by industry. However, the weigh matrices,  $Q$  and  $R$  in full-state feedback LQR design and the uncertainty weight functions,  $W_p$  and  $W_u$  in  $H_\infty$  control are fixed, which obviously can not satisfied the various operating circumstances. Though the full-model linear systems with the  $H_\infty$  executed tolerable dynamic action, the nonlinear system coupled with the  $H_\infty$  control can only have acceptable performance to track a small portion of the poppet displacement of sine waves of 10 HZ shown in Figure 4-21. The LQG control presented in this dissertation is not a suitable solution of the control design for the tracking problem no matter it is associated with the linear system or the nonlinear system. Therefore, when  $H_\infty$  and LQG control algorithm is applied to the

real system with widely various working pressures, a strategy of getting proper robust internal gains will be required for the global system.

#### 5.4 Contributions

This dissertation is trying to mainly make contributions for the metering poppet topic in two areas: system modeling and control design. This work presented the nonlinear and linear analytical models for a two-stage metering poppet system that contains a critically-centered 3-way spool as the pilot device, a common poppet valve as the flow distributor and a simple poppet back-side chamber condition. A clear linear expression of the flow force was derived to investigate its effect on stability.

In this work, three linear control methods were used to make the closed-loop system. It is shown that modified PI control is one of the good choices for industrial application. How to choose the appropriate gains for a PI controller was also decided numerically. LQG control and  $H_\infty$  control were proved to satisfy the local system behavior, instead of the global one. If a strategy can be conceived to achieve the global performance, they also could be acceptable control approaches in practice. The work of the nonlinear controller that is based on Du's work was proved to be globally asymptotically stable and valuable. The effects of some important key parameters on the system stability were discussed. The leakage across the poppet land and the hole containing it has surprising negative influence on the system stability.

## CHAPTER 6. FUTURE WORK

### 6.1 System Modeling

The modeling work can be enriched by adding more components to the system, for example complex load conditions (a cylinder with loading, a pump), spool dynamics or transient delivery line effect, etc. The experimental data of transient flow force and leakage across the poppet land is a good collection for exploring the reason of system instability. Furthermore experimental identification of the control design, especially for the nonlinear and modified PI control is also encouraged to be covered in the future work, though part of the work has been done by industry. If the first-hand data of unstable situation that occurs in industry can be collected, it is good for engineers to make a detailed model of that system to understand the root causes of the instability. The leakage across the poppet land and the bore containing it and the back-side pipeline leakage are theoretically proved to be negative influences on the system open-loop stability. Considering that leakages dissipate the disturbance energy, it is worth while to investigate this conclusion in real physical systems.

### 6.2 Control Design

It has been mentioned in Chapter 5, the LQG and  $H_\infty$  controller in this dissertation are locally favorable to the regulating behavior. They only can reveal regional stability property. When they are applied to the real physical word, fixed control specifications will put them at disadvantage. Therefore, it is necessary to create a robust gain scheduling strategy for the all-around system. Rong Zhang [11] developed a LPV (Linear Parameter



Varying) method in his PhD. thesis to deal with the similar problem. Additionally, the unmodelled uncertainty can be counted in to improve  $H_\infty$  control.

The nonlinearity of the flowing direction of the fluid passing the poppet opening and the pipeline fixed-area orifice was not involved in system modeling and control design. The switch process when the fluid across the poppet suddenly changes its flowing direction could contribute to untraceable stability problems. Especially the linear formation of the flow force is not advisable at this case, because this split second can cause infinite flow gains that are unacceptable for calculation. Consequently, more future work can be done to smooth this process. The way to measure the transient flow force needs to be examined to explain the relationship between the transient flow force and the system stability.

## REFERENCE

- [1] Du, Hongliu, An E/H Control Design for Poppet Valves in Hydraulic System, *ASME, The Fluid Power and Systems Technology Division (Publication) FPST*, Vol. 9, p. 141-148, 2002
- [2] Pfeiffer, Ferris, Dynamics and Stability Issues of Poppet Type Pressure Relief Valves, Master Thesis, *University of Missouri at Columbia*, 2004
- [3] Stone, J. A., Discharge Coefficients and Steady-State Flow Forces for Hydraulic Poppet Valves, *Transactions of the ASME*, 82, p.144-154, March, 1960
- [4] Funk, James E., Poppet Valve Stability, *Journal of Basic Engineering*, Ser. D, Vol.86, p. 207-212, June, 1964
- [5] Kasai, Kohji, On the Stability of a Poppet Valve with an Elastic Support, *Bulletin of JSME*, Vol. 11, No.48, p.1068-1083, 1968
- [6] Johnson, B. L. and D. E. Wandling, Actual Popping Pressure of a Relief Valve with a Real Helical Spring Under Dynamic Load, *Transactions of the ASME*, p. 1142-1146, November, 1960
- [7] Roberts, Brian J., Poppet Valves for Directional Control, *Machine Design*, 60,18,ABI/INFORM Global, p. 119-122, 11, August, 1988
- [8] Johnston, D. N., K. A. Edge and N.D. Vaughan, Experimental Investigation of Flow and Force Characteristics of Hydraulic Poppet and Disc Valves, *Processing Institution Mechanical Engineering*, Vol. 205, p. 161-170, 1991

- [9] Ito, Kazumi, Koji Takahashi and Kiyoshi Inoue, Flow in a Poppet Valve, *JSME International Journal, Series B: Fluids and Thermal Engineering*, Vol. 36(1), p. 42-50, 1993
- [10] Shin, Yung C., Static and Dynamic Characteristics of a Two Stage Pilot Relief Valve, *Transactions of the ASME*, Vol.113, p. 260-268. , June, 1991
- [11] Zhang, Rong, Andrew G. Alleyne and Eko A. Prasetyawan, Performance Limitations of A Class of Two-stage Electro-hydraulic Flow Valves, *International Journal of Fluid Power*, Vol. 3, No. (1), p. 1-7, 2002
- [12] Opendenbosch, Patrick, Nader Sadegh and J. Book Wayne, Modeling and Control of an Electro-hydraulic Poppet Valve, *Proceeding International Mechanical Engineering Congress and Exposition, Anaheim, California*, November, 2004
- [13] Satoru, Hayashi and Ohi Kiyotoshi, Global Stability of A Poppet Valve Circuit, *The Journal of Fluid Control*, Vol. 21, Issue 4, p. 48-63 , 1993
- [14] Dorato, Peter, A Historical Review of Robust Control, *IEEE Control Systems*, p. 44-47, April, 1987
- [15] Lewis, F. L., Applied Optimal Control and Estimation, *Prentice-Hall*, 1992
- [16] Bennett, Stuart, A Brief History of Automatic Control, *IEEE Control Systems*, Vol. 16, Issue 3, p. 17-25, June, 1996
- [17] Bryson, Arthur E., Optimal Control-1950-1985, *IEEE Control Systems*, Vol. 16, Issue 3, p. 26-33, June, 1996
- [18] Atherton, Derek P., Early Developments in Nonlinear Control, *IEEE Control Systems*, Vol. 16, Issue 3, p. 34-43, June, 1996

- [19] Doyle, J. C. and G. Stein, Robustness with Observers, *IEEE Transaction on Automatic Control*, Vol. AC-24, p. 607-611, August, 1979
- [20] Doyle, John C. and Gunter Stein, Multivariable Feedback Design: Concepts for a Classical/Modern Synthesis, *IEEE Transactions on Automatic Control*, Vol. AC-26, No. 1, February, 1981
- [21] Athans, Michael, A Tutorial on LQG/LTR Method, *Proceeding American Control Conference, Seattle, WA*, p. 1289-1296, June, 1986
- [22] Zames, George, Feedback and Optimal Sensitivity: Model Reference Transformations, Multiplicative Seminorms, and Approximate Inverses, *IEEE Transactions on Automatic Control*, Vol. AC-26, No.2, April, 1981
- [23] Zames, George and Bruce A. Francis, Feedback, Minimax Sensitivity, and Optimal Robustness, *IEEE Transactions on Automatic Control*, Vol. AC-28, No.5, May, 1983
- [24] Doyle, John C., Keith Glover, Pramod P. Khargonekar and Bruce A. Francis, State-space Solutions to Standard  $H_2$  and  $H_\infty$  Control Problems, *IEEE Transactions on Automatic Control*, Vol. 34, No. 8, August, 1989
- [25] Slotine, Jean-Jacques E. and Weiping Li, *Applied Nonlinear Control*, Prentice Hall, 1991
- [26] Astrom, Karl Johan and Bjorn Wittenmark, *Adaptive Control*, Prentice Hall, December, 1994
- [27] Isidori, Alberto, *Nonlinear Control Systems*, Springer-Verlag, August 1995

- [28] Astrom, Karl J., Adaptive Control Around 1960, *IEEE Control Systems*, Vol. 16, Issue 3, p. 44-49, June, 1996
- [29] Yao, Bin, F. Bu, and G. C. T. Chiu, Nonlinear Adaptive Robust Control of Electro-hydraulic Systems Driven by Double-rod Actuators, *International Journal of Control*, Vol.74, No.8, p. 761-775, 2001
- [30] Zhang, Rong, Andrew Alleyne, Modeling and  $H_2/H_\infty$  MIMO Control of an Earthmoving Vehicle Powertrain, *Journal of Dynamic Systems, Measurement, and Control*, Vol. 124, p. 625-636, December, 2002
- [31] Fales, Roge, E. Spencer, K. Chipperfield, F. Wagner, Atul Kelkar, Modeling and Control of a Wheel Loader With a Human-in-the-Loop Assessment Using Virtual Reality, *Journal of Dynamic Systems, Measurement, and Control*, Vol. 27, Issue 3, p. 415-423, September, 2005
- [32] Manring, Noah D., Hydraulic Control Systems, *John Wiley & Sons*, April 2005
- [33] Skogestad, Sigurd and Ian Postlethwaite, Multivariable Feedback Control, *John Wiley & Sons*, February, 2004
- [34] Zhou, Kemin, and John C. Doyle, Essentials of Robust Control, *Prentice Hall*, September, 1997
- [35] Special Issue on the LQG Problem, *IEEE Transaction on Automatic Control*, December, 1971
- [36] Wandling, D. E. and B. L. Johnson, Hydraulic Poppet Valve Stability, *National Combined Farm, Construction and Industrial Machinery and Powerplant Meetings, Milwaukee, Wis.*, September 11-14, 1972

- [37] Guillaume, D. W. and D. DeVries, A Valve with Seat-slope Proportional to Flow Area at All Poppet Positions, *Review of Scientific Instruments (0034-6748)*, Vol. 62, No. 1, p.247-248, January 1991
- [38] Vaughan, N. D. and D. N. Johnston, K.A. Edge, Numerical Simulation of Fluid Flow in Poppet Valves, *Processing Institution Mechanical Engineering*, Vol. 206, p. 119-127, 1992
- [39] Schexnayder, Lawrence F., Poppet Valve with Force Feedback Control, *U.S. Patent 5 421 545*, June 6, 1995
- [40] Hyde, Richard Alden, H Aerospace Control Design- A VSTOL Flight Application, *Springer-Verlag*, October, 1995
- [41] Hayashi, Satoru, Instability of Poppet Valve Circuit, *JSME International Journal, Series C*, Vol. 38, No. 3, p. 357-366, 1995
- [42] Khalil, Hassan K., Nonlinear Systems, *Prentice Hall*, December 1995
- [43] Bushnell, Linda G., On the History of Control, *IEEE Control Systems*, Vol. 16, Issue 3, p. 14-16, June, 1996
- [44] Michel, Anthony N., Stability: The Common Thread in the Evolution of Feedback Control, *IEEE Control Systems*, Vol. 16, Issue 3, p. 50-60, June, 1996
- [45] Zames, George, Input-Output Feedback Stability and Robustness, 1955-85, *IEEE Control Systems*, Vol. 16, Issue 3, p. 61-66, June, 1996
- [46] Phillips, Charles L. and Royce D. Harbor, Feedback Control Systems, *Prentice Hall*, 1996

- [47] Manring, Noah D. and Robert E. Johnson, Optimal Orifice Geometry for a Hydraulic Pressure-Reducing Valve, *Journal of Dynamics Systems, Measurement, and Control*, Vol.119, p. 467-473, September, 1997
- [48] Woods, W. A. and P. G. Brown, Flow Area of Multiple Poppet Valve, *Proceedings of the Institution of Mechanical Engineers. Part D: Journal of Automobile Engineering (0954-4070)*, Vol. 211 (5), p. 407-412, 1997
- [49] Nadarajah, S., S. Balabani, M. J. Tindal and M. Yiammeskis, The Turbulence Structure of the Annular Non-swirling Flow Past an Axisymmetric Poppet Valve, *Proceedings of the Institution of Mechanical Engineers. Part C: Journal of Mechanical Engineering Science (0954-4062)*, Vol. 212 (6), p. 455-471, February, 1998
- [50] Nadarajah, S., S. Balabani, M. J. Tindal and M. Yiammeskis, The Effect of Swirl on the Annular Flow Past an Axisymmetric Poppet Valve, *Proceedings of the Institution of Mechanical Engineers. Part C: Journal of Mechanical Engineering Science (0954-4062)*, Vol. 212 (6), p. 473-484, February, 1998
- [51] Hayashi, Satoru, Nonlinear Phenomena in Hydraulic Systems, *Fifth International Conference on Fluid Power Transmission and Control, Hangzhou, China*, p. 28-32., April, 2001
- [52] Barber, Dennis and Michael Paik, Hydraulic Poppet Valve with Force Feedback, *U.S. Patent 6869060*, December 11, 2001
- [53] Vonderwell, M. P., A Summary of Metering Poppet Valve Research Efforts, *Company Document of Caterpillar Inc.*, September, 2002

- [54] Zhang, Rong, Multivariable Robust Control of Nonlinear Systems with Application to an Electro-Hydraulic Powertrain, PhD Dissertation, *University of Illinois at Urbana-Champaign*, 2002
- [55] Chenvisuwat, Thum, Sung-Hwan Park and Ato Kitagawa, Development of Hydraulic Friction Brake for Railway Rolling Stock (Part I: Static Behavior of Poppet-type Brake Pressure Control Valve), *JSME International Journal Series C*, Vol. 47, No. 4, p. 1149-1155, 2004
- [56] Chenvisuwat, Thum, Sung-Hwan Park and Ato Kitagawa, Development of Hydraulic Friction Brake for Railway Rolling Stock (Part II: Dynamic Analysis and Performance Evaluation of Hydraulic Brake System Using Poppet-type Brake Pressure Control Valve), *JSME International Journal Series C*, Vol. 47, No. 4, p. 1166-1174, 2004
- [57] Yang, Xiaolong, Dwight Stephenson and Michael Paik, Bidirectional Pilot Operated Control Valve, *U.S. Patent 6328275*, March 22, 2005



## VITA

Yamin Luo was born on January 29, 1976 in Su zhou, Anhui, China. She received her Bachelor of Science degree in Mechanical Engineering in 1997 from Anhui University of Science and Technology in Huainan, Anhui, China where is Yamin's second hometown not only because she spent four fantastic years for BS study but also she was raised by her dear grandmother for eight years in this lovely city. After that, she took a position as a Technical Instructor at Shanghai Diesel Engine Co. Ltd. that is a first-class engine company in China. Three years later, she was enrolled in the Master program in the School of Power Machinery and Energy Engineering in Shanghai Jiao Tong University in China. She earned a Master of Science degree in Mechanical Manufacturing and Automation in 2003. In the same year, she was recruited by Intel Products (Shanghai) Co. Ltd as a Manufacturing Supervisor in March. Yamin entered the University of Missouri at Columbia in August 2003 to pursue a doctoral degree in Mechanical Engineering under the supervision of Prof. Noah Manring. Her research focuses on hydraulic control of a two-stage metering poppet valve system. Subsequent to graduation, she will be joining to Hydraulic Control Research in Caterpillar Inc. in Peoria, Illinois.